SPECTROSCOPIC AND COMPUTATIONAL STUDIES OF IONIC CLUSTERS AS MODELS OF SOLVATION AND ATMOSPHERIC REACTIONS

Thesis by

Keith T. Kuwata

In Partial Fulfillment of the Requirements

for the Degree of

Doctor of Philosophy

California Institute of Technology

Pasadena, California

1998

(Submitted 17 April 1998)

"Those countries in Europe which are still influenced by priests, are exactly the countries where there is still singing and dancing and coloured dresses and art in the open-air. Catholic doctrine and discipline may be walls; but they are the walls of a playground. Christianity is the only frame which has preserved the pleasures of Paganism. We might fancy some children playing on the flat grassy top of some tall island in the sea. So long as there was a wall round the cliff's edge they could fling themselves into every frantic game and make the place the noisiest of nurseries. But the walls were knocked down, leaving the naked peril of the precipice. They did not fall over; but when their friends returned to them they were all huddled in terror in the centre of the island; and their song had ceased."

--G. K. Chesterton, *Orthodoxy*

ACKNOWLEDGMENTS

Seven years of graduate school can give a person a great diversity of experiences, within the laboratory and without. This has certainly been true of my years here at Caltech. But somehow, after doing many different things with many different people, we are required to write a thesis, to attempt some synthesis, to tell one (long) scientific story. The problem is that all systematic treatments are fundamentally false, or at least contrived, extrinsic to the vicissitudes and multitudes of chance insights that characterize research. Yet without some generalizations, we could not talk or even think about science. So, with an earnest desire to graduate, I attempt a synthesis of my graduate work in this thesis.

However, the smooth (smoothed?) scientific story we tell is challenged by this brief section of Acknowledgments. These few pages draw us nearer to reality, for they admit explicitly that our time at Caltech was not fundamentally about science, nor even about the multitude of techniques we employed to do science. Rather, our graduate student careers were fundamentally about relationships. Other people brought us to Caltech, helped us through Caltech, and welcome us after Caltech. My seven years in graduate school have been filled with people who have encouraged me to live vigorously as a scientist and as a human being.

I first thank my advisor, Prof. Mitchio Okumura, for the example of his passion for science, and for his support of my sundry research endeavors here. He has taught me the need both to ask important scientific questions, and to engage the myriad of technical

details required to answer these questions. I hope that my future career can follow the patterns of scientific care and delight that he has set forth for me.

I also thank my predecessors in the Okumura group I did not have the opportunity to work with on a daily basis. Yi-Bin Cao impressed upon me the single-minded focus required to excel in chemical physics. Chrissy Nelson and Teresa Moore gave me a good amount of practical help with the synthesis of chlorine nitrate, and well as insights into stratospheric chemistry. Post-docs Bermi Haas and Xu Zhang and master's student Todd Fuelberth also were generous with their scientific advice and their friendship.

That I have new experimental data to report in this thesis is due to the sacrificial contributions of Jong-Ho Choi and Matt Johnson. In 1994, Jong-Ho gave me a thorough initiation into our lab's original time-of-flight mass spectrometer, and taught me the mechanics of ion spectroscopy during many long nights of scanning chloride-water clusters. Matt Johnson, during his incredibly hectic winter and spring of 1995, still managed to teach me most of what I know about our optical parametric oscillator, and gave me a vision for the deep partnerships possible on a chemical physics experiment.

I also appreciate the generous assistance from our post-docs Ted Dibble and Thomas Schindler, for their work with me in lab, and their detailed advice about academic careers. Undergrad Jessie Haldeman provided a lot of help and an enjoyable sardonic sense of humor while pursuing the photoelectron spectroscopy of chlorine nitrate.

I also must express my ongoing thanks to the current members of the Okumura group. Jim Spotts and I shared a windowless room in 101 Noyes in our first year of grad

school, and we now share an equally sunless, even more isolated (and therefore productive) space in 34 Noyes in our last few months of grad school. I can only stand from afar and admire his doing the archetypal chemical physics thesis, from planning, to building, to getting data (lots of it), to analyzing data (an overwhelming amount of that). I express my gratitude for his sharp insights into chemistry, and I wish him great success in his future in developmental biology.

I also thank Alex Wong and Julio Lobo for their dedication to the time-of-flight experiment (at the beginning and the end of my time in lab), and their helpfulness with all the business of lab. I wish them, and our new students, Lance Christensen, Eva Garland, and Daniel Paik, a rewarding time here at Tech.

And thanks to so many other people here at Tech: Mike Roy, Ray Garcia, and Guy Duremberg in the machine shop; Tom Dunn, for his electronic wizardry at key points in my time here; Dian Buchness, who keeps this whole grad school enterprise hanging together; and the other wonderful people on staff.

Thanks also to my incredible professors at Harvey Mudd--researchers and educators who brought me here, and whose examples sustained me during my years here. I am especially grateful to Profs. Kerry Karukstis and Bob Cave. And thanks to those professors at UCLA willing to give me a chance with my post-doc, Ken Houk and Suzanne Paulson.

And without any good transition, I delight to acknowledge the people in the Caltech Christian Fellowship who have blessed me in the disparate stages of my life here. Early on, thanks to Janice Peters, to Charles and Margat Werner, to Sue Melnik, to

Yvonne Lung. Thanks to wonderful partners in ministry: Daniel Chang, Tony Chang, and Kurt Kramer. And thanks to the folks in grad group who have challenged me to integrate Christian and scientific lifestyles: Brad and Sherri Minch, Paul and Beth Hasler, Matt and Erica Carlson, Gary Holt, Jeff and Kim Copeland, Jeremy Kua and Aileen Chang.

My life has been deeply affected by the priests and congregation at the Episcopal Church of the Ascension in Sierra Madre. Frs. Michael Bamberger, Spencer Edwards, Roger Wood, and Stuart Ruth have all taught me the wisdom and delight of the Anglican expression of the Catholic faith.

In the background are two people who have faithfully loved me and who have been patient during all the vicissitudes of seven years of graduate school. I express my love and thanks to my mother and father, and wish them only happiness and peace.

Very much in the foreground in the past couple of years is someone who could inspire truly awful and long-winded (but very sincere) prose from me at 4:30 of the morning I intend to turn this in. There is nothing melodramatic in saying I would not be here, two weeks away from my Ph.D., without the astonishing love of my fiancée, Alexa Tharalson. What with the turmoil in my life and hers, I'm not sure we've ever had a romantic high to fall from. Alexa has led me by the hand into the real world, the world of real relationships, of give and take every day, of bearing each other's sorrows. I pledge my love to her, and I rejoice in the certainty of her love for me. And, of course, I dedicate this thesis (such as it is) to her.

ABSTRACT

Ionic clusters are useful as model systems for the study of fundamental processes in solution and in the atmosphere. Their structure and reactivity can be studied in detail using vibrational predissociation spectroscopy, in conjunction with high level *ab initio* calculations. This thesis presents the applications of infrared spectroscopy and computation to a variety of gas-phase cluster systems.

A crucial component of the process of stratospheric ozone depletion is the action of polar stratospheric clouds (PSCs) to convert the reservoir species HCl and chlorine nitrate ($ClONO_2$) to photochemically labile compounds. Quantum chemistry was used to explore one possible mechanism by which this activation is effected:

$$Cl^- + ClONO_2 \rightarrow Cl_2 + NO_3^- \qquad (1)$$

Correlated *ab initio* calculations predicted that the direct reaction of chloride ion with $ClONO_2$ is facile, which was confirmed in an experimental kinetics study. In the reaction a weakly bound intermediate Cl_2--NO_3^- is formed, with ~70% of the charge localized on the nitrate moiety. This enables the Cl_2--NO_3^- cluster to be well solvated even in bulk solution, allowing (1) to be facile on PSCs.

Quantum chemistry was also applied to the hydration of nitrosonium ion (NO^+), an important process in the ionosphere. The calculations, in conjunction with an infrared spectroscopy experiment, revealed the structure of the gas-phase clusters $NO^+(H_2O)_n$. The large degree of covalent interaction between NO^+ and the lone pairs of the H_2O ligands is contrasted with the weak electrostatic bonding between iodide ion and H_2O.

Finally, the competition between ion solvation and solvent self-association is explored for the gas-phase clusters $Cl^-(H_2O)_n$ and $Cl^-(NH_3)_n$. For the case of water, vibrational predissociation spectroscopy reveals less hydrogen bonding among H_2O ligands than predicted by *ab initio* calculations. Nevertheless, for $n \geq 5$, cluster structure is dominated by water-water interactions, with Cl^- only partially solvated by the water cluster. Preliminary infrared spectra and computations on $Cl^-(NH_3)_n$ indicate that NH_3 preferentially binds to Cl^- ion instead of forming inter-solvent networks.

CHAPTER 1

Introduction

The chemical and physical properties of ions are clearly important for understanding a wide variety of chemical phenomena. There is fundamental interest in the nature of solvation in liquids, both under conditions of normal pH and under conditions of high acidity. A detailed understanding of ion chemistry is also important for describing processes in the upper atmosphere.

The importance of ions is predicated on their electric charge. Electrostatics provides the driving force for the strong interactions of ions with solvent, and the often rapid reactions in both the stratosphere and ionosphere. Felicitously, what makes ions important also make them very amenable to study in the laboratory. For decades, mass spectrometry has been used to study the reactivity and physical properties of ions in the gas phase.

However, we have to consider the relevance of gas-phase measurements on ions to the questions of solvation and chemistry in the upper atmosphere. Much of the phenomena we seek to understand takes place in the context of macroscopic systems. The exact measurements possible for bare ions may not be applicable to the systems of interest. At the same time, direct experimental probes of bulk properties can reveal only so much about the fundamental solvent structure and reactivity of ions.

Workers in the past few decades have sought to bridge this gap between the gas and condensed phases by the study of ionic clusters, defined as bare ions with a countable number of solvent molecules. Using a variety of techniques, ions with a distribution of solvent molecule numbers can be both generated and mass selected. The chemical and physical properties of ions can then be measured as a function of the number of solvent

molecules. Thus, we can study explicitly the extrapolation from gas-phase to condensed phase properties.

While much attention is still being focused on the generation of larger ions (particularly biological molecules like polypeptides) with one or more solvent molecules, recent work has also focused on the development of spectroscopic techniques appropriate for studying ionic clusters. While electronic spectroscopy is appropriate and informative for quantitative studies of bare ions and monosolvated ions, this technique becomes less useful for the study of larger clusters. Infrared spectroscopy would be a more direct probe of the intermolecular forces within ionic clusters, but low absorption cross sections, low infrared fluence (particularly of tunable light sources), and low ion density all conspired again such an approach.

The first, and still quite fruitful, solution to these problems was the use of vibrational predissociation induced by the infrared output of optical parametric oscillators. Techniques pioneered in the late 1970's allowed for the parametric down-conversion of intense monochromatic laser light (such as the fundamental (1.06 μm) of Nd:YAG lasers) by non-linear optical crystals such as lithium niobate ($LiNbO_3$), tuned by precise control either of crystal angle or temperature. Problems with the low ion densities and IR absorption cross sections were avoided by doing photofragment spectroscopy. Infrared absorptions were inferred by the induction of vibrational predissociation, the breaking of ion-solvent bonds at resonant frequencies. Technology also existed for the precise counting of the daughter ion fragments that was required.

A complementary approach to interpolating between the gas and condensed phases has been the use of *ab initio* quantum chemistry techniques. The advances in

computer technology have allowed for the accurate computation of electrostatic properties of polyatomic ions. These properties can then be used to model the effect of solvation. Alternatively, the evolution in ion properties with solvation can be studied explicitly, as one or more solvent molecules are added to an ion, and its properties calculated. Thus, extrapolation to the condensed phase can be explored by *ab initio* calculations in a way conceptually analogous to the infrared spectroscopy of mass-selected ionic clusters.

This thesis discusses studies of ions and ionic clusters by mass spectrometry, infrared spectroscopy, and *ab initio* calculations. Throughout, we will emphasize the interactions between experiment and theory.

We begin in Chapter 2 with the question of ozone depletion in the Antarctic stratosphere. As chemical physicists, our inclination was to consider the possible roles of ions in driving the activation of chlorine reservoir species on polar stratospheric clouds. Kevin Crellin and Bernd-Michael Haas used Fourier-transform ion cyclotron resonance mass spectrometry to study the reaction of chloride ion with chlorine nitrate. Chapter 2 focuses on *ab initio* calculations done in conjunction with the experimental work to understand the potential energy surface for this reaction, and to enable us to extrapolate our gas-phase results to the condensed phase context of polar stratospheric clouds.

In Chapter 3, we turn our attention to the ion chemistry of the ionosphere. Jong-Ho Choi and other workers used vibrational predissociation spectroscopy to study in detail the chemistry of nitrosonium ion as a function of the number of water molecules. Their experiment demonstrated the power of ionic clusters as models of reactions in the atmosphere. Chapter 3 will discuss the *ab initio* calculations we performed to help

interpret the infrared spectra of smaller $NO^+(H_2O)_n$ clusters. We also present calculations on $I^-(H_2O)$, the spectroscopy of which we performed with Matthew Johnson and Chi-Kin Wong. The points of agreement and disagreement between experiment and theory for these systems reveal subtleties about both approaches.

The reactivity study in Chapter 2 raises the more fundamental question of the solvation of Cl^- ion in polar stratospheric clouds, and in other mesoscopic systems. A large body of computational work suggested that Cl^- ion would be incompletely solvated even in large gas-phase water clusters, but there was no direct experimental evidence for such structures. In Chapter 4 we report infrared spectroscopy done with Jong-Ho Choi to probe solvation within the clusters $Cl^-(H_2O)_n$, n = 1-7. Questions about the vibrational spectrum of the $Cl^-(H_2O)$ monohydrate motivated a study of the related system $Cl^-(H_2O)(CCl_4)$. Our experimental work was supplemented by *ab initio* studies on the smaller chloride clusters. Discrepancies between experiment and theory in part challenged the accuracy of early experimental reports, and in part revealed the inadequacy of static quantum chemical treatments of ionic cluster structure.

In Chapter 5, we continue our exploration of Cl^- ion solvation by reporting preliminary spectra of chloride-ammonia clusters, $Cl^-(H_2O)_n$, n = 1-5. This is ongoing work being continued by Julio Lobo. We also present *ab initio* calculations for some of the possible structural isomers of these systems. The data to date reveal a simple picture of ion solvation, but further spectroscopic and computational work could reveal a great deal more.

CHAPTER 2

An *Ab Initio* Study of the Activation of Chlorine Nitrate by Chloride and Its Implications for the Stratosphere

2.1 INTRODUCTION

Measurements of trace constituents in the stratosphere[1] indicate that the reaction

$$ClONO_2 + HCl \rightarrow Cl_2 + HNO_3 \qquad (1)$$

is crucial for converting the chlorine reservoir species $ClONO_2$ and HCl into photochemically labile Cl_2 in the Antarctic stratosphere. While (1) is extremely slow in the gas phase ($k < 1.5 \times 10^{-19}$ $cm^3 molecule^{-1} s^{-1}$),[2] a number of kinetics studies[3,4,5,6] have established the facility of the reaction on the surface of polar stratospheric clouds (PSCs).

Although the kinetics studies, done on laboratory models of PSCs, have established the overall stoichiometry of the above reaction, its fundamental mechanism is not completely established. It has been suggested that (1) takes part in two steps:

$$ClONO_2 + H_2O \rightarrow HOCl + HNO_3 \qquad (2)$$

$$HOCl + HCl \rightarrow Cl_2 + H_2O \qquad (3)$$

Reactions (2) and (3) have also been found to be rapid on model PSCs. The isotopic studies of Hanson[7] and the very recent computations of Bianco and Hynes[8] provide evidence that (2) proceeds by a direct reaction of chlorine nitrate and water, with homolytic cleavage of the Cl-O bond.

This does not preclude ionic pathways, however, for the overall transformation of (1).[9,10] This is consistent with experiments[11] and dynamics calculations[12] which suggest that HCl may chemisorb dissociatively on PSC aerosols under typical stratospheric conditions.

Molina and co-workers[9] suggested that (1) occurs by proton catalysis:

$$H^+ + ClONO_2 \rightarrow HONO_2\text{--}Cl^+ \qquad (2)$$

The putative intermediate $HONO_2$--Cl^+ would expel Cl^+ as a leaving group, which would in turn combine with Cl^- and leave the PSC surface as Cl_2.

A mass spectrometry experiment by Nelson and Okumura[13] suggested a different picture of proton catalysis. They found that when $ClONO_2$ is allowed to react with

protonated water clusters ($H_3O^+(H_2O)_n$) ($<n> \approx 14$) at large collision energies, the major product is NO_2^+. They proposed that H^+ activates $ClONO_2$ as follows:

$$H^+ + ClONO_2 \rightarrow HOCl—NO_2^+ \rightarrow HOCl + NO_2^+ \quad (3)$$

Further support for this mechanism came from the extensive *ab initio* computations of Lee and Rice,[14] who predicted that HOCl--NO_2^+ is the most stable isomer of protonated chlorine nitrate. The binding energy (0 K) was estimated to be 12.9 ± 2.0 kcal/mol, using the CCSD(T) level of theory with large atomic natural orbital basis sets. The recent vibrational spectroscopic work of Okumura and co-workers[15] has provided direct evidence for the HOCl--NO_2^+ intermediate.

However, the relevance of HOCl--NO_2^+ to the heterogeneous chemistry of the stratosphere has been questioned by other experimental studies. In a selected-ion flow tube study, van Doren *et al.*[16] found NO_2^+ to be only a minor product of the reaction of H_3O^+ and $ClONO_2$; $H_3O^+(H_2O)_n$ (n = 1-3) did not react with $ClONO_2$ at all. Using Fourier-transform ion-cyclotron resonance (FT-ICR) mass spectrometry, Schindler *et al.*[17] found that the dominant product of the reaction of $H_3O^+(H_2O)_n$ ($<n> \approx 18$) with $ClONO_2$ was $H_3O^+(H_2O)_m(HNO_3)$. The mechanism proposed was a direct reaction of H_2O with $ClONO_2$, although proton transfer from a H_3O^+ was believed to assist this reaction. Proton catalysis is therefore believed to be relevant to PSC chemistry, but not through a HOCl--NO_2^+ intermediate.

In this chapter we would like to explore the existence of another ionic mechanism for reaction (1) on PSCs. It is possible that chlorine nitrate is activated by the direct reaction of chloride. The following are plausible reaction pathways:

$$Cl^- + ClONO_2 \rightarrow Cl_2 + NO_3^- \quad (4)$$

$$Cl^- + ClONO_2 \rightarrow Cl_2O + NO_2^- \quad (5)$$

$$Cl^- + ClONO_2 \rightarrow Cl_2O^- + NO_2^- \quad (6)$$

$$Cl^- + ClONO_2 \rightarrow ClO^- + ClNO_2 \quad (7)$$

From gas-phase thermochemical data[18] we know that reaction (4) is exothermic by -24.6 kcal/mol. Reactions (5), (6) and (7) are endothermic by ~22, ≥ 30, and ~25 kcal/mol, respectively.

We can expect that the exothermic pathway, reaction (4), proceeds with little barrier in the gas phase. The second-order rate constant of a similar exothermic ion-molecule reaction,

$$Cl^- + N_2O_5 \rightarrow ClNO_2 + NO_3^-, \qquad (8)$$

was measured by Davidson *et al.*[19] to be 9.4×10^{-10} $cm^3molecule^{-1}s^{-1}$, that is, almost at the collision limit.

In order to study the direct reaction of chloride with chlorine nitrate, we have performed *ab initio* calculations on various intermediates $Cl_2NO_3^-$ for reactions (4)-(7). In analogy to the work of Lee and Rice, we anticipated the existence of a stable, weakly bound complex, Cl_2--NO_3^-. Our computational results, which are consistent with a FT-ICR measurement of the rate constant,[20] will show that (4) is quite facile in the gas phase. We will then discuss how to extend our gas-phase results to an understanding of the heterogeneous processes taking place on PSCs.

2.2 COMPUTATIONAL METHODS

We explored sections of the Cl^- + $ClONO_2$ potential energy surface in the vicinity of plausible reactive intermediates (Figures 1-3), $Cl_2(NO_3)^-$, $Cl(NO_3Cl)^-$, and $Cl_2O(NO_2)^-$, for pathways (4)-(7). Most calculations were performed on a Cray Y-MP using the Gaussian 92 system of programs,[21] with some preliminary work done on a Hewlett-Packard 9000 using Gaussian 90.[22]

The geometries of these complexes were optimized using analytical gradients at the Hartree-Fock (HF)[23] and the second-order Møller-Plesset (MP2)[24] levels of theory. Some treatment of dynamic electron correlation, as is afforded by the MP2 method, is

necessary for even a qualitative determination of the geometry of weakly bound complexes.

The optimized structures were then characterized as minima, transition states, or higher-order stationary points by calculating harmonic vibrational frequencies. Most frequencies were obtained using analytical second derivatives, but some MP2 frequencies were obtained by numerical differentiation of the analytical gradients.

A variety of basis sets was used in the calculation of equilibrium geometries and vibrational frequencies. The smallest was the 6-31G(*d*) basis set of Pople and co-workers,[25] and is designated DZP. The next basis set, designated TZ+P, was constructed as follows: The *sp* basis functions for O and N were taken from the 6-311G basis of Pople and co-workers.[26] The *sp* basis functions for Cl were taken from the [12*s*9*p*/6*s*5*p*] contraction of McLean and Chandler.[27] A set of five *d* polarization functions was added to each atom: the 3*d* exponents for O and N were 1.292 and 0.913, and the 3*d* exponent for Cl was 0.750.[27] A set of diffuse *sp* functions, determined by Clark *et al.*[28] was also added to each atom.

Lee and Schaefer[29] have shown that a number of diffuse *s* and *p* basis functions are necessary to describe accurately the charge distribution of an anionic system, at least at the self-consistent field level. Therefore, the TZ+P basis set was expanded by an additional set of *sp* functions on each atom, giving rise to a basis designated as TZ2+P. The exponents (α_s =0.0143 and α_p =0.0176 for Cl, α_{sp}=0.0259 for O, α_{sp} =0.0195 for N) were obtained following the procedure of Lee and Schaefer.[29]

Jankowski *et al.*[30] have shown that the equilibrium geometry and energy of a molecule are equally improved by adding a second set of *d* polarization functions and by adding a first set of *f* polarization functions. Another basis set, TZ+2Pf, was thus constructed by adding to the 6-311+G basis the following functions determined by Frisch *et al.*:[31] two sets of five *d* functions (α_d = 1.5000 and 0.3750 for Cl, α_d = 2.5840 and

0.6460 for O, α_d =1.8260 and 0.4565 for N) and a set of seven *f* functions (α_f =0.700 for Cl, α_f =1.400 for O, α_f =1.000 for N).

The DZP, TZ+P, TZ2+P, and TZ+2Pf basis sets were used in HF geometry optimizations. The DZP, TZ+P, and TZ2+P basis sets were used in the MP2 geometry optimizations. For MP2 calculations, all electrons were correlated at the DZP level, and core electrons were frozen for the larger basis sets (except for a TZ+P calculation of the fragments listed below).

To estimate the binding energies of the $Cl_2NO_3^-$ intermediates, we also calculated HF and MP2 equilibrium geometries and vibrational frequencies for Cl^-, Cl_2, NO_3^-, and $ClONO_2$. The same basis sets were used for the fragments as for the $Cl_2NO_3^-$ complexes.

To obtain more accurate estimates of the binding energy of Cl_2--NO_3^-, we performed single point calculations using the coupled-cluster method including all single and double excitations (CCSD).[32] All CCSD calculations neglected the contribution of excitation of core electrons. The CCSD energies of Cl_2--NO_3^-, Cl^-, Cl_2, NO_3^-, and $ClONO_2$ were determined at various MP2-optimized geometries. In addition, the standard 6-31+G(*d*) (DZ+P) basis,[25,28] which was not used in the geometry optimizations, was used for the CCSD calculations.

It should be noted that the HF, MP2, and CCSD methods are all size-consistent, meaning that ΔE_e may be calculated rigorously as the difference of the electronic energy of the complex and the electronic energies of the corresponding fragments.

We anticipated that the binding energy of the Cl_2--NO_3^- complex would be overestimated at the MP2 and CCSD levels of theory due to the incompleteness of the basis sets. To compensate for this basis set superposition error (BSSE), the well-established counterpoise correction[33] was employed. At a given level of theory and basis set, the energy of every given monomer (Cl^-, $ClONO_2$, Cl_2, and NO_3^-) was

recomputed as follows: Basis functions of the monomer were placed at the optimized geometry of that monomer; basis functions for the other atoms were placed at the optimized geometry of the Cl_2--NO_3^- complex. The nuclear charges of the other atoms were set to zero.

Finally, we were interested in the partial charges of the species in reaction (4). Reed *et al.*[34] have noted that the conventional Mulliken analysis of the self-consistent-field (SCF) density matrix gives partial charges that often are not consistent with the observable physical properties of a system. We therefore obtained partial charges of Cl_2--NO_3^-, NO_3^-, and $ClONO_2$ from a more accurate natural population analysis of the MP2 density matrices of the MP2/TZ2+P wave functions. For the sake of comparison, we performed a Mulliken analysis of the SCF density for the same wave functions.

2.3 RESULTS AND DISCUSSION

A. $Cl_2NO_3^-$ Isomers. Three $Cl_2NO_3^-$ stationary points (Figure 1) were identified in the calculations. Table 1 gives their relative stabilities. The optimized geometries and vibrational frequencies of $Cl_2O(NO_2)^-$ (Figure 1), which has C_{2v} symmetry, are reported in Tables 2 and 3; those of $Cl(NO_3Cl)^-$ are reported in Tables 4 and 5. The isomer $Cl_2O(NO_2)^-$ has one imaginary frequency (at the HF level), the Cl-O antisymmetric stretch (Table 3). We note a difference of almost 40 kcal/mol in the HF and MP2 results. It is well known[35] that the heights of transition states are grossly overestimated by the HF method. However, even with the MP2 value, $Cl_2O(NO_2)^-$ is predicted to be 21.5 kcal/mol less stable than the ground state isomer, and is therefore probably not relevant to stratospheric chemistry.

Another stable isomer of $Cl_2NO_3^-$, $Cl(NO_3Cl)^-$ (Figure 2), is predicted to be a true minimum of the potential energy surface at both the HF and MP2 levels (Table 5).

We would expect significant binding of Cl^- to the N site of $ClONO_2$, since the partial charge on the N of $ClONO_2$ (see Table 16) is +0.66. However, since $Cl(NO_3Cl)^-$ is over 20 kcal/mol less stable than the ground state $Cl_2NO_3^-$ isomer, we can assume that its role in the stratosphere will also be minor.

All levels of theory indicate that, unlike $Cl_2O(NO_2)^-$ and $Cl(NO_3Cl)^-$, the $Cl_2(NO_3)^-$ complex is a weakly bound intermediate, Cl_2--NO_3^-, whose constituents resemble the final products of the reaction of Cl^- and $ClONO_2$. The region of the potential energy surface in the vicinity of the Cl_2--NO_3^- minimum was explored (at the HF level) with the following results: Chloride ion approaches the Cl atom of $ClONO_2$, slightly *trans* to the N, without any barrier. Based upon the orientation of the electric dipole of $ClONO_2$, the Cl^- would be expected to approach the Cl-O bond making an angle of 158°. However, at a Cl--Cl separation of ~3 Å, the angle of approach is actually ~176°. When we optimized only the Cl--Cl and Cl-O bond lengths, we found chloride to be weakly bound (r(Cl-Cl) ≅ 2.7 Å) to chlorine nitrate. Optimizing all the bond lengths and angles, however, resulted in a great reorganization in the structure of the complex, as discussed below. As noted above, the absence of a barrier in the formation of the intermediate Cl_2--NO_3^- is consistent with the FT-ICR kinetics study by Haas *et al.*[20] The reaction rate of chloride ions with chlorine nitrate was determined to be $k = (9.2 \pm 3.0) \times 10^{-10}$ cm^3s^{-1} (298 K), close to the ion-dipole collision limit.

B. The Structure of Cl_2--NO_3^-. The MP2-optimized geometry of $Cl_2(NO_3)^-$ (Table 8) shows that $ClONO_2$ (Table 9) is greatly perturbed by the binding of chloride ion. With the largest basis set, the Cl-O bond in $ClONO_2$ is lengthened by 0.44 Å. On the other hand, the Cl-Cl bond formed in the complex is only 0.17 Å longer than that of molecular chlorine. Also, the three N-O bond lengths in $Cl_2(NO_3)^-$ are no more that 0.04 Å different from the N-O bond lengths in free nitrate ion. Moreover, each of the three ONO bond angles in the complex is within 3° of 120°. We can conclude, then, that the

binding of chloride to chlorine nitrate results in a complex of molecular chlorine and nitrate, Cl_2--NO_3^-.

The HF results (Tables 6 and 7) give roughly the same picture of the Cl_2--NO_3^- intermediate, but the Cl—Cl and Cl—O bond lengths predicted are very different. The Cl-O bond in $ClONO_2$ is lengthened by almost 1 Å in the complex. This reflects a gross underestimate of the binding between the incipient Cl_2 and NO_3^- moieties in the intermediate (see below), which is typical for HF theory. This is also reflected in the optimized geometries of the $Cl(NO_3Cl)^-$ intermediate (Table 4). The intermolecular Cl—N bond is predicted to be more than 0.3 Å at the HF level than at the MP2 level. Table 8 shows the importance of having sufficient valence *s* and *p* functions in the basis set. The intermolecular Cl···O bond is predicted to be 0.12 Å longer with the TZ+P basis than with the DZP basis. Also, the Cl_2--NO_3^- complex is predicted to be planar at the MP2/DZP level, as well as at the HF level (Table 7). However, with larger basis sets, MP2 theory predicts that Cl_2--NO_3^- will be very slightly twisted out of plane. (Since the system deviates from planarity by $\leq 0.1°$, it will be reasonable later to characterize the normal modes as if the system had C_s symmetry.)

However, further uncontraction of the *sp* basis set beyond TZ+P proved unnecessary in determining the equilibrium geometry. The second set of diffuse *sp* functions in the TZ2+P basis set gave virtually the same optimized geometries for all species considered. Also, a comparison of the two MP2/TZ+P results for Cl_2, NO_3^-, and $ClONO_2$ (Table 9) indicates that the correlation of core electrons has little effect on the optimized geometry.

Additional polarization functions, however, would undoubtedly change the MP2 prediction of the system's geometry. The effect of adding more *d* and *f* functions to the basis can be see even at the HF level (Tables 10 and 11), especially on those geometrical parameters involving Cl atoms. We would expect the effect to be even more dramatic at

the MP2 level, for which several sets of polarization functions are required to saturate the space, as noted by Jankowski *et al.*[30] Unfortunately, the limitations of our computational resources made MP2 calculations on Cl_2--NO_3^- with basis sets larger than TZ2+P impossible with the computing resources available.

We can estimate the reliability of our results for Cl_2--NO_3^- by comparing our geometries for Cl_2 and $ClONO_2$ with the experimental values[36] in Table 9. The most serious discrepancy between theory and experiment is in the value of $r(N\text{-}O_1)$. Our overestimate of the $N\text{-}O_1$ bond length arises from the neglect of triple excitations in the second-order Møller-Plesset treatment, as Lee and Rice[14] note. This discrepancy should not prove crucial, however, in our calculation of the energetics of the chloride reaction. Our calculations indicate that shortening the $N\text{-}O_1$ bond to the experimental length of 1.499 Å increases the MP2/TZ2+P energy by only ~0.4 kcal/mol.

C. Vibrational Frequencies of Cl_2--NO_3^-. Harmonic vibrational frequencies and intensities of $Cl_2(NO_3)^-$ are listed in Tables 10 and 12. A comparison of the infrared spectrum of the intermediate, and those of the reactants and products (Tables 11 and 13), supports our picture of the complex as Cl_2--NO_3^-. At the highest level of theory (MP2/TZ2+P), the Cl-O stretch is dramatically red-shifted from 790 cm^{-1} in $ClONO_2$ to 181 cm^{-1} in the complex. On the other hand, the $N\text{-}O_1$ stretch, which is at 516 cm^{-1} in $ClONO_2$, is blue-shifted to 1361 cm^{-1} in Cl_2--NO_3^-, and becomes the most intense peak in the infrared spectrum. The position of this mode is in between the symmetric (1077 cm^{-1}) and antisymmetric (1495 cm^{-1}) N-O stretches in free NO_3^-. We see, then, that the attachment of chloride to chlorine nitrate has given rise to a distinct NO_3^- moiety. Nevertheless, the complex is bound fairly strongly; the Cl-Cl stretch in Cl_2--NO_3^-, at 312 cm^{-1}, is almost 250 cm^{-1} to the red of the Cl-Cl stretch in molecular chlorine.

Generally speaking, the MP2 vibrational frequencies of Cl_2--NO_3^- are well converged with respect to increasing the number of *sp* basis functions, as we saw above

for the calculated geometries. This is less the case, however, for the low frequency *A"* modes. Comparing the MP2 frequencies of $ClONO_2$ to the experimental fundamentals,[37] we see that the error varies with the type of mode, being worst for the N-O antisymmetric stretch and the O_1-N-O_3 bend. Also, two of the theoretical frequencies are misassigned. Significantly, the modes for which MP2 theory gives very inaccurate positions have HF harmonic frequencies (Table 10) which are actually lower than the MP2 harmonic frequencies. Typically, HF frequencies have larger anharmonic corrections. This indicates that the inaccuracy is not due solely to the neglect of anharmonic corrections to the *ab initio* values, but of inadequacies in the MP2 method. This seems to be especially true of modes involving the NO_3 moiety, which has considerable double-bond character. We would anticipate, however, that in using the *ab initio* frequencies to estimate ΔE_o, the errors in the frequencies of $ClONO_2$ and $Cl_2NO_3^-$ would mostly cancel.

D. Energetics of Cl_2--NO_3^-. It is useful to estimate thermodynamic quantities of the Cl_2--NO_3^- complex. We are specifically interested in the energy changes for the reactions

$$Cl^- + ClONO_2 \rightarrow Cl_2\text{--}NO_3^- \qquad (4a)$$

and

$$Cl_2\text{--}NO_3^- \rightarrow Cl_2 + NO_3^- \qquad (4b)$$

Sums and differences of the appropriate electronic energies give estimates of ΔE(4a) and ΔE(4b) at 0 K. The calculation of harmonic vibrational frequencies, discussed above, allows us to correct ΔE for the effects of zero-point vibrational energies, yielding ΔE_o(4a) and ΔE_o(4b). Assuming ideal-gas behavior, we can then use the standard equations of statistical thermodynamics to estimate ΔH_{298}(4a) and ΔH_{298}(4b), the enthalpy changes at room temperature. Moreover, since the sum of reactions (4a) and (4b) yields a reaction

$$Cl^- + ClONO_2 \rightarrow Cl_2 + NO_3^- \qquad (4)$$

whose experimental value of ΔH_{298} is known, we have a way to test the reliability of our *ab initio* thermodynamic quantities.

Table 14 reports the thermochemistry of (4a) and (4b) calculated at the HF, MP2, and CCSD levels. As noted before, CCSD calculations were performed using MP2-optimized geometries. This approximation should have little effect. Comparing the CCSD/DZ+P energies at two MP2 geometries, we find differences of no more than 0.1 kcal/mol.

The chloride affinity, $-\Delta E$(4a), is not strongly dependent on the level of theory. Although the affinity increases with expansion of the basis set at all three levels of theory, it is reasonably well converged to a range of 33-37 kcal/mol. The zero-point correction to the energy is also well converged and independent of the level of theory. At the highest level of theory, CCSD/TZ+P//MP2/TZ2+P, $-\Delta E_0$(4a) = 36.0 kcal/mol.

The binding energy of the intermediate, ΔE_0(4b), is far more strongly dependent on the level of theory, as we might expect for a weakly bound complex. Because the HF method cannot describe dispersion interactions explicitly, we would expect it to underestimate the magnitude of the binding energy. This expectation is borne out by the calculations. The HF value of ΔE_0(4b) is converged to 6.6 kcal/mol. The MP2 estimate of ΔE_0(4b) is 13-14 kcal/mol. The CCSD value of ΔE_0(4b) is 9.2 kcal/mol with the largest basis set used.

The binding energy of Cl_2--NO_3^- is also strongly dependent on the size of the basis set. At all levels of theory, the predicted value of ΔE_0(4b) is far larger for the smallest basis set (DZP) than for all others. With the CCSD calculations, adding a set of diffuse *sp* functions to the DZP basis decreased the binding energy by almost 6 kcal/mol.

At our highest level of theory, increasing the number of polarization functions should have a dramatic effect on both ΔE_0(4a) and ΔE_0(4b). In lieu of calculations with additional *d* and *f* functions, however, we report counterpoise corrections of the basis set

superposition error (BSSE) (Table 15). At the HF/TZ2+P level, the corrections are BSSE(4a) -0.8 kcal/mol and for ΔE_0(4b) is -0.6 kcal/mol. The small magnitude of the correction indicates that the basis set is nearly saturated at the Hartree-Fock level. However, the correlated (MP2 and CCSD) calculations dramatically reveal the inadequacies of the basis set, particularly in describing $ClONO_2$. Even at the highest level of theory, CCSD/TZ+P, the BSSE of (4a) is nearly –5 kcal/mol. The BSSE for (4b) is smaller, and better converged, to –3 kcal/mol. The large error associated with the DZP basis is consistent with recent work by Hu and Truhlar,[38] who note that the BSSE will be large especially when there are insufficient *s* and *p* functions in the basis set.

Using the (unscaled) harmonic frequencies to estimate enthalpy changes, our final 298 K predictions are ΔH_{298}(4a) = -30.6 kcal/mol and ΔH_{298}(4b) = 5.9 kcal/mol. The top of Figure 5 illustrates these gas-phase results.

Finally, we compare our *ab initio* values (Table 15) to experimental data. At our highest level of theory, we predict that ΔH_{298} for

$$Cl^- + ClONO_2 \rightarrow Cl_2 + NO_3^- \qquad (4)$$

is -24.6 kcal/mol, in exact (albeit fortuitous) agreement with the experimental value. As noted above, inaccuracies in the MP2-optimized geometries may lead to energy differences of ~0.5 kcal/mol.

E. Partial Charges of Cl_2--NO_3^-, NO_3^-, and $ClONO_2$. The results of the natural population analysis of the reactants, intermediate, and products of reaction (4) are listed in Table 16. The partial charges confirm our picture of the reaction intermediate as a weakly bound complex of molecular chlorine and nitrate ion. We see that about 70% of the negative charge on the reactant chloride has been transferred to nitrate in the intermediate.

In Table 17 we note, for comparison, the partial charges obtained from a Mulliken analysis of the SCF density. It is evident that they differ radically from the natural

population charges. The most dramatic discrepancy is in the nature of the nitrogen atom. According to the Mulliken analysis, N is the most negative site in $ClONO_2$ and Cl_2--NO_3^-; according to natural population analysis, N is the most positive site in these species. We have found that Cl^- binds to the N of $ClONO_2$, forming a stable complex. The long (~3.1 Å) separation between Cl^- and N (Table 4) suggests that the Cl--N bond is mostly electrostatic in nature. This is consistent with the large positive partial charge assigned to the N by natural population analysis. The Mulliken partial charges, on the other hand, are completely unreliable to characterize the current system.

F. Relevance to Heterogeneous Chemistry in the Stratosphere. We now consider how to apply our gas-phase *ab initio* results to an understanding of heterogeneous processes in the stratosphere. One question is the availability of chloride ions for reaction with chlorine nitrate on PSCs. The two main molecules competing with $ClONO_2$ for Cl^- ion on the surface of PSCs are H_2O and HNO_3. In the current work, we have found that the chloride affinity of chlorine nitrate is 31 kcal/mol. It is known experimentally[39] that in the gas phase, Cl^- binds to H_2O by (14.7 ± 0.3) kcal/mol. This suggests that chloride ion will react far more readily with $ClONO_2$ than associate with H_2O.

The magnitude of the chloride affinity of HNO_3 would be the sum of the overall exothermicity of the reaction $Cl^- + HNO_3 \rightarrow HCl + NO_3^-$, and the enthalpy of formation of the ion-dipole complex NO_3^---HCl. From standard thermochemical data,[18] it is known that ΔH_{298} = -9 kcal/mol for the overall reaction. While the binding enthalpy of NO_3^---HCl is not known, we can estimate it based on existing ion-molecule clustering data. Yamdagni and Kebarle[40] observed that in hydrogen-bonded complexes B^---HX, the strength of the hydrogen bond is linearly correlated to the acidity of HB. For X = Cl, a linear extrapolation of hydrogen bond enthalpies[41] *vs.* gas-phase acidities[18] suggests that the formation of NO_3^---HCl is exothermic by -19 kcal/mol. Hence, the Cl^- affinity of

HNO_3 is estimated to be 28 kcal/mol, roughly the same as that determined for $ClONO_2$. We anticipate, therefore, that if HCl is dissociatively ionized on PSCs, a significant fraction of the Cl^- will be free to activate adsorbed $ClONO_2$.

This is in contrast to the proton-catalyzed activation of $ClONO_2$, shown in reaction (3) above. Lee and Rice[14] have noted that since the gas-phase proton affinity of HNO_3 is higher than that of $ClONO_2$, chlorine nitrate should be less reactive on PSCs rich in nitric acid (neglecting the effect of adsorbed HCl). This prediction based only on gas-phase thermochemistry has been borne out in experiments with model PSCs.[4,42]

Another issue we may attempt to address is the extent of charge delocalization in the reactive intermediate. In a typical organic S_N2 reaction, the transition complex has its negative charge delocalized throughout the structure, meaning that in the solution phase, the intermediate will be solvated far more weakly than either the reactant or product anions. This gives rise to a significant barrier along the reaction coordinate, often slowing down the rate of a given solution-phase S_N2 reaction by many orders of magnitude compared to the gas phase.[43]

However, for our system, the extent to which charge is localized in Cl_2--NO_3^- (Table 16) suggests that this transition complex will be well solvated in the condensed phase. Some semi-quantitative estimate of the hydration enthalpy may be made by application of the Born model,[44,45] which asserts that the interaction energy between a charged sphere of radius r and a continuous dielectric medium of constant ε is given by

$$E = \frac{(ze)^2(1-1/\varepsilon)}{8\pi\varepsilon_o r}$$

The solvation energy should then vary as the square of the charge, $(ze)^2$. Representing the Cl_2--NO_3^- intermediate as the sum of charged spheres at the attacking Cl atom and the three O atoms, we estimate the solvation enthalpy thus:

$$\Delta H_{\text{hyd}} = \Delta H_{\text{hyd}}(\text{Cl}^-)\left(\frac{z(\text{Cl}_1)}{z_o(\text{Cl}_1)}\right)^2 + \Delta H_{\text{hyd}}(\text{NO}_3^-)\frac{1}{3}\sum_i\left(\frac{z(\text{O}_i)}{z_o(\text{O}_i)}\right)^2$$

with z and z_o representing the partial charges in the complex and in free Cl^- and NO_3^-, respectively. Although absolute values of the hydration enthalpy of ions are difficult to determine, reasonable estimates given by Marcus[45] are $\Delta H_{\text{hyd}}(Cl^-)$ = -90 kcal/mol and $\Delta H_{\text{hyd}}(NO_3^-)$ = -79 kcal/mol. The Born model predicts that in our intermediate, the hydration will be somewhat attenuated down to a value of $\Delta H_{\text{hyd}}(Cl_2NO_3^-)$ = -65 kcal/mol. However, as the bottom of Figure 5 illustrates, the predicted intermediate is solvated well enough not to give rise to a barrier even in solution. As far as the overall thermochemistry of the reaction, an early measurement[46] gives $\Delta H_{\text{hyd}}(Cl_2)$ = -6.5 kcal/mol, and an atmospheric modeling study estimates that $\Delta H_{\text{hyd}}(ClONO_2)$ = -15 kcal/mol. These data suggest that the overall activation of $ClONO_2$ by Cl^- ion will be slightly exothermic in solution.

2.4 CONCLUSION

Our calculations predicted that the reaction of Cl^- with chlorine nitrate is facile in the gas phase, which was confirmed by an ICR measurement of the rate constant. A detailed examination of the reaction coordinate revealed a weakly bound complex of molecular chlorine and nitrate ion. With the formation of this intermediate, the chloride affinity of $ClONO_2$ is predicted to be ~31 kcal/mol, which is larger than the chloride affinity either of H_2O or of HNO_3. Moreover, the extent of charge delocalization within the Cl_2--NO_3^- is small, and it is predicted not to give rise to a barrier even in solution. While the direct reaction of $ClONO_2$ with H_2O is now known to be facile, this negative

ion mechanism is also likely to be relevant in the heterogeneous chemistry of the Antarctic stratosphere.

2.5 REFERENCES AND NOTES

(1) Webster, C. R.; May, R. D.; Toohey, D. W.; Avallone, L. M.; Anderson, J. G.; Newman, P.; Lait, L.; Schoeberl, M. R.; Elkins, J. W.; Chan, K. R. *Science* **1993**, *261*, 1130.

(2) Atkinson, R.; Aschmann, S. M.; Tuazon, E. C.; Goodman, M. A.; Winer, A. M. *J. Atmos. Chem.* **1987**, *5*, 83.

(3) Tolbert, M. A.; Rossi, M. J.; Malhotra, R.; Golden, D. M. *Science* **1987**, *238*, 1258.

(4) Hanson, D. R.; Ravishankara, A. R. *J. Geophys. Res.* **1991**, *96*, 5081.

(5) Moore, S. B.; Keyser, L. F.; Leu, M. T.; Turco, R. P.; Smith, R. H. *Nature* **1990**, *345*, 333.

(6) Abbatt, J. P. D.; Molina, M. J. *J. Phys. Chem.* **1992**, *96*, 7674.

(7) Hanson, D. R. *J. Phys. Chem.* **1995**, *99*, 13059.

(8) Bianco, R.; Hynes, J. T. *J. Phys. Chem. A* **1998**, *102*, 309.

(9) Wofsy, S. C.; Molina, M. J.; Salawitch, R. J.; Fox, L. E.; McElroy, M. B. *J. Geophys. Res.* **1988**, *93*, 2442.

(10) Burley, J. D.; Johnson, H. S. *Geophys. Res. Let.* **1992**, *19*, 1359.

(11) Abbatt, J. P. D.; Beyer, K. D.; Fucaloro, A. F.; McMahon, J. R.; Wooldridge, P. J.; Zhang, R.; Molina, M. J. *J. Geophys. Res.* **1992**, *97*, 15819.

(12) Kroes, G.-J.; Clary, D. C. *J. Phys. Chem.* **1992**, *96*, 7079.

(13) Nelson, C. M.; Okumura, M. *J. Phys. Chem.* **1992**, *96*, 6112.

(14) Lee, T. J.; Rice, J. E. *J. Phys. Chem.* **1993**, *97*, 6637

(15) Choi, J.-H.; Kuwata, K. T.; Cao, Y.-B.; Haas, B.-M.; Okumura, M. *J. Phys. Chem. A* **1997**, *101*, 6753.

(16) van Doren, J. M.; Viggiano, A. A.; Morris, R. A. *J. Am. Chem. Soc.* **1994**, *116*, 6957.

(17) Schindler, T.; Berg, C.; Niedner-Schatteburg, G.; Bondybey, V. E. *J. Chem. Phys.* **1996**, *104*, 3998.

(18) (a) Lias, S. G.; Bartmess, J. E.; Liebman, J. F.; Holmes, J. L.; Levin, R. D.; Mallard, W. G. *J. Phys. Chem. Ref. Data* **1988**, *17*, Suppl. 1. (b) Atkinson, R.; Baulch, D. L.; Cox, R. A.; Hampson, R. F.; Kerr, J. A. *J. Phys. Chem. Ref. Data* **1992**, *21*, 1125.

(19) Davidson, J. A.; Viggiano, A. A.; Howard, C. J.; Dotan, I.; Fehsenfeld, F. C.; Albritton, D. L.; Ferguson, E. E. *J. Chem. Phys.* **1978**, *68*, 2085.

(20) Haas, B.-M.; Crellin, K. C.; Kuwata, K. T.; Okumura, M. *J. Phys. Chem.* **1994**, *98*, 6740.

(21) Frisch, M. J.; Trucks, G. W.; Head-Gordon, M.; Gill, P. M. W.; Wong, M. W.; Foresman, J. B.; Johnson, B. G.; Schlegel, H. B.; Robb, M. A.; Replogle, E. S.; Gomperts, R.; Andres, J. L.; Raghavachari, K.; Binkley, J. S.; Gonzalez, C.; Martin, R. L.; Fox, D. J.; Defrees, D. J.; Baker, J.; Stewart, J. J. P.; Pople, J. A. *Gaussian 92, Revision D.2.* Gaussian Inc., Pittsburgh, PA, 1992.

(22) Frisch, M. J.; Head-Gordon, M.; Trucks, G. W.; Foresman, J. B.; Schlegel, H. B.; Raghavachari, K.; Robb, M.; Binkley, J. S.; Gonzalez, C.; Defrees, D. J.; Fox, D. J.; Whiteside, R. A.; Seeger, R.; Melius, C.; Baker, J.; Martin, R. L.; Kahn, L. R.; Stewart, J. J. P.; Topiol, S.; Pople, J. A. *Gaussian 90, Revision J.* Gaussian Inc., Pittsburgh, PA, 1990.

(23) Roothaan, C. C. J. *Rev. Mod. Phys.* **1951**, *23*, 69.

(24) Møller, C.; Plesset, M. S. *Phys. Rev.* **1934**, *46*, 618.

(25) (a) Hehre, W. J.; Ditchfield, R.; Pople, J. A. *J. Chem. Phys.* **1972**, *56*, 2257. (b) Hariharan, P. C.; Pople, J. A. *Theor. Chem. Acta* **1973**, *28*, 213.

(26) Krishnan, R.; Binkley, J. S.; Seeger, R.; Pople, J. A. *J. Chem. Phys.* **1980**, *72*, 650.

(27) McLean, A. D.; Chandler, G. S. *J. Chem. Phys.* **1980**, *72*, 5639.

(28) Clark, T.; Chandrasekhar, J.; Spitznagel, G. W.; Schleyer, P. v. R. *J. Comput. Chem.* **1983**, *4*, 294.

(29) Lee, T. J.; Schaefer III, H. F. *J. Chem. Phys.* **1985**, *83*, 1784.

(30) Jankowski, K.; Becherer, R.; Scharf, P.; Schiffer, H.; Ahlrichs, R. *J. Chem. Phys.* **1985**, *82*, 1413.

(31) Frisch, M. J.; Pople, J. A.; Binkley, J. S. *J. Chem. Phys.* **1984**, *80*, 3265.

(32) Bartlett, R. J. *J. Phys. Chem.* **1989**, *93*, 1697.

(33) Liu, B.; McLean, A. D. *J. Chem. Phys.* **1973**, *59*, 4557.

(34) Reed, A. E.; Weinstock, R. B.; Weinhold, F. *J. Chem. Phys.* **1985**, *83*, 735.

(35) Wladkowski, B. D.; Lim, K. F.; Allen, W. D.; Brauman, J. I. *J. Am. Chem. Soc.* **1992**, *114*, 9136.

(36) (a) Edwards, H. G. M.; Good, E. A. M.; Long, D. A. *J. Chem. Soc. Faraday Trans. II* **1975**, 927. (b) Casper, B.; Lambotte, P.; Minkwitz, R.; Oberhammer, H. *J. Phys. Chem.* **1993**, *97*, 9992.

(37) (a) Huber, K. P.; Herzberg, G. *Molecular Spectra and Molecular Structure. IV. Constants of Diatomic Molecules*; Van Nostrand Reinhold: New York, 1977. (b) Miller, R. H.; Bernitt, D. L.; Hisatsune, I. C. *Spectrochim. Acta* **1967**, 23A, 223.

(38) Hu, W.-P.; Truhlar, D. G. *J. Phys. Chem.* **1994**, *98*, 1049.

(39) Zhao, X. G.; Gonzalez-Lafont, A.; Truhlar, D. G.; Steckler, R. *J. Chem. Phys.* **1991**, *94*, 5544, and references therein.

(40) Yamdagni, R.; Kebarle, P. *J. Am. Chem. Soc.* **1971**, *93*, 7139.

(41) Keesee, R. G.; Castleman, A. W., Jr. *J. Phys. Chem. Ref. Data* **1986**, *15*, 1011.

(42) Leu, M.-T.; Moore, S. B.; Keyser, L. F. *J. Phys. Chem.* **1991**, *95*, 7763.

(43) Olmstead, W. N.; Brauman, J. I. *J. Am. Chem. Soc.* **1977**, *99*, 4219.

(44) Born, M. *Z. Phys.* **1920**, *21*, 45.

(45) Marcus, Y. *Ion* Solvation; John Wiley and Sons Ltd.: Chichester, 1985.

(46) Wartenberg, H. V.; Werth, H. *Z. Phys. Chem.* **1930**, *151*, 109.

TABLE 1: Relative Energetics[a] of $Cl_2NO_3^-$ Isomers

Isomer	HF/TZ+P	MP2/TZ+P
$Cl_2(NO_3)^-$	0.0	0.0
$Cl(NO_3Cl)^-$	+30.5	+23.2
$Cl_2O(NO_2)^-$ [b]	+59.6	+21.5

[a] Energies in kcal/mol

[b] A transition state (one imaginary frequency) at the HF level. Vibrational frequencies were not computed at the MP2 level.

TABLE 2: Optimized Geometries of $Cl_2O(NO_2)^-$ with the TZ+P Basis Set[a,b]

	HF	MP2
r(Cl-O_1)	2.134	2.178
r(O_1-N)	1.384	1.466
r(N-O_2)	1.171	1.212
θ(Cl-O_1-Cl)	97.2	96.1
θ(O_2-N-O_2)	115.8	115.9

[a] Bond lengths in Å; bond angles in deg.

[b] Atoms are labeled as in Figure 1.

TABLE 3: Harmonic Vibrational Frequencies and Infrared Intensities for $Cl_2O(NO_2)^-$ [a]

	Approx Description	HF/TZP
$\omega_1(A_1)$	NO_2 sym stretch	1552(321)
$\omega_2(A_1)$	NO_2 sym bend	1056(162)
$\omega_3(A_1)$	NO_2 sym bend	792(5)
$\omega_4(A_1)$	Cl_2O bend + NO_2 bend	290(0)
$\omega_5(A_1)$	Cl_2O sym bend	157(3)
$\omega_6(A_2)$	Cl_2O wag + NO_2 wag	135(0)
$\omega_7(B_1)$	NO_2 antisym stretch	1872(835)
$\omega_8(B_1)$	NO_2 antisym bend	688(1)
$\omega_9(B_1)$	Cl_2O--NO_2 bend	201(1)
$\omega_{10}(B_2)$	NO_3 umbrella	880(0)
$\omega_{11}(B_2)$	Cl_2O--NO_2 bend	215(5)
$\omega_{12}(B_2)$	Cl_2O antisym stretch	456*i*(2898)

[a] Frequencies in cm^{-1}; infrared intensities in km/mol.

TABLE 4: Optimized Geometries of $Cl(NO_3Cl)^-$ with the TZ+P Basis Set[a,b]

	HF	MP2
$r(Cl_1\text{-}O_1)$	1.663	1.694
$r(O_1\text{-}N)$	1.372	1.640
$r(N\text{-}O_2)$	1.166	1.180
$r(N\text{-}O_3)$	1.165	1.183
$r(N\text{-}Cl_2)$	3.390	3.065
$\theta(Cl_1\text{-}O_1\text{-}N)$	116.4	110.5
$\theta(O_1\text{-}N\text{-}O_2)$	118.4	115.4
$\theta(O_1\text{-}N\text{-}O_3)$	111.0	106.7
$\theta(O_1\text{-}N\text{-}Cl_2)$	89.0	99.4
$\tau(Cl_1\text{-}O_1\text{-}N\text{-}O_2)$	1.0	-12.0
$\tau(Cl_1\text{-}O_1\text{-}N\text{-}O_3)$	179.0	172.8
$\tau(Cl_1\text{-}O_1\text{-}N\text{-}Cl_2)$	89.0	78.7

[a] Bond lengths in Å; bond angles in deg.

[b] Atoms are labeled as in Figure 2.

TABLE 5: Harmonic Vibrational Frequencies and Infrared Intensities for $Cl(NO_3Cl)^-$ with the TZ+P Basis Set[a,b]

	Approx Description	HF	MP2
ω_1	O_2NO_3 antisym stretch	1903(732)	2039(207)
ω_2	O_2NO_3 sym stretch	1545(382)	1360(202)
ω_3	N-O_1 stretch	1073(239)	778(133)
ω_4	Cl-O stretch + O_2NO_3 bend	967(40)	758(36)
ω_5	O_1NO_2 bend	875(44)	599(28)
ω_6	O_2NO_3 bend	802(5)	492(40)
ω_7	Cannot be determined	551(3)	313(126)
ω_8	Cannot be determined	315(1)	230(0)
ω_9	Cannot be determined	155(0)	141(1)
ω_{10}	Cannot be determined	88(0)	118(32)
ω_{11}	NO_3 umbrella	78(24)	92(1)
ω_{12}	N--Cl stretch	51(4)	28(4)

[a] Frequencies in cm^{-1}; infrared intensities in km/mol.

[b] Atoms are labeled as in Figure 2.

TABLE 6: HF Geometries of Cl_2--NO_3^- with Various Basis Sets[a,b]

	DZP	TZ+P	TZ2+P	TZ+2Pf
$r(Cl_1\text{-}Cl_2)$	2.034	2.030	2.030	2.006
$r(Cl_2\text{-}O_1)$	2.511	2.588	2.588	2.631
$r(O_1\text{-}N)$	1.239	1.232	1.232	1.223
$r(N\text{-}O_2)$	1.218	1.216	1.216	1.215
$r(N\text{-}O_3)$	1.218	1.215	1.215	1.213
$\theta(Cl_1\text{-}Cl_2\text{-}O_1)$	174.9	174.7	174.7	174.8
$\theta(Cl_2\text{-}O_1\text{-}N)$	120.0	126.1	126.1	124.4
$\theta(O_1\text{-}N\text{-}O_2)$	119.8	119.6	119.6	119.6
$\theta(O_1\text{-}N\text{-}O_3)$	119.2	119.6	119.6	119.6
$\tau(Cl_1\text{-}Cl_2\text{-}O_1\text{-}N)$	180.0	180.0	180.0	180.0
$\tau(Cl_2\text{-}O_1\text{-}N\text{-}O_3)$	0.0	0.0	0.0	0.0
$\tau(Cl_2\text{-}O_1\text{-}N\text{-}O_3)$	180.0	180.0	180.0	180.0

[a] Bond lengths in Å; bond angles in deg.

[b] Atoms are labeled as in Figure 3.

TABLE 7: HF Geometries of Cl_2, NO_3^-, and $ClONO_2$ with Various Basis Sets[a,b]

	DZP	TZ+P	TZ2+P	TZ+2Pf
Cl_2				
r(Cl-Cl)	1.990	2.000	2.000	1.981
NO_3^-	1.226	1.222	1.222	1.220
r(N-O)				
$ClONO_2$				
r(Cl-O_1)	1.666	1.663	1.663	1.646
r(O_1-N)	1.372	1.372	1.372	1.369
r(N-O_2)	1.172	1.166	1.166	1.164
r(N-O_3)	1.172	1.165	1.165	1.164
θ(Cl-O_1-N)	115.8	116.4	116.4	116.0
θ(O_1-N-O_2)	118.6	118.4	118.4	118.4
θ(O_1-N-O_3)	110.7	111.0	111.0	111.0
τ(Cl-O_1-N-O_2)	0.0	0.0	0.0	0.0

[a] Bond lengths in Å; bond angles in deg.

[b] Atoms are labeled as in Figure 4.

TABLE 8: MP2 Geometries of Cl_2--NO_3^- with Various Basis Sets[a,b]

	DZP	TZ+P	TZ2+P
$r(Cl_1\text{-}Cl_2)$	2.288	2.192	2.194
$r(Cl_2\text{-}O_1)$	2.030	2.145	2.144
$r(O_1\text{-}N)$	1.329	1.302	1.302
$r(N\text{-}O_2)$	1.239	1.239	1.239
$r(N\text{-}O_3)$	1.247	1.244	1.244
$\theta(Cl_1\text{-}Cl_2\text{-}O_1)$	175.3	175.2	175.3
$\theta(Cl_2\text{-}O_1\text{-}N)$	115.4	118.4	118.2
$\theta(O_1\text{-}N\text{-}O_2)$	120.6	119.9	119.9
$\theta(O_1\text{-}N\text{-}O_3)$	114.8	116.9	116.9
$\tau(Cl_1\text{-}Cl_2\text{-}O_1\text{-}N)$	180.0	180.0	179.9
$\tau(Cl_2\text{-}O_1\text{-}N\text{-}O_3)$	0.0	0.1	0.1
$\tau(Cl_2\text{-}O_1\text{-}N\text{-}O_3)$	180.0	180.1	180.1

[a] Bond lengths in Å; bond angles in deg.

[b] Atoms are labeled as in Figure 3.

TABLE 9: MP2 Geometries of Cl_2, NO_3^-, and $ClONO_2$ with Various Basis Sets[a,d]

	DZP	TZ+P	TZ+P full[b]	TZ2+P	Exp[c]
Cl_2					
r (Cl-Cl)	2.015	2.024	2.024	2.024	1.988
NO_3^-					
r(N-O)	1.269	1.262	1.261	1.262	
$ClONO_2$					
r(Cl-O_1)	1.702	1.700	1.700	1.701	1.673
r(O_1-N)	1.547	1.557	1.557	1.557	1.499
r(N-O_2)	1.202	1.190	1.190	1.190	1.196
r(N-O_3)	1.206	1.192	1.192	1.192	1.196
θ(Cl-O_1-N)	111.1	112.0	111.8	111.8	113.0
θ(O_1-N-O_2)	117.3	116.9	116.8	116.8	118.6
θ(O_1-N-O_3)	107.7	107.7	107.8	107.8	108.8
τ(Cl-O_1-N-O_2)	0.0	0.0	0.0	0.0	0.0

[a] Bond lengths in Å; bond angles in deg.

[b] Core electrons were included in correlation.

[c] Cl_2 data from ref. 36a; $ClONO_2$ data from ref. 36b.

[d] Atoms are labeled as in Figure 4.

TABLE 10: HF Harmonic Vibrational Frequencies and Infrared Intensities for Cl_2--NO_3^- with Various Basis Sets[a,b]

	Approx Description	DZP	TZ+P	TZ2+P
$\omega_1(A')$	O_2NO_3 antisym stretch	1689(696)	1605(908)	1604(911)
$\omega_2(A')$	N-O_1 stretch	1609(1016)	1550(1109)	1550(1112)
$\omega_3(A')$	N-O sym stretch	1244(23)	1237(19)	1237(18)
$\omega_4(A')$	O_1NO_3 bend	804(6)	806(3)	804(0)
$\omega_5(A')$	O_2NO_3 bend	802(1)	805(0)	806(3)
$\omega_6(A')$	Cl-Cl stretch	505(132)	546(85)	548(83)
$\omega_7(A')$	Cl-Cl--O IP shear	147(6)	128(7)	128(9)
$\omega_8(A')$	Cl--O stretch	124(64)	106(39)	106(36)
$\omega_9(a')$	NO_3 rock	66(5)	47(4)	46(4)
$\omega_{10}(A'')$	NO_3 umbrella	978(47)	973(29)	971(30)
$\omega_{11}(A'')$	Cl-Cl--O OP shear	147(2)	123(2)	122(2)
$\omega_{12}(A'')$	NO_3 wag	33(0)	30(0)	31(0)

[a] Frequencies in cm^{-1}; infrared intensities in km/mol.

[b] Atoms are labeled as in Figure 3.

TABLE 11: HF Harmonic Vibrational Frequencies and Infrared Intensities for Cl_2, NO_3^-, and $ClONO_2$ with Various Basis Sets[a,b]

	Approx Description	DZP	TZ+P	TZ2+P
Cl_2				
$\omega(\sigma_g)$	Cl-Cl stretch	600(0)	604(0)	605(0)
NO_3^-				
$\omega_1(A_1')$	N-O sym stretch	1244(0)	1235(0)	1235(0)
$\omega_2(A_2'')$	NO_3 umbrella	984(50)	977(30)	976(31)
$\omega_3(E')$	N-O antisym stretch	1655(710)	1573(878)	1572(886)
$\omega_4(E')$	O-N-O bend	797(1)	801(0)	800(0)
$ClONO_2$				
$\omega_1(A')$	N-O antisym stretch	1952(647)	1912(789)	1912(789)
$\omega_2(A')$	N-O sym stretch	1558(380)	1539(393)	1539(392)
$\omega_3(A')$	O-N-O bend	1060(240)	1056(277)	1057(276)
$\omega_4(A')$	Cl-O St	962(55)	964(46)	964(46)
$\omega_5(A')$	N-O_1 stretch	790(3)	798(6)	799(5)
$\omega_6(A')$	O_1-N-O_3 bend	548(2)	547(3)	547(3)
$\omega_7(A')$	N-O-Cl IP bend	313(1)	312(1)	312(1)
$\omega_8(A'')$	NO_2 OP wag	882(34)	884(27)	882(27)
$\omega_9(A'')$	Cl-O_1-N-O_2 torsion	125(0)	122(0)	120(0)

[a] Frequencies in cm^{-1}; infrared intensities in km/mol.

[b] Atoms are labeled as in Figure 4.

TABLE 12: MP2 Harmonic Vibrational Frequencies and Infrared Intensities for Cl_2--NO_3^- with Various Basis Sets[a,b,c]

	Approx Description	DZP	TZ+P	TZ2+P
$\omega_1(A')$	O_2NO_3 antisym stretch	1726(182)	1623(335)	1622(336)
$\omega_2(A')$	N-O_1 stretch	1377(1250)	1364(1485)	1361(1490)
$\omega_3(A')$	N-O sym stretch	1034(285)	1059(191)	1058(192)
$\omega_4(A')$	O_1-N-O_3 bend	739(49)	746(35)	745(34)
$\omega_5(A')$	O_2-N-O_3 bend	713(3)	727(1)	726(1)
$\omega_6(a')$	Cl--Cl stretch	272(660)	312(244)	312(232)
$\omega_7(A')$	Cl-Cl--O IP shear	293(24)	240(166)	239(167)
$\omega_8(A')$	Cl--O stretch	236(19)	184(358)	181(374)
$\omega_9(A')$	NO_3 rock	99(3)	83(16)	82(16)
$\omega_{10}(A'')$	NO_3 umbrella	795(14)	796(5)	778(6)
$\omega_{11}(A'')$	Cl-Cl--O OP shear	221(1)	191(1)	175(1)
$\omega_{12}(A'')$	NO_3 wag	55(1)	20(0)	5(0)

[a] Frequencies in cm^{-1}; infrared intensities in km /mol.

[b] The equilibrium geometry of the complex is not perfectly planar with the TZ+P and TZ2+P basis sets; the symmetries of the normal modes are therefore only approximate.

[c] Atoms are labeled as in Figure 3.

TABLE 13: MP2 Harmonic Vibrational Frequencies and Infrared Intensities for Cl_2, NO_3^-, and $ClONO_2$ with Various Basis Sets[a,c]

	Approx Description	DZP	TZ+P	TZ2+P	Exp[b]
Cl_2					
$\omega(\sigma_g)$	Cl-Cl stretch	546(0)	547(0)	547(0)	560(0)
NO_3^-					
$\omega_1(A_1')$	N-O sym stretch	1082(0)	1078(0)	1077(0)	
$\omega_2(A_2'')$	NO_3 umbrella	838(19)	823(4)	811(5)	
$\omega_3(E')$	N-O antisym stretch	1582(466)	1498(654)	1495(668)	
$\omega_4(E')$	O-N-O bend	711(2)	720(0)	719(0)	
$ClONO_2$					
$\omega_1(A')$	N-O antisym stretch	1969(157)	1964(225)	1963(225)	1735(vs)
$\omega_2(A')$	N-O sym stretch	1324(220)	1321(235)	1321(234)	1292(vs)
$\omega_3(A')$	O-N-O bend	763(170)	767(107)	768(107)	809(s)
$\omega_4(A')$	Cl-O stretch	800(23)	790(87)	790(86)	780(ms)
$\omega_5(A')$	N-O_1 stretch	531(84)	516(81)	516(81)	560(s)
$\omega_6(A')$	O_1-N-O_3 bend	397(88)	374(141)	373(141)	434(m)
$\omega_7(A')$	N-O-Cl IP bend	252(0)	246(2)	248(2)	270(vvw)
$\omega_8(A'')$	NO_2 OP wag	697(10)	699(6)	688(7)	711(w)
$\omega_9(A'')$	Cl-O_1-N-O_2 torsion	130(1)	118(1)	113(1)	121(vvw)

[a] Frequencies in cm^{-1}; infrared intensities in km /mol.

[b] Cl_2 data from ref. 37a; $ClONO_2$ data from ref. 37b.

[c] Atoms are labeled as in Figure 4.

TABLE 14: Energetics[a] (0 K) of the Reactions $Cl^- + ClONO_2 \rightarrow Cl_2\text{--}NO_3^-$ (4a) and $Cl_2\text{--}NO_3^- \rightarrow Cl_2 + NO_3^-$ (4b)

Level of Theory	$-\Delta E$(4a)	$-\Delta E_0$(4a)	ΔE(4b)	ΔE_0(4b)
HF/DZP	34.3	34.4	9.3	8.7
HF/TZ+P	36.3	36.6	6.9	6.4
HF/TZ2+P	36.5	36.8	7.1	6.6
HF/TZ+2Pf	38.3		7.1	
MP2/DZP	33.1	32.1	21.8	21.0
MP2/TZ+P	33.5	32.7	13.8	13.2
MP2/TZ2+P	33.7	33.0	14.2	13.6
CCSD/DZP//MP2/TZ+P[b]	35.9	35.1	15.9	15.3
CCSD/DZ+P//MP2/TZ+P[b]	35.5	34.7	10.4	9.7
CCSD/DZ+P//MP2/TZ2+P[b]	35.5	34.8	10.3	9.7
CCSD/TZ+P//MP2/TZ2+P[b]	36.8	36.0	9.8	9.2

[a] Energies in kcal/mol.

[b] Indicates that a single-point CCSD energy is calculated at an MP2-optimized geometry. The zero-point corrections to the electronic energies are done with the corresponding MP2 harmonic frequencies.

TABLE 15: Basis Set Superposition Errors (BSSE) for the Reaction Energetics of $Cl^- + ClONO_2 \rightarrow Cl_2\text{--}NO_3^-$ (4a) and $Cl_2\text{--}NO_3^- \rightarrow Cl_2 + NO_3^-$ (4b), and the Overall Thermochemistry Predicted for $Cl^- + ClONO_2 \rightarrow Cl_2 + NO_3^-$ (ΔH_{298}(4)) [a]

Level of Theory	BSSE(4a)	BSSE(4b)	ΔH_{298}(4)
HF/TZ2+P	-0.6	-0.8	-29.7
MP2/TZ2+P	-4.9	-3.4	-17.4
CCSD/DZP//MP2/TZ+P[b]	-5.5	-5.3	-19.2
CCSD/DZ+P//MP2/TZ2+P[b]	-4.6	-3.0	-22.9
CCSD/TZ+P//MP2/TZ2+P[b]	-4.8	-3.1	-24.6

[a] Energies in kcal/mol.

[b] Indicates that a single-point CCSD energy is calculated at an MP2-optimized geometry. The zero-point corrections to the electronic energies are done with the corresponding MP2 harmonic frequencies.

TABLE 16: Natural Population Analysis (MP2 Density) Partial Charges of the Chemical Species in the Reaction $Cl^- + ClONO_2 \rightarrow Cl_2\text{--}NO_3^- \rightarrow Cl_2 + NO_3^-$[a]

	$Cl^- + ClONO_2$	$Cl_2\text{--}NO_3^-$	$Cl_2 + NO_3^-$
$z(Cl_1)$	-1	-0.29	0
$z(Cl_2)$	+0.25	+0.04	0
$z(O_1)$	-0.45	-0.49	-0.55
$z(O_2)$	-0.23	-0.45	-0.55
$z(O_3)$	-0.23	-0.47	-0.55
$z(N)$	+0.66	+0.66	+0.65

[a] Atoms are labeled as in Figure 3.

TABLE 17: Mulliken Partial Charges (SCF Density) of the Chemical Species in the Reaction $Cl^- + ClONO_2 \rightarrow Cl_2\text{--}NO_3^- \rightarrow Cl_2 + NO_3^-$[a]

	$Cl^- + ClONO_2$	$Cl_2\text{--}NO_3^-$	$Cl_2 + NO_3^-$
$z(Cl_1)$	-1	-0.22	0
$z(Cl_2)$	+0.05	-0.03	0
$z(O_1)$	+0.12	-0.13	-0.29
$z(O_2)$	+0.17	-0.11	-0.29
$z(O_3)$	+0.21	-0.08	-0.29
$z(N)$	-0.55	-0.43	-0.13

[a] Atoms are labeled as in Figure 3.

2.6 FIGURE CAPTIONS

Figure 1. MP2 geometry of the $(Cl_2O)(NO_2)^-$ isomer.

Figure 2. MP2 geometry of the $Cl(NO_3Cl)^-$ isomer.

Figure 3. MP2 geometry of the Cl_2--NO_3^- isomer.

Figure 4. MP2 geometry of $ClONO_2$.

Figure 5. Enthalpy diagram of the reaction coordinate of (4) in both the gas phase (top) and in the bulk aqueous phase (bottom.)

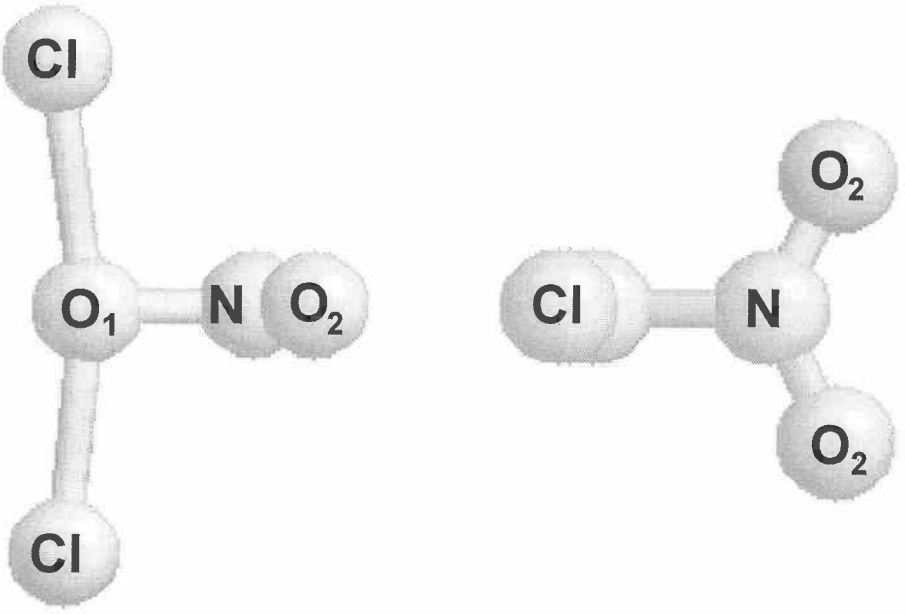

Figure 1

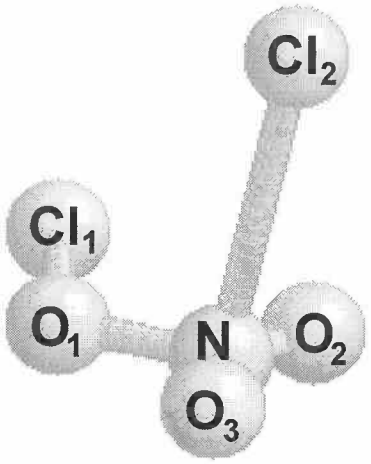

Figure 2

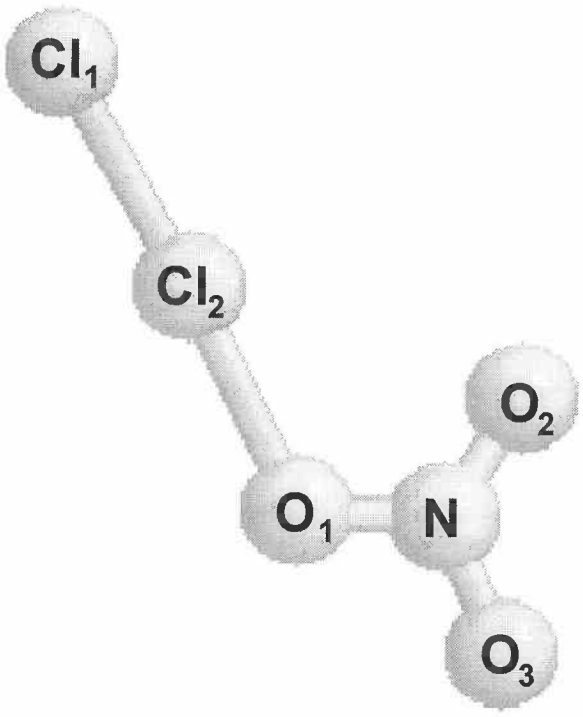

Figure 3

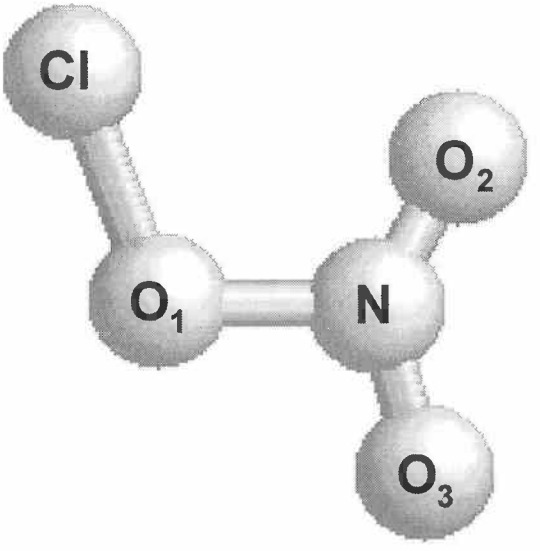

Figure 4

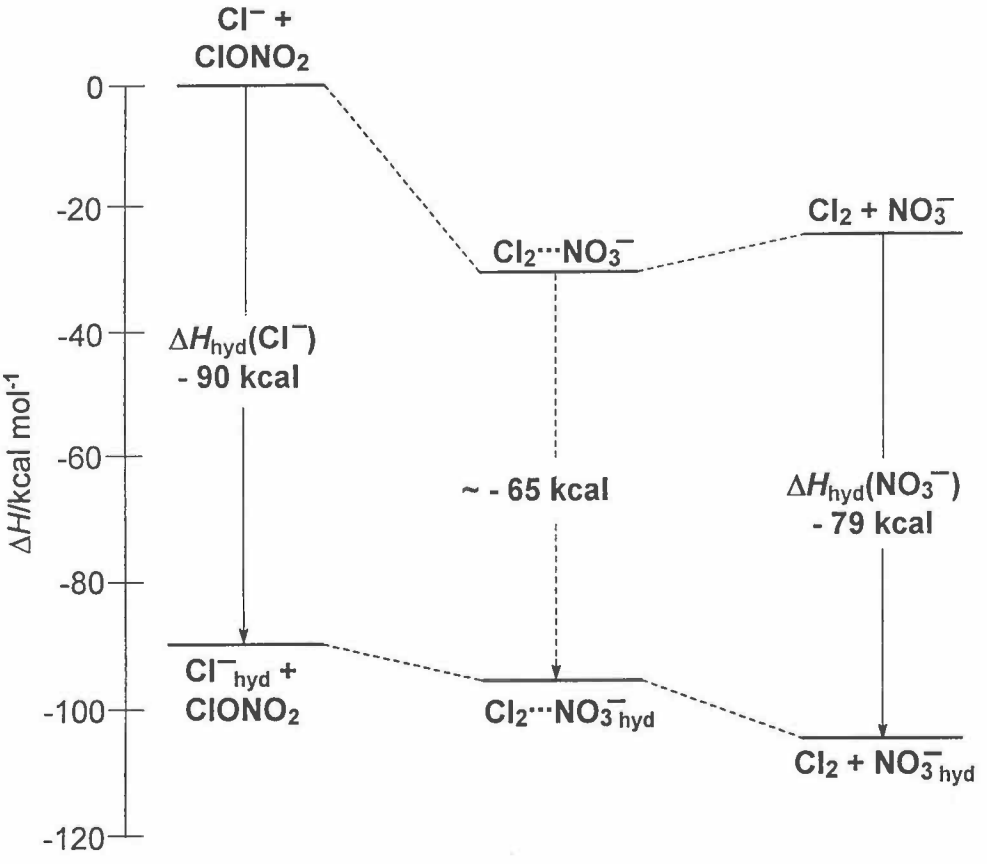
Cl⁻ +
ClONO2
0
-20
-40
-60
-80
-100
-120
ΔH/kcal mol-1
ΔHhyd(Cl⁻)
- 90 kcal
Cl2···NO3⁻
Cl2 + NO3⁻
~ - 65 kcal
ΔHhyd(NO3⁻)
- 79 kcal
Cl⁻hyd +
ClONO2
Cl2···NO3⁻hyd
Cl2 + NO3⁻hyd

Figure 5

CHAPTER 3

Computational Studies of Ion Solvation: The Systems $H_2NO_2^+$, $NO^+(H_2O)_2$, and $I^-(H_2O)$

3.1 INTRODUCTION

The solvation of ions in the gas phase involves a complex interplay of electrostatic and covalent bonding forces. Species and structures can exist in the gas phase that are not typically observed in bulk solution. However, the properties of these atypical species can enable us to provide detailed modeling of condensed phase behavior, and reveal the mechanistic details of chemical reactions under extreme conditions. Vibrational spectroscopy of gas-phase hydrates in our laboratory has revealed much along these lines, and further insight has come from our *ab initio* studies of these hydrates. In this chapter we will discuss computations performed to explore the hydration of nitrosonium cation (NO^+) and iodide anion (I^-). We will also discuss the application of our computation results to the experimental spectra obtained in our laboratory. The $NO^+(H_2O)_n$ and the $I^-(H_2O)_n$ systems typify the two lines of investigation we have pursued.

NO^+ and its hydrates play an important role in the ion chemistry of Earth's upper atmosphere.[1] Because of the low ionization potential of NO radical (9.25 eV),[2] it is readily ionized in the D-region of the ionosphere. However, measurements of the positive ion composition in the ionosphere[3] indicate that the D-region is dominated by the hydronium ion hydrates, $H_3O^+(H_2O)_n$, with the distribution peaked at $n = 1$. It is now known[4] that NO^+ undergoes a sequence of solvation steps to form a hydrated cluster ion, $NO^+(H_2O)_3$. This cluster subsequently reacts with another water molecule to form the hydrated hydronium ions:

$$NO^+(H_2O)_3 + H_2O \rightarrow H_3O^+(H_2O)_2 + HONO \qquad (1)$$

NO^+ is also known to exist in aqueous solution under conditions of high acidity (pH ≤ 1).[5] The nitrosonium ion is a key intermediate in the nitrosation reactions of organic compounds. Kinetics study suggest that protonated nitrous acid, $H_2NO_2^+$, is a weakly bound complex of NO^+ and H_2O (Figure 1a) in equilibrium with NO^+:

$$H^+ + HONO \leftrightarrow NO^+(H_2O) \leftrightarrow NO^+ + H_2O \qquad (2)$$

Both experimental and theoretical physical chemistry studies have explored the hydration chemistry of NO^+ and its relationship to HONO. Kebarle and co-workers[6] used pulsed high-pressure mass spectrometry to obtain hydration enthalpies of $\Delta H_{0,1} = -18.5 \pm 1.5$ kcal/mol for NO^+ and $\Delta H_{1,2} = -16.1 \pm 1.0$ kcal/mol for $NO^+(H_2O)$. Burdett and Hayhurst[7] found a similar value of $\Delta H_{0,1} = -19.3 \pm 2.4$ kcal/mol. There have been no direct probes, however, of the structure of these gas-phase clusters.

Several theoretical calculations[8,9,10] had examined the optimized geometries of $H_2NO_2^+$, although at the time this work described in this Chapter was published, no theoretical studies of the higher hydrates of NO^+ had been performed. The consensus was that the most stable form of $H_2NO_2^+$ is an ion-molecule complex between NO^+ and H_2O, rather than a purely covalently bound cation. The highest level calculations to date had been performed by de Petris *et al.*,[10] who predicted that protonated nitrous acid has six different isomers which are true minima on the potential energy hypersurface. For the lowest energy form, $NO^+(H_2O)$, they obtained an enthalpy of formation $\Delta H^\circ_f = 160 \pm 2$ kcal/mol, in very good agreement with the experimental value of 159.0 ± 1.5 kcal mol^{-1}.[2] They found that the next lowest energy isomers are formed by protonating either the nitrogen atom to form $HON(H)O^+$ (Figure 1b) or the terminal oxygen to form $N(OH)_2^+$

(Figure 1c). Neither isomer, both of which were calculated to be > 40 kcal/mol less stable than $NO^+(H_2O)$, has been observed experimentally.

The gas-phase hydration of halide ions will be discussed thoroughly in Chapter 4. For now, it suffices to say that while the sequential hydration of I^- does not drive chemistry, as it does for NO^+, interesting structural questions are nevertheless raised. The large polarizability of halide ions favors their asymmetric hydration in small clusters. This, in turn, provides the opportunity for water molecules to form strong hydrogen bonding networks. Halide ions end up incompletely solvated on the surface of a water cluster. A competition exists, then, between hydrogen bonding to the ion and hydrogen bonding to the solvent. Which force wins out likely depends on the number of water molecules. Solvation of I^- may be particularly poor, since its large 5*s* and 5*p* valence orbitals will overlap poorly with the 1*s* orbital of hydrogen. It is plausible that the hydration of iodide ion may depend largely on the electrostatic attraction between the charge on I^- and the water dipole.

In contrast, the solvation of NO^+ in water clusters should have significant covalent character. The $n = 2$ valence orbitals of N and O should overlap each other well. The structure of these clusters is determined by this fundamental chemical question: which is the most basic site? Previous work suggests that the internal O atom is the most basic site of free HONO in the gas phase. Yet gas-phase kinetics studies, and normal solution-phase chemistry, tells us that H_3O^+ is the only cation present in bulk water under most conditions.

Clearly the structure of $NO^+(H_2O)_n$, like that of $I^-(H_2O)_n$, will depend on *n*. The nature of the OH (and possibly NH) stretches, as revealed by infrared spectroscopy in the ~3 μm region, will be sensitive probes of the cluster structure. In cationic systems like $NO^+(H_2O)_n$, direct solvation of the ion will be effected by the O lone pairs in H_2O; the details of the solvation will be revealed by subtle perturbations of the OH stretches of water. In a sense, the 3 μm infrared spectra of solvated anionic clusters probe cluster structures more directly. Here, the OH groups are participating in the hydrogen bonding that defines the structure, and their stretch frequencies will be perturbed significantly.

Our laboratory has successfully used vibrational predissociation spectroscopy coupled with tandem mass spectrometry to probe both solvent-induced chemistry and surface solvation of ions.[11,12,13,14,15] In particular, this technique has been applied to the systems $NO^+(H_2O)_n$ (n = 1-5)[16] and $I^-(H_2O)$.[17] These experimental studies were accompanied by *ab initio* calculations of the vibrational spectra for the three major isomers of $H_2NO_2^+$ (Figure 1), the putative ground state isomer of $NO^+(H_2O)_2$ (Figure 2a), and the two major isomers of $I^-(H_2O)$ (Figure 4). This chapter will focus on our computational results, their relationship to other computational studies, and their relationship to the experimental spectra, which have been presented in previous theses.[18,19]

3.2 COMPUTATIONAL METHODS

Calculations were done using the Gaussian 92 system of programs[20] on a Cray Y-MP supercomputer. Optimized geometries and vibrational frequencies of $H_2NO_2^+$, $NO^+(H_2O)_2$, and $I^-(H_2O)$ were computed at the Hartree-Fock[21] (HF) and the second-

order Mϕller-Plesset[22] (MP2) levels of theory. The $NO^+(H_2O)_n$ MP2 calculations involved the correlation of all electrons; the $I^-(H_2O)$ MP2 calculations neglected the correlation of core electrons. The $NO^+(H_2O)_n$ vibrational frequencies were all calculated analytically. Because of the use of effective core potentials for I (see below), all $I^-(H_2O)$ vibrational frequencies were calculated numerically. $H_2NO_2^+$ and $NO^+(H_2O)_2$ geometries and frequencies are reported in Tables 2-9; $I^-(H_2O)$ geometries and frequencies are reported in Tables 15-18.

To predict the thermochemistry of protonated nitrous acid clusters more accurately, energies were computed at the coupled cluster with single and double excitations (CCSD) level of theory,[23] with the systems fixed at the MP2 optimized geometries. Because both the MP2 and CCSD levels of theory are size-consistent, binding energies may be calculated simply as the sum and difference of the appropriate electronic energies. Corrections for zero-point vibrational energy and for binding enthalpies (298.15 K) were made to the CCSD energies using the MP2-level vibrational frequencies. All CCSD calculations neglected the correlation of core electrons. The thermochemistry of the NO^+ hydrates is reported in Tables 10-12. Predictions of the thermochemistry of the $I^-(H_2O)$ isomers were made only at the HF and MP2 levels, as noted in Tables 19 and 20.

A variety of basis sets were employed for the two sets of calculations. The geometries and vibrational frequencies of $NO^+(H_2O)_n$ were all determined with the standard 6-31G** basis set of Pople and co-workers.[24] A first set of CCSD energies was also computed with 6-31G**. More accurate CCSD calculations were performed with

the 6-311G** and the 6-311G(2*df*, 2*pd*) basis sets,[25] the construction of which was discussed in Chapter 2. These bases provided more flexibility in both the valence and polarization spaces. Note that none of the basis sets used to describe protonated nitrous acid clusters included diffuse basis functions. These functions were deemed not to be necessary for the accuracy of the wave functions of cationic systems.

One set of diffuse *sp* functions, however, was necessary for an accurate description of the $I^-(H_2O)$ isomers. As discussed in Chapter 2, the standard functions developed by Clark *et al.*[26] were used. (The results of Chapter 2 indicated that an additional set of diffuse functions had little effect on the MP2 predictions and were thus not employed.) The 6-311++G** basis set was used for the H and O atoms in the system.

The basis set used to describe the iodine atom merits special discussion. It is possible to treat all 53 of iodine's electrons explicitly (in so-called all-electron calculations), but this is computationally burdensome. It is common to approximate the core electrons of atoms below the third row of the periodic table with numerical potentials whose eigenvectors (the so-called pseudo-orbitals) match the behavior of the all-electron valence orbitals. The analytic fits to the numeric potentials, called effective core potentials (ECPs), are readily corrected to account for relativistic effects. Thus, ECP calculations on heavy atoms can be as accurate as all-electron calculations on the same systems.

Our basis set for I was constructed following the work of Hu and Truhlar,[27] and Wadt and Hay.[28] The latter used three uncontracted Gaussians to describe each valence *s* electron (exponents α = 0.7242, 0.4653, 0.1336) and *p* electron (exponents α = 1.2900,

0.3180, 0.1053). To this Hu and Truhlar added a *d* polarization function (α = 0.262) and diffuse *s*, *p*, and *d* functions (α_s = 0.034, α_p = 0.039, α_d = 0.0873). The iodine ECP derived by Wadt and Hay involved functions of the form

$$\sum_k d_k r^{n_k} \exp(-\zeta_k r^2)$$

with parameters listed in Table 1.

In order to relate the *ab initio* frequencies to experimental values, we also computed the vibrational frequencies of H_2O and compared them with the experimental values of 3657 cm^{-1} (A_1) and 3756 cm^{-1} (B_2).[29] For $NO^+(H_2O)_n$, the MP2/6-31G** values of 3894 cm^{-1} (A_1) and 4032 cm^{-1} (B_2) led to a scaling factor of 0.935. Our scaled *ab initio* values are compared in Table 13 with experimental vibrational frequencies of $NO^+(H_2O)$ and $NO^+(H_2O)_2$ measured in our laboratory. For $I^-(H_2O)$, the MP2/6-311++G** values of 3885 cm^{-1} (A_1) and 4003 cm^{-1} (B_2) led to a scaling factor of 0.940. Table 21 compares our experimental values with our scaled *ab initio* predictions.

Finally, some idea of the nature of the bonding within these ionic clusters can be gleaned from the partial charges. Since we were not concerned with the condensed phase solvation of these ionic complexes (unlike in Chapter 2), a Mulliken population analysis of the self-consistent field density was deemed sufficient. The partial charges of $NO^+(H_2O)_n$ are reported in Table 14, the partial charges of $I^-(H_2O)$ in Table 22.

3.3 RESULTS AND DISCUSSION

A. *Ab Initio* Results on $H_2NO_2^+$ Isomers. Our *ab initio* calculations predicted that the ground state isomer of protonated nitrous acid is the ion-dipole complex of nitrosonium ion, NO^+, and water, formed by the protonation of the internal oxygen atom

of HONO. This agreed with previous *ab initio* studies. As shown in Figure 1a, the oxygen atom of the water binds to the nitrogen end of the cation, which carries ~70% of the charge (Table 14).

Table 2 shows that the geometries of the NO^+ and H_2O moieties do not differ significantly from those of free NO^+ and H_2O. The N···O separation (2.202 Å) is about twice as long as the $N{\equiv}O^+$ triple bond. The complex has a plane of symmetry bisecting the H_2O angle. However, unlike the ion-dipole complex $NO_2^+(H_2O)$ (as characterized by Lee and Rice[30]), the $NO^+(H_2O)$ lacks a rotational axis of symmetry. Instead, the intermolecular O=N···O bond angle is significantly bent at 100.2°; the water molecule is oriented with a lone pair pointed towards the N atom. This geometry probably reflects the fact that the lone pair electrons of the O atom of H_2O are donating density into the empty π^* orbitals of NO^+, which have significant *p* character on the N atom. This is consistent with the slight decrease in the positive partial charge on N, from +0.76 in free NO^+ to +0.71 in the $NO^+(H_2O)$ complex (Table 14).

While the Hartree-Fock N···O bond length is ~0.1 Å longer than the MP2 prediction (Table 2), the two levels of theory give the same qualitative structure. However, the HF description of $NO^+(H_2O)$ is inadequate in other ways, as discussed below. Although the same level of theory was supposedly used, our MP2/6-31G** optimized geometry of $NO^+(H_2O)$ differs slightly from that reported by De Petris *et al.*[10] In particular, we predict a slightly shorter N···O bond than the previous value of 2.204 Å.

Two other $H_2NO_2^+$ isomers, formed by protonation of the other basic sites of nitrous acid, were also characterized by our calculations. Protonation of the nitrogen

atom gave the planar C_s isomer $HON(H)O^+$, shown in Figure 1b. Protonation of the terminal oxygen atom gave the W-shaped C_{2v} isomer $N(OH)_2^+$, shown in Figure 1c. The HF and MP2 geometries (Tables 3 and 4) both indicate that $HON(H)O^+$ and $N(OH)_2^+$ are covalently bound cations. However, the HF and MP2 predictions of the NO bond lengths are notably different, particularly for the N-O_2 bond of $HON(H)O^+$. Both levels of theory may be expected to be inadequate in describing the double bond character of the N-O_2 interaction. As discussed for the $ClONO_2$ calculations in Chapter 2, inclusion of triple excitations is necessary for accurate predictions of the N-O_2 bond length. Our results are again consistent with, but not identical to, the earlier calculations of de Petris *et al.*[10]

All of the MP2 harmonic vibrational frequencies for $NO^+(H_2O)$, $N(OH)_2^+$, and $HON(H)O^+$ (Tables 6-8) were calculated to be real, confirming that the optimized structures in Figure 1 are all minima of the $H_2NO_2^+$ potential energy hypersurface. However, the HF calculations of $NO^+(H_2O)$ predicted one imaginary frequency corresponding to the twisting of the H atoms into the plane defined by the O=N···O bond angle. Early HF calculations by Nguyen and Hegarty[9] predicted such a planar $NO^+(H_2O)$ adduct to be the ground state $H_2NO_2^+$ structure, an idea later refuted by the MP2 calculations of de Petris *et al.*[10] This result underscores the importance of treating electron correlation explicitly to describe non-covalently bonding systems accurately.

We also note that the isomer $NO^+(H_2O)$ is predicted to have an infrared spectrum distinct from the other two $H_2NO_2^+$ isomers. The OH and NH stretches of $HON(H)O^+$ and $N(OH)_2^+$ will all lie to the red of ~3400 cm^{-1} (Tables 7 and 8, scaled by 0.935), while the water-like OH stretches of $NO^+(H_2O)$ should lie to the blue of ~3600 cm^{-1} (Table 13).

All our calculations predict that the two covalently bound $H_2NO_2^+$ isomers are more than 30 kcal/mol less stable than the ion-dipole adduct $NO^+(H_2O)$ (Table 10). However, the magnitudes of the relative stabilities vary dramatically. The difference in the relative stabilities of $N(OH)_2^+$ and $HON(H)O^+$ at the HF level, 8.5 kcal/mol, is far larger than any other prediction, and is probably grossly in error. At our highest level of theory, CCSD/6-311G(2*df*, 2*pd*), $N(OH)_2^+$ is predicted to be 33 kcal/mol less stable than $NO^+(H_2O)$, and $HON(H)O^+$ is 3 kcal/mol higher in energy. The small difference in the $N(OH)_2^+$ and $HON(H)O^+$ energies are consistent with the MP4/6-311G** predictions of de Petris *et al.*[10] However, the previously reported values, +41.5 kcal/mol for $N(OH)_2^+$ and +41.7 kcal/mol for $HON(H)O^+$, are over 25% higher. Quantitative predictions of the relative stability of these metastable isomers are clearly difficult to obtain. The uncertainty in even our high level *ab initio* predictions is at least 3 kcal/mol. We therefore cannot say definitively if $N(OH)_2^+$ or $HON(H)O^+$ is more stable. However, we can say for certain that the $H_2NO_2^+$ chemistry of the upper atmosphere will be dominated by $NO^+(H_2O)$, and that $N(OH)_2^+$ and $HON(H)O^+$ will be observed in the laboratory only under extreme conditions.

The $NO^+(H_2O)$ binding enthalpy is far more converged with respect to the level of theory (Table 11) than the relative stabilities of the $H_2NO_2^+$ isomers. As was seen for $Cl_2\cdots NO_3^-$ in Chapter 2, the highest level CCSD calculations predict binding energies intermediate between the HF and MP2 predictions. It is interesting to note that for all correlated calculations, ΔH_{298} values decrease with increasing levels of theory. Our

highest theoretical treatment, CCSD/6-311G(2*df*, 2*pd*), gave a value of ΔH_{298} = 20.9 kcal/mol.

B. Interpretation of the $H_2NO_2^+$ Vibrational Spectrum. In the vibrational predissociation experiment performed in this laboratory, the only photofragment ion detected upon infrared excitation of $H_2NO_2^+$ was NO^+, indicating that a single water molecule evaporated upon vibrational excitation.

The infrared spectrum of protonated nitrous acid exhibited a single vibrational band in the 2700-3800 cm^{-1} range (Figure 2a) centered at 3605 cm^{-1}. This band was only 50 cm^{-1} lower in frequency than the symmetric stretch of the water monomer. Closer examination revealed that the band was a doublet with maxima at 3599 cm^{-1} and 3611 cm^{-1}.

The experimental results on the n = 1 cluster confirmed the *ab initio* predictions that the most stable form of $H_2NO_2^+$ is the weakly bound ion-molecule complex, $NO^+(H_2O)$. The photochemistry observed is most easily explained by the breaking of the intermolecular bond. The frequency of the observed vibrational band, 3605 cm^{-1}, agrees within 1% of the scaled MP2 frequency of the H_2O symmetric stretch, 3571 cm^{-1} (Table 13). The previous experimental measurements[6,7] of the $H_2NO_2^+$ binding enthalpies, 18.5 ± 1.5 kcal/mol and 19.3 ± 2.4 kcal/mol, are in good agreement with the prediction of ΔH_{298} = 20.9 kcal/mol for the isomer $NO^+(H_2O)$.

The only discrepancy between the experimental results and the proposed structure is the absence of the antisymmetric stretch in the experimental spectrum, which is predicted to occur at 3686 cm^{-1} (scaled) with an intensity 80% of that of the symmetric

stretch (Table 13). The discrepancy cannot be accounted for by an alternative structure of $H_2NO_2^+$. The scaled OH symmetric and antisymmetric stretching frequencies of $N(OH)_2^+$, predicted at 3375 and 3350 cm^{-1} (Table 8), are more than 200 cm^{-1} below the observed transition. The spectrum of $HON(H)O^+$ would consist of two distinct bands (for the OH and NH stretches) split by ~200 cm^{-1}, and shifted 300-500 cm^{-1} to the red of the observed band (Table 7). Moreover, there is no experimental evidence for the production of these isomers with ion sources typically used in laboratory experiments.

The reason for the absence of an antisymmetric H_2O stretch absorption may lie in the fact that the experimental data are not absorption spectra, but rather two-photon dissociation spectra. It is plausible that the multiphoton absorption process is highly inefficient for ν_3 relative to ν_1 absorption. In the free H_2O monomer, the anharmonicity constants[31] are $x_{11} = -43$ cm^{-1}, $x_{13} = -155$ cm^{-1}, and $x_{33} = -46$ cm^{-1}. Thus, the $\nu_1 \rightarrow 2\nu_1$ and $\nu_3 \rightarrow 2\nu_3$ transitions are off resonance from the fundamentals by over ~170 cm^{-1}. However, the $\nu_1 \rightarrow \nu_1 + \nu_3$ transition is at 3600 cm^{-1}, which is reasonably close to the ν_1 frequency of 3657 cm^{-1}. Thus, two photon excitation of the symmetric stretch will be far more efficient because the second photon can excite the red-shifted antisymmetric stretch hot band transition. The $0 \rightarrow \nu_1 \rightarrow \nu_1 + \nu_3$ process is therefore a near-resonant two photon process. While the frequencies differ in the $n = 1$ cluster, this effect should still be qualitatively correct. Thus, two-photon dissociation was observed for ν_1, while the ν_3 band was too weak to be detected experimentally. The weakness of two photon ν_3 absorption is also consistent with the appearance of the antisymmetric stretch band in all larger hydrates of NO^+ and its increase in intensity with cluster size relative to the ν_1

band. An increasing fraction of these more weakly bound larger clusters will require only one photon to dissociate.

C. *Ab Initio* Calculations of $NO^+(H_2O)_2$. At the time the work described in this chapter was published, there had been no previous theoretical work on the $n = 2$ clusters. For our calculations, then, we assumed that the isomer of interest would be of the form $NO^+(H_2O)_2$, with both of the water ligands binding to the nitrogen atom of the NO^+, as in $n = 1$. We postulated the presence of at least C_s and perhaps C_{2v} symmetry. The putative structure was fully optimized under these symmetry constraints at both the HF and the MP2 levels. Due to the presence of several low frequency (< 200 cm^{-1}) modes, it was necessary to use stringent convergence criteria. The HF minimum was converged to a maximum force of 3×10^{-8} hartree/bohr and to a maximum displacement of 9×10^{-5} bohr. The MP2 minimum was converged to a maximum force of 7×10^{-8} hartree/bohr and to a maximum displacement of 4×10^{-6} bohr.

The optimized HF and MP2 structures both had C_s symmetry, with the symmetry plane bisecting the intermolecular angle O···N···O (Figure 3a). However, as reported in Table 5, the HF structure was nearly C_{2v} planar (the torsions deviate from 180° or 0° in the second decimal place), while at the MP2 level, the NO^+ moiety was predicted to be nearly perpendicular with respect to the O···N···O plane. Similarly, MP2 theory predicts that the two ion-solvent bonds are almost perpendicular to each other (θ(O···N···O) = 109.9°), while HF theory predicts a more linear structure (156.6°). This indicates that, as with $n = 1$, the water molecules interact with the p orbitals of the N atom. One H_2O donates lone pair density into the π_x^* orbital, the other into the π_y^* orbital. That MP2

theory does a far better job than HF theory of describing the electronic structure of intermolecular bonds is to be expected. This picture of the electronic structure is consistent with the Mulliken partial charges (Table 14), which shows a decrease of 0.05*e* on the N atom upon formation of the $NO^+(H_2O)_2$ complex.

The dipole-dipole interaction between the H_2O molecules at the computed geometry is repulsive. Using the Mulliken charges, we computed that this effect alone would favor by 0.5 kcal/mol having the waters on opposing sides of the nitrogen atom. However, at the MP2 level, this latter geometry (C_{2v} symmetry, with the H_2O molecules on opposite sides and the O···N···O angle at 180°) is 0.5 kcal mol^{-1} higher in energy; thus, the weak dipole repulsion is offset by other factors. Nevertheless, the MP2 ion-solvent bond lengths are 2.318 Å (Table 5), ~0.1 Å longer than the N···O in the n = 1 cluster (Table 2). This suggests a lack of cooperativity in the hydration of NO^+; that is, the binding of a second H_2O weakens both ion-solvent bonds slightly.

Harmonic vibrational frequencies (Table 9) showed that both the HF and the MP2 optimized structures were potential energy minima. The HF frequencies are generally only slightly larger (<10%) than the MP2 frequencies, due to the greater effect of anharmonicity. However, the HF prediction for the N=O stretch is over 30% larger than the MP2 prediction. This shows the almost complete failure of non-correlated methods to describe adequately the potential between multiply bonded atoms. The low frequency of the O···N···O bend, 33 cm^{-1}, indicates that the potential energy surface is very flat along this coordinate. The equilibrium O···N···O bond angle, calculated with a modest 6-31G** basis set, should therefore be treated with caution.

The energy required to remove one water from $NO^+(H_2O)_2$ was computed at various levels of theory (Table 12). As with the $NO^+(H_2O)$ calculations, estimates of ΔH_{298} decrease monotonically with increasing level of correlated theory. The CCSD/6-311G** value of ΔH_{298} = 17.1 kcal mol^{-1} is in good agreement with the value of 16.1±1.0 kcal mol^{-1} measured by Kebarle and co-workers, although larger basis sets would likely improve the agreement still further. The slight decrease in the binding enthalpy of water to $NO^+(H_2O)$ *vs.* the binding enthalpy of water to NO^+ is consistent with the longer ion-solvent bond lengths in n = 2 noted earlier.

D. Interpretation of the $NO^+(H_2O)_2$ Vibrational Spectrum. The n = 2 cluster predissociated by loss of one H_2O only. There were two absorption bands in the 2700–3800 cm^{-1} region (Figure 2b). The lower frequency band at 3622 cm^{-1} was sharp and resembled in shape and position the band observed for $NO^+(H_2O)$. The higher frequency absorption centered at ~3695 cm^{-1} was broad. Based on the proximity of these bands to the H_2O monomer stretch frequencies, we assigned these bands to the symmetric and antisymmetric stretch modes of water ligands respectively. The predicted OH stretch spectrum consists of the symmetric and antisymmetric H_2O bands at scaled frequencies of 3607 cm^{-1} and 3719 cm^{-1} with similar intensities (Table 13). The *ab initio* band positions agree well with experiment, but not the relative intensities. However, unlike the n = 1 cluster, the antisymmetric stretch band at least was observable for n = 2. The lower binding energy means that a non-negligible fraction of the $NO^+(H_2O)_2$ ions can predissociate by one-photon excitation of the antisymmetric OH stretch. The weakening

of the ion-solvent interaction is also reflected in the slight blue shift (+15 cm^{-1}) of the symmetric OH stretch.

The consistent picture provided by our spectroscopy experiment and *ab initio* calculations seemed to support the notion that in $NO^+(H_2O)_2$, NO^+ is directly solvated by both water molecules. However, very recent quantum molecular dynamics calculations by Ye and Cheng[32] challenge this picture. They predict that a $n = 2$ isomer in which the second H_2O binds to the first H_2O (Figure 3b) is the global minimum by ~3 kcal/mol. A preliminary HF calculation we have performed on this "water dimer isomer" (our term) does identify it as a stationary point, but it is ~4 kcal/mol less stable than the global minimum we have identified. This notwithstanding, we also know from the quantum chemistry that the $n = 2$ global potential is very flat along several coordinates (Table 9), and a dynamical treatment may be necessary for quantitative predictions of structure and vibrational frequencies at finite temperatures. (Simulation of the rotationally resolved $n = 1$ OH stretch band indicated for the $NO^+(H_2O)_n$ experiment a rotational temperature of 120 K.)

That being said, it is not clear that the current quantum dynamics study[32] affords reliable predictions. The simulation of the 300 K vibrational spectrum (Figure 2c) differs markedly from the experimental spectrum (Figure 2b) for $NO^+(H_2O)_2$. The theoretical spectrum does not predict the broad antisymmetric OH stretch to the blue of the sharp symmetric OH stretch band. Likewise, experiment does not indicate the presence of any bands to the red of 3600 cm^{-1} that could correspond to hydrogen bonding between the waters.

Moreover, the absolute and relative band positions predicted by the quantum dynamics simulation[32] are dubious. The free OH stretches are predicted to blue shift ~200 cm^{-1} in going from $n = 1$ (simulated spectrum not shown) to $n = 2$. Our experiment, on the other hand, indicates the blue shift is only ~15 cm^{-1}. Our *ab initio* calculations, while not quantitative in accuracy, do predict a blue shift of less than 40 cm^{-1}. Likewise, the intra-shell OH stretches are predicted in the simulation to be in the range 2500-2600 cm^{-1}, well to the red of any putative water-bound OH stretch in $NO^+(H_2O)_2$. (Our preliminary HF calculations on the "water dimer isomer" suggest that such a mode will be at ~3400 cm^{-1}.) While it is possible that our spectroscopy experiment missed absorptions to the red of 3600 cm^{-1}, the quantum dynamics calculation fails to account for the bands that are seen, and the authors fail to qualify the validity of their calculations in light of the discrepancies with experiment. Nevertheless, quantum molecular dynamics studies that more seriously engage the available experimental data should prove useful in the simulation of the structure and vibrational spectra of ionic clusters. The work to be discussed in Chapter 4 suggests the need and potential use of quantum dynamics simulations for systems such as $Cl^-(H_2O)_n$, where hydrogen bonding among the H_2Os is clearly important even for $n = 2$.

E. *Ab Initio* Calculations for $I^-(H_2O)$. The calculations identified two isomers of $I^-(H_2O)$, reflecting the two driving forces in halide ion solvation. The ground state (Figure 4a) C_s structure is bound by one strong, nearly linear hydrogen bond between the I^- and the H_2O. The bridged C_{2v} structure (Figure 4b) is bound by the ion-dipole force. It consists of two equivalent, highly bent hydrogen bonds between the I^- and the H_2O.

Table 15 compares the HF and MP2 predictions for the linear isomer. At the HF level, the $I^-\cdots H$ bond lengths are ~0.25 Å longer, and the hydrogen bonds are ~9° less linear. This indicates that the strength of the hydrogen bonds is predicted to be weaker at the HF level. The same effect is seen for the bridged isomer (Table 16); the $I^-\cdots H$ separations are predicted to be ~0.2 Å greater at the HF level. Thus, as we found for $NO^+(H_2O)$ and $NO^+(H_2O)_2$, HF theory predicts weaker intermolecular interactions between the ion and the solvent molecule(s) than are predicted at levels of theory that account for electron correlation.

The linear $I^-(H_2O)$ isomer is predicted to have all real vibrational frequencies, and is thus a minimum at both the HF and MP2 levels (Table 17). HF and MP2 calculations give the same qualitative picture of two chemically distinct OH stretches, one near the average of the OH stretches of free H_2O monomer, the other red-shifted by almost 200 cm^{-1}. HF and MP2 theory also give a consistent picture of the C_{2v} bridged isomer (Table 18). Both predict the C_{2v} stationary point to be a transition state for the exchange of hydrogen atoms via the B_2 H_2O rocking mode. Because the two OH stretches of the bridged isomer are chemically equivalent, they will be split only by harmonic (and anharmonic) coupling. Both levels of theory predict the OH stretches to be split by ~60 cm^{-1}, and red shifted by less than 100 cm^{-1} from the H_2O monomer bands. In both cases, because we are solvating an anion, the frequencies of the OH stretches directly probe the intermolecular interactions and could be dramatically shifted by different chemical environments. This contrasts with the solvation in $NO^+(H_2O)$ and

$NO^+(H_2O)_2$, where very strong intermolecular bonds (16-20 kcal/mol) shift the OH stretches by ≤ 50 cm^{-1} (Table 13).

The $I^-(H_2O)$ global potential is very flat along the rocking coordinate; the harmonic frequency is only ~100 cm^{-1}. This is further reflected by the relative stability of the linear and bridged isomers (Table 19). At the MP2 level, the electronic energy barrier to H-atom exchange, including zero-point vibrational energy, is only 0.2 kcal/mol. The two isomers are essentially degenerate. (In fact, if the rocking frequency were not removed from the calculation of the linear isomer ZPE, the bridged isomer would be predicted to be more stable.) This ambiguity is reflected by the earlier HF calculations of Hiraoka *et al.*,[33] who predicted the C_{2v} structure to be the ground state isomer using the 3-21+G* basis set.

Table 20 compares our theoretical estimate of the binding energy of $I^-(H_2O)$ with the experimental measurements of Kebarle and co-workers,[34] and Keesee and Castleman.[35] The MP2/6-311++G** estimate of ΔH_{298} = 9.4 kcal/mol agrees reasonably well with the experimental measurements of 10-11 kcal/mol. It is interesting that *ab initio* theory seems to underestimate the strength of the intermolecular bond in this diffuse anionic system, whereas *ab initio* theory overestimated the strength of the bonding in the cationic $NO^+(H_2O)$ and $NO^+(H_2O)_2$.

F. Interpretation of the $I^-(H_2O)$ Vibrational Spectrum. Infrared excitation of the $I^-(H_2O)$ cluster from 3200-3800 cm^{-1} led only to the loss of the water molecule. The action spectrum (Figure 5) revealed two dominant features: a broad, structured band centered at ~3415 cm^{-1}, and a sharp band at 3710 cm^{-1}. Apart from any theoretical

calculations, the experimental spectrum by itself indicates that $I^-(H_2O)$ consists of one OH group which is strongly red-shifted by hydrogen bonding to the ion, and another OH group which is basically unperturbed. This picture of $I^-(H_2O)$ is consistent with the linear isomer in Figure 4a.

Since the experimental vibrational bands were not rotationally resolved, however, a quantitative assignment of structure requires some recourse to theory. Hence we compare experimental frequencies with the scaled *ab initio* spectra for both the linear and bridged isomers. Table 21 clearly shows that the red shifts and relative intensities predicted for the linear structure agree much better with the experimental spectrum than those for the bridged structure. However, the bonded OH stretch prediction is more than 100 cm^{-1} too high. While this is consistent with the MP2 underestimate of the $I^-(H_2O)$ binding energy (Table 20) and the very small transfer of charge from I^- to H_2O (Table 22), the discrepancy is still notable. Given the far better agreement between experiment and theory for the bonded OH stretch of $Cl^-(H_2O)$ (to be discussed in Chapter 4), this suggests that the $I^-\cdots$H-O potential is highly anharmonic. A detailed study of this potential would be useful.

Nevertheless, both the bonded and free OH stretches are clearly observed in the $I^-(H_2O)$, and with roughly the relative intensities predicted by MP2 theory. This was not the case for $NO^+(H_2O)$, nor was it the case for $Cl^-(H_2O)$, as we shall see in the next chapter. This is perhaps surprising in light of the small forces keeping the ionic hydrogen bond reasonably linear. One might have expected the bridged C_{2v} isomer, with OH stretches in the ~3600 cm^{-1} region, also to be sampled. The salient physical parameter for

the observation of free OH stretches appears to be the intermolecular bond enthalpy. $I^-(H_2O)$, bound by ~10 kcal/mol, is predissociated by one photon. Both $Cl^-(H_2O)$ ($\Delta H_{298} \approx 15$ kcal/mol) and $NO^+(H_2O)$ ($\Delta H_{298} = 19$ kcal/mol) require two photons to predissociate. OH stretch anharmonicities will shift the second photon (in a one-color experiment) out of resonance. The shallowness of the intermolecular potential, however, does appear to affect the observation of water-bound OH stretches, as will be discussed in Chapter 4.

3.4 CONCLUSION

Our *ab initio* calculations for the isomers of $H_2NO_2^+$, $NO^+(H_2O)_2$, and $I^-(H_2O)$ generally provided information that was consistent with our experimental vibrational spectra, as well as the thermochemical data. MP2 theory afforded predictions of cluster geometries and vibrational frequencies that were qualitatively different from HF theory, particularly for the ground state $NO^+(H_2O)$ and $NO^+(H_2O)_2$ isomers. For the systems we studied, CCSD theory provided binding energies of nearly quantitative accuracy. The only significant discrepancy between our experimental data and theory is the absence of the symmetric OH stretch band in the $NO^+(H_2O)$. The details of the predissociation mechanism provide a likely explanation. In spite of the flatness of parts of the global potentials for these clusters, our static quantum chemical methods proved adequate in accounting for the experimental observations. Quantum mechanical treatments of the dynamics will prove to be necessary, however, in explaining the vibrational spectra of $Cl^-(H_2O)_n$ clusters.

3.5 REFERENCES AND NOTES

(1) (a) Ferguson, E. E.; Fehsenfeld, F.; Albritton, D. L. *Gas Phase Ion Chemistry*, Ed. M. T. Bowers, Academic Press, New York (1979); (b) Brasseur, G.; Solomon, S. *Aeronomy of the Middle Atmosphere*, D. Reidel, Dordrecht, Holland (1986).

(2) Lias, S. G.; Bartmess, J. E.; Liebman, J. F.; Holmes, J. L; Levin, R. D.; Mallard, W. G. *J. Phys. Chem. Ref. Data* **1988**, *17*, Suppl. 1.

(3) Narcisi, R. S.; Bailey, A. D. J. *Geophys.Res.* **1965**, *70*, 3687.

(4) (a) Fehsenfeld, F. C.; Ferguson, E. E. *J. Geophys. Res.* **1969**, *74*, 2217. (b) Lineberger, W. C.; Puckett, L. J. *Phys. Rev.* **1969**, *187*, 286.

(5) Patai, S. *The Chemistry of Amino, Nitroso, and Nitro Compounds and Their Derivatives* (Wiley, New York,1982) and references therein.

(6) French, M. A.; Hills, L. P.; Kebarle, P. *Can. J. Chem.* **1973**, *51*, 456.

(7) Burdett, N. A.; Hayhurst, A. N. *J. Chem. Soc. Faraday Trans. I* **1982**, 78, 2997.

(8) (a) Dewar, M. J. S.; Shanshal, M.; Worley, S. D. *J. Am. Chem. Soc.* **1969**, 91, 3590. (b) Jorgensen, K. A.; Lawessen, S. O. *J. Chem. Soc., Perkin Trans. 2* **1985**, 231. (c) Dargelos, A.; El Ouadi, S.; Liotard, D.; Chaillet, M.; Elguero, J. *Chem. Phys. Lett.* **1977**, *51*, 545. (d) Edwards, W. D.; Weinstein, H. *Chem. Phys. Lett.* **1978**, *56*. 582.

(9) Nguyen, M. T.; Hegarty, A. F. *J. Chem. Soc., Perkin Trans. 2* **1984**, 2037.

(10) de Petris, G.; Marzio, A. D.; Grandinetti, F. *J. Phys. Chem.* **1991**, *95*, 9782.

(11) Cao, Y.; Choi, J.-H.; Haas, B.-M.; Johnson, M. S.; Okumura, M. *J. Phys. Chem.* **1993**, *97*, 5215.

(12) Cao, Y.; Choi, J.-H.; Haas, B.-M.; Johnson, M. S.; Okumura, M. *J. Chem. Phys.* **1993**, *99*, 9307.

(13) Cao, Y.; Choi, J.-H.; Haas, B.-M.; Okumura, M. *J. Phys. Chem.* **1994**, *98*, 12176.

(14) Choi, J.-H.; Kuwata, K. T.; Cao, Y.-B.; Haas, B.-M.; Okumura, M. *J. Phys. Chem. A* **1997**, *101*, 6753.

(15) Choi, J.-H.; Kuwata, K. T.; Cao, Y.-B.; Okumura, M. *J. Phys. Chem. A* **1998**, *102*, 503.

(16) Choi, J.-H.; Kuwata, K. T.; Haas, B.-M.; Cao, Y.-B.; Johnson, M. S.; Okumura, M. *J. Chem. Phys.* **1994**, *100*, 7153.

(17) Johnson, M. S.; Kuwata, K. T.; Wong, C.-K.; Okumura, M. *Chem. Phys. Lett.* **1996**, *260*, 551.

(18) Choi, J.-H. Ph.D. Thesis, California Institute of Technology, 1995.

(19) Johnson, M. S. Ph.D. Thesis, California Institute of Technology, 1996.

(20) Frisch, M. J.; Trucks, G. W.; Head-Gordon, M.; Gill, P. M. W.; Wong, M. W.; Foresman, J. B.; Johnson, B. G.; Schlegel, H. B.; Robb, M. A.; Replogle, E. S.; Gomperts, R.; Andres, J. L.; Raghavachari, K.; Binkley, J. S.; Gonzalez, C.; Martin, R. L.; Fox, D. J.; Defrees, D. J.; Baker, J.; Stewart, J. J. P.; Pople, J. A. *Gaussian 92, Revision D.2.*, Gaussian, Inc., Pittsburgh, PA, 1992.

(21) Roothaan, C. C. J. *Rev. Mod. Phys.* **1951**, *23*, 69.

(22) Mϕller, C.; Plesset, M. S. *Phys. Rev.* **1931**, *46*, 618.

(23) Bartlett, R. J. *J. Phys. Chem.* **1989**, *93*, 1697.

(24) (a) Hehre, W. J.; Ditchfield, R.; Pople, J. A. *J. Chem. Phys.* **1972**, *56*, 2257. (b) Hariharan, P. C.; Pople, J. A. *Theor. Chim. Acta.* **1973**, *28*, 213.

(25) Frisch, M. J.; Pople, J. A.; Binkley, J. S. *J. Chem. Phys.* **1984**, *80*, 3265.

(26) Clark, T.; Chandrasekhar, J.; Spitznagel, G. W.; Schleyer, P .V. R. *J. Comput. Chem.* **1983**, *4*, 294.

(27) Hu, W.-P.; Truhlar, D. G. *J. Phys. Chem.* **1994**, *98*, 1049.

(28) Wadt, W. R.; Hay, P. J. *J. Chem. Phys.* **1985**, *82*, 284.

(29) Herzberg, G. *Molecular Spectra and Molecular Structure, III, Electronic Spectra of Polyatomic Molecules,* (van Nostrand Reinhold, New York, 1966).

(30) Lee, T. J.; Rice, J. E. *J. Phys. Chem.* **1992**, *96*, 650.

(31) Herzberg, G. *Molecular Spectra and Molecular Structure II, Infrared and Raman Spectra of Polyatomic Molecules* (van Nostrand Reinhold, New York, 1945).

(32) Ye, L.; Cheng, H.-P. *J. Chem. Phys.* **1998**, *108*, 2015.

(33) Hiraoka, K.; Mizuse, S.; Yamabe, S. *J. Phys. Chem.* **1988**, *92*, 3943.

(34) Arshadi, M.; Yamdagni, R.; Kebarle, P. *J. Phys. Chem.* **1970**, *74*, 1475.

(35) Keesee, R. G.; Castleman, Jr., A. W. *Chem. Phys. Lett.* **1980**, *71*, 139.

TABLE 1: The Effective Core Potential for Iodine as Derived by Wadt and Hay[a]

n_k	ζ_k	d_k
	f potential	
0	1.0715702	-0.0747621
1	44.1936028	-30.0811224
2	12.9367609	-75.3722721
2	3.1956412	-22.0563758
2	0.8589806	-1.6979585
	s-f potential	
0	127.9202670	2.9380036
1	78.6211465	41.2471267
2	36.5146237	287.8680095
2	9.9065681	114.3758506
2	1.9420086	3.76547714
	p-f potential	
0	13.0035304	2.2222630
1	76.0331404	39.4090831
2	24.1961684	177.4075002
2	6.4053433	77.9889462
2	1.5851786	25.7547641
	d-f potential	
0	40.4278108	7.0524360
1	28.9084375	33.3041635
2	15.6268936	186.9453875
2	4.1442856	71.9688361
2	0.9377235	9.3630657

[a] From ref. 28.

TABLE 2: Optimized Geometries of $NO^+(H_2O)$, NO^+, and H_2O at Various Levels of Theory[a,b]

	HF/ 6-31G**	MP2/ 6-31G**
$NO^+(H_2O)$		
$r(N\text{-}O_1)$	1.043	1.108
$r(N\cdots O_2)$	2.321	2.202
$r(H\text{-}O_2)$	0.948	0.968
$\theta(O_1\text{-}N\text{-}O_2)$	100.5	100.2
$\theta(N\text{-}O_2\text{-}H)$	125.5	119.5
$\theta(H\text{-}O_2\text{-}H)$	106.0	104.9
$\tau(H\text{-}O_2\text{-}N\text{-}O_1)$	101.1	±114.4
NO^+		
$r(N\text{-}O)$	1.040	1.103
H_2O		
$r(O\text{-}H)$	0.943	0.961
$\theta(H\text{-}O\text{-}H)$	105.9	103.9

[a] Bond lengths in Å; bond angles in deg.

[b] Atoms labeled as in Figure 1a.

TABLE 3: Optimized Geometries of $HON(H)O^+$ at Various Levels of Theory[a,b]

	HF/ 6-31G**	MP2/ 6-31G**
$r(H_1\text{-}O_1)$	0.965	0.992
$r(O_1\text{-}N)$	1.275	1.296
$r(N\text{-}O_2)$	1.141	1.200
$r(N\text{-}H_2)$	1.027	1.041
$\theta(H_1\text{-}O_1\text{-}N)$	110.9	108.7
$\theta(O_1\text{-}N\text{-}O_2)$	125.7	126.1
$\theta(O_1\text{-}N\text{-}H_2)$	111.9	110.7
$\tau(H_1\text{-}O_1\text{-}N\text{-}O_2)$	0	0.0
$\tau(H_1\text{-}O_1\text{-}N\text{-}H_2)$	180.0	180.0

[a] Bond lengths in Å; bond angles in deg.

[b] Atoms are labeled as in Figure 1b.

TABLE 4: Optimized Geometries of $N(OH)_2^+$ at Various Levels of Theory[a]

	HF/ 6-31G**	MP2/ 6-31G**
r(H-O)	0.964	0.989
r(O-N)	1.227	1.272
θ(H-O-N)	109.6	106.2
θ(O-N-O)	109.5	107.2
τ(H-O-N-O)	180.0	180.0

[a] Bond lengths in Å; bond angles in deg.

TABLE 5: Optimized Geometries of the $NO^+(H_2O)_2$ C_s Isomer at Various Levels of Theory[a,b]

	HF/ 6-31G**	MP2/ 6-31G**
$r(N\text{-}O_1)$	1.044	1.107
$r(N\cdots O_2)$	2.373	2.318
$r(O_2\text{-}H_1)$	0.946	0.965
$r(O_2\text{-}H_2)$	0.947	0.965
$\theta(O_1\text{-}N\text{-}O_2)$	101.7	95.9
$\theta(O\cdots N\cdots O)$	156.6	109.9
$\theta(N\text{-}O_2\text{-}H_1)$	120.1	125.2
$\theta(N\text{-}O_2\text{-}H_2)$	133.9	121.5
$\theta(H_1\text{-}O_2\text{-}H_2)$	106.0	104.4
$\tau(O_2\text{-}N\text{-}O_1\text{-}O_2)$	180.0	110.7
$\tau(H_1\text{-}O_2\text{-}N\text{-}O_1)$	±180.0	±106.6
$\tau(H_2\text{-}O_2\text{-}N\text{-}O_1)$	0.0	±111.2

[a] Bond lengths in Å; bond angles in deg.

[b] Atoms labeled as in Figure 3a.

TABLE 6: Harmonic Vibrational Frequencies and Infrared Intensities of the $NO^+(H_2O)$ Isomer at Various Levels of Theory[a]

	Approx Description	HF/ 6-31G**	MP2/ 6-31G**
$\omega_1(A')$	O-H sym stretch	4101(119)	3820(196)
$\omega_2(A')$	N-O stretch	2816(106)	2099 (92)
$\omega_3(A')$	H_2O bend	1793(104)	1682 (65)
$\omega_4(A')$	H_2O wag	399(376)	472 (272)
$\omega_5(A')$	N···O stretch	283(51)	281 (101)
$\omega_6(A')$	O-N···O bend	219(6)	248 (10)
$\omega_7(A'')$	O-H antisym stretch	4199(186)	3942 (159)
$\omega_8(A'')$	H_2O rock	447(101)	470 (56)
$\omega_9(A'')$	H_2O twist	5*i* (3)	116 (36)

[a] Frequencies in cm^{-1}; infrared intensities in km /mol.

TABLE 7: Harmonic Vibrational Frequencies and Infrared Intensities of the HON(H)O$^+$ Isomer at Various Levels of Theory[a,b]

	Approx Description	HF/ 6-31G**	MP2/ 6-31G**
$\omega_1(A')$	O-H_1 stretch	3895(356)	3550 (320)
$\omega_2(A')$	N-H_2 stretch	3538(182)	3355 (135)
$\omega_3(A')$	N-O_2 stretch	2103(214)	1656 (159)
$\omega_4(A')$	O_1NH_2 bend + N-O_2 stretch	1667(19)	1509 (83)
$\omega_5(A')$	H_1O_1N bend + N-O_1 stretch	1562(7)	1430 (9)
$\omega_6(A')$	O_1NH_2 bend + N-O_1 stretch	1299(332)	1239 (215)
$\omega_7(A')$	O_1NO_2 IP bend	754(65)	668 (53)
$\omega_8(A'')$	$O_1N(H_2)O_2$ umbrella	1183(67)	1065 (110)
$\omega_9(A'')$	O_1NO_2 op bend	660(253)	752 (181)

[a] Frequencies in cm^{-1}; infrared intensities in km /mol.

[b] Atoms are labeled as in Figure 1b.

TABLE 8: Harmonic Vibrational Frequencies and Infrared Intensities of the $N(OH)_2^+$ Isomer at Various Levels of Theory[a]

	Approx Description	HF/ 6-31G**	MP2/ 6-31G**
$\omega_1(A_1)$	O-H sym stretch	3932(142)	3610 (105)
$\omega_2(A_1)$	N-O sym stretch + NOH bend	1749(131)	1539 (77)
$\omega_3(A_1)$	N-O sym stretch	1420(25)	1280 (22)
$\omega_4(A_1)$	O-N-O bend	782(19)	713 (20)
$\omega_5(A_2)$	O-N-O shear	813(0)	760 (0)
$\omega_6(B_1)$	N-O-H shear	884(310)	875 (291)
$\omega_7(B_2)$	O-H antisym stretch	3905(863)	3583 (848)
$\omega_8(B_2)$	N-O antisym stretch + NOH bend	1681(136)	1560 (115)
$\omega_9(B_2)$	N-O antisym stretch + ONO shear	1419(604)	1293 (439)

[a] Frequencies in cm^{-1}; infrared intensities in km /mol.

TABLE 9: Harmonic Vibrational Frequencies and Infrared Intensities of the $NO^+(H_2O)_2$ C_s Isomer at Various Levels of Theory[a,b]

	Approx Description	HF/ 6-31G**	MP2/ 6-31G**
$\omega_1(A')$	O-H antisym stretch	4213 (292)	3978 (180)
$\omega_2(A')$	O-H sym stretch	4114 (14)	3859 (75)
$\omega_3(A')$	N-O stretch	2800 (101)	2097 (36)
$\omega_4(A')$	H_2O bend	1794 (20)	1698 (82)
$\omega_5(A')$	H_2O rock	425 (165)	423 (126)
$\omega_6(A')$	H_2O wag	378 (764)	397 (482)
$\omega_7(A')$	N···O sym stretch	202 (2)	254 (52)
$\omega_8(A')$	N···OH bend	27 (0)	201 (14)
$\omega_9(A')$	H_2O twist	65 (6)	105 (22)
$\omega_{10}(A')$	O···N···O bend	85 (0)	33 (0)
$\omega_{11}(A'')$	O-H antisym stretch	4213 (32)	3977 (66)
$\omega_{12}(A'')$	O-H sym stretch	4112 (179)	3857 (132)
$\omega_{13}(A'')$	H_2O bend	1793 (194)	1693 (69)
$\omega_{14}(A'')$	H_2O wag	360 (0)	379 (118)
$\omega_{15}(A'')$	H_2O rock	414 (56)	375 (84)
$\omega_{16}(A'')$	N···O antisym stretch	238 (23)	224 (4)
$\omega_{17}(A'')$	N···OH bend	318 (41)	207 (1)
$\omega_{18}(A'')$	H_2O OP twist	28 (0)	26 (7)

[a] Frequencies in cm^{-1}; infrared intensities in km /mol.

[b] OP=out of phase.

TABLE 10: Stabilities[a] of the Protonated Nitrous Acid Isomers $N(OH)_2^+$ and $HON(H)O^+$ Relative to the Ground State $NO^+(H_2O)$

	$N(OH)_2^+$		$HON(H)O^+$	
Level of Theory	ΔE_e	ΔE_0	ΔE_e	ΔE_0
HF/6-31G**	32.7	36.0	41.0	44.5
MP2/6-31G**	38.3	41.2	37.8	40.8
CCSD/6-31G**[b]	31.4	34.3	35.1	38.1
CCSD/6-311G(2*df*,2*pd*)[b]	29.7	32.7	32.8	35.8

[a] Energies in kcal/mol.

[b] At the MP2/6-31G** optimized geometry, with the MP2/6-31G** harmonic vibrational frequencies.

TABLE 11: Energetics[a] of the Reaction $NO^+(H_2O) \rightarrow NO^+ + H_2O$

Source of Data	ΔE_e	ΔE_0	ΔH_{298}
HF/6-31G**	22.4	20.7	21.8
MP2/6-31G**	25.1	23.1	23.8
CCSD/6-31G**[b]	23.9	21.9	22.6
CCSD/6-311G**[b]	22.4	20.4	21.2
CCSD/6-311G(2*df*,2*pd*)[b]	22.2	20.2	20.9
Experiment (Ref. 6)			18.5±1.5
Experiment (Ref. 7)			19.3±2.4

[a] Energies in kcal/mol.

[b] At the MP2/6-31G** optimized geometry, with the MP2/6-31G** harmonic vibrational frequencies.

TABLE 12: Energetics[a] of the Reaction $NO^+(H_2O)_2 \rightarrow NO^+(H_2O) + H_2O$

Source of Data	ΔE_e	ΔE_0	ΔH_{298}
HF/6-31G**	18.9	17.3	16.8
MP2/6-31G**	19.5	18.0	18.0
CCSD/6-31G**[b]	18.9	17.4	17.5
CCSD/6-311G**[b]	18.6	17.1	17.1
Experiment (Ref. 6)			16.1±1.0

[a] Energies in kcal/mol.

[b] At the MP2/6-31G** optimized geometry, with the MP2/6-31G** harmonic vibrational frequencies.

TABLE 13: Experimental and (Scaled) *Ab Initio* Vibrational Frequencies and Infrared Intensities of $NO^+(H_2O)$ and $NO^+(H_2O)_2$[a]

	Approx Description	Experiment	MP2/6-31G**
$NO^+(H_2O)$			
	O-H sym stretch	3599, 3611	3571(196)
	O-H antisym stretch		3686(159)
$NO^+(H_2O)_2$			
	O-H sym stretch	3622	3607(207)[b]
	O-H antisym stretch	3695	3719(247)[b]

[a] Frequencies in cm^{-1}; infrared intensities in km /mol.

[b] The absolute infrared intensity reported is the sum of the in-phase and out-of-phase linear combinations of each H_2O ligand mode.

TABLE 14: Mulliken Partial Charges (SCF Density) of the Chemical Species NO^+, H_2O, $NO^+(H_2O)$, and $NO^+(H_2O)_2$[a,b]

	NO^+, H_2O	$NO^+(H_2O)$	$NO^+(H_2O)_2$
z(N)	+0.76	+0.71	+0.71
$z(O_1)$	+0.24	+0.19	+0.18
$z(O_2)$	-0.68	-0.71	-0.72
z(H)	+0.34	+0.40	+0.39

[a] Atoms are labeled as in Figures 1a and 3a.

[b] The four H atoms in $NO^+(H_2O)_2$, although strictly not all equivalent by symmetry, have the same partial charges to two decimal places.

TABLE 15: Optimized Geometries of the Linear C_s $I^-(H_2O)$ Isomer and H_2O at Various Levels of Theory[a,b]

	HF/ 6-311++G**	MP2/ 6-311++G**
$I^-(H_2O)$		
$r(I^- \cdots H_1)$	3.052	2.805
$r(H_1\text{-}O)$	0.947	0.970
$r(O\text{-}H_2)$	0.942	0.961
$\theta(I^-\text{-}H_1\text{-}O)$	139.3	147.8
$\theta(H_1\text{-}O\text{-}H_2)$	102.2	99.2
$\tau(I^-\text{-}H_1\text{-}O\text{-}H_2)$	0.0	0.0
H_2O		
r(O-H)	0.941	0.960
θ(H-O-H)	106.2	103.5

[a] Bond lengths in Å; bond angles in deg.

[b] Atoms are labeled as in Figure 4a.

TABLE 16: Optimized Geometries of the Bridged C_{2v} $I^-(H_2O)$ Isomer and H_2O at Various Levels of Theory[a]

	HF/ 6-311++G**	MP2/ 6-311++G**
$I^-(H_2O)$		
$r(I^-\cdots H)$	3.302	3.117
r(O-H)	0.944	0.964
θ(I^--H-O)	116.4	117.5
θ(H-O-H)	101.6	98.0
τ(I^--H-O-H)	0.0	0.0
H_2O		
r(O-H)	0.941	0.960
θ(H-O-H)	106.2	103.5

[a] Bond lengths in Å; bond angles in deg.

TABLE 17: Harmonic Vibrational Frequencies and Infrared Intensities of the Linear C_s $I^-(H_2O)$ Isomer at Various Levels of Theory[a]

	Approx Description	HF/ 6-31G**	MP2/ 6-31G**
$\omega_1(A')$	Free OH stretch	4194(61)	3938(42)
$\omega_2(A')$	Bonded OH stretch	4084(200)	3749(358)
$\omega_3(A')$	H_2O bend	1785(236)	1694(192)
$\omega_4(A')$	H_2O rock	128(94)	174(78)
$\omega_5(A')$	$I^-\cdots H$ stretch	93(5)	111(3)
$\omega_6(A'')$	H_2O wag	550(180)	561(113)

[a] Frequencies in cm^{-1}; infrared intensities in km/mol.

TABLE 18: Harmonic Vibrational Frequencies and Infrared Intensities of the Bridged C_{2v} $I^-(H_2O)$ Isomer at Various Levels of Theory[a]

	Approx Description	HF/ 6-31G**	MP2/ 6-31G**
$\omega_1(A_1)$	Sym OH stretch	4124(85)	3846(94)
$\omega_2(A_1)$	H_2O bend	1785(283)	1697(274)
$\omega_3(A_1)$	$I^-\cdots H$ stretch	92(2)	108(2)
$\omega_4(B_1)$	H_2O wag	541(198)	539(140)
$\omega_5(B_2)$	Antisym OH stretch	4180(60)	3904(33)
$\omega_6(B_2)$	H_2O rock	94*i*(114)	129*i*(108)

[a] Frequencies in cm^{-1}; infrared intensities in km/mol.

TABLE 19: Stability[a] of the $I^-(H_2O)$ Bridged Isomer Relative to the Ground State Linear Isomer

Level of Theory	ΔE_e	ΔE_0
HF/6-311++G**	0.04	0.06
MP2/6-311++G**	+0.1	+0.2

[a] Energies in kcal/mol.

TABLE 20: Energetics[a] of the Reaction $I^-(H_2O) \rightarrow I^- + H_2O$

Source of Data	ΔE_e	ΔE_0	ΔH_{298}
MP2/6-311++G**	10.7	9.7	9.4
Experiment (Ref. 34)			10.2
Experiment (Ref. 35)			11.1

[a] Energies in kcal/mol.

TABLE 21: Experimental and (Scaled) *Ab Initio* Vibrational Frequencies (MP2/6-311++G) and Infrared Intensities of the Linear and Bridged $I^-(H_2O)$ Isomers**[a]

Approx Description	Experiment	Linear	Bridged
Bonded OH stretch	~3415[b]	3524(358)	
OH sym stretch			3615(94)
Free OH stretch	3710	3702(42)	
O-H antisym stretch			3669(33)

[a] Frequencies in cm^{-1}; infrared intensities in km /mol.

[b] The center of the system, which had four sub-bands.

TABLE 22: Mulliken Partial Charges (SCF Density) of the Chemical Species I^-, H_2O, and $I^-(H_2O)$[a]

	I^-, H_2O	$I^-(H_2O)$
$z(I)$	-1.00	-0.98
$z(H_1)$	+0.25	+0.26
$z(O)$	-0.51	-0.51
$z(H_2)$	+0.25	+0.23

[a] Atoms are labeled as in Figure 4a.

3.6 FIGURE CAPTIONS

Figure 1. Isomers of protonated nitrous acid, with structures optimized at the MP2/6-31G** level of theory. (a) $NO^+(H_2O)$. (b) $HON(H)O^+$. (c) $N(OH)_2^+$.

Figure 2. Vibrational spectra of $NO^+(H_2O)_n$ clusters. (a) The experimental $n = 1$ spectrum. (b) The experimental $n = 2$ spectrum. (c) The $n = 2$ spectrum predicted in quantum molecular dynamics simulations by Ye and Cheng (ref. 32). The experimental data has been previously reported in the thesis of J.-H. Choi, and the theoretical spectrum is taken from ref. 32.

Figure 3. Isomers of $NO^+(H_2O)_2$. (a) The structure identified by our MP2/6-31G** calculations. (b) The "water dimer" isomer predicted to be the $n = 2$ global minimum by Ye and Cheng; the figure is taken from ref. 32.

Figure 4. Isomers of $I^-(H_2O)$, as predicted by MP2/6-31G** calculations. (a) The linear C_s isomer. (b) The bridged C_{2v} isomer.

Figure 5. The experimental vibrational spectrum of $I^-(H_2O)$. The data has been previously reported in the thesis of M. S. Johnson.

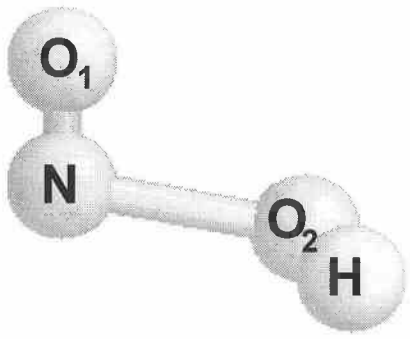

Figure 1a

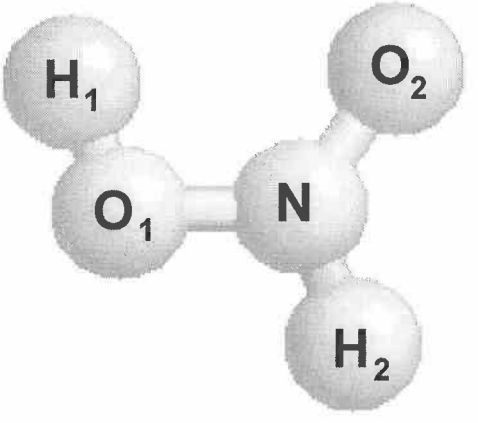

Figure 1b

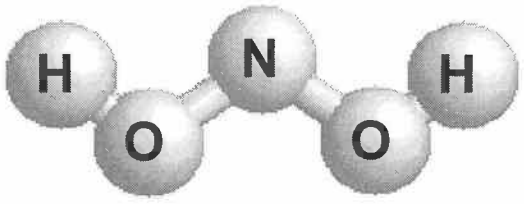

Figure 1c

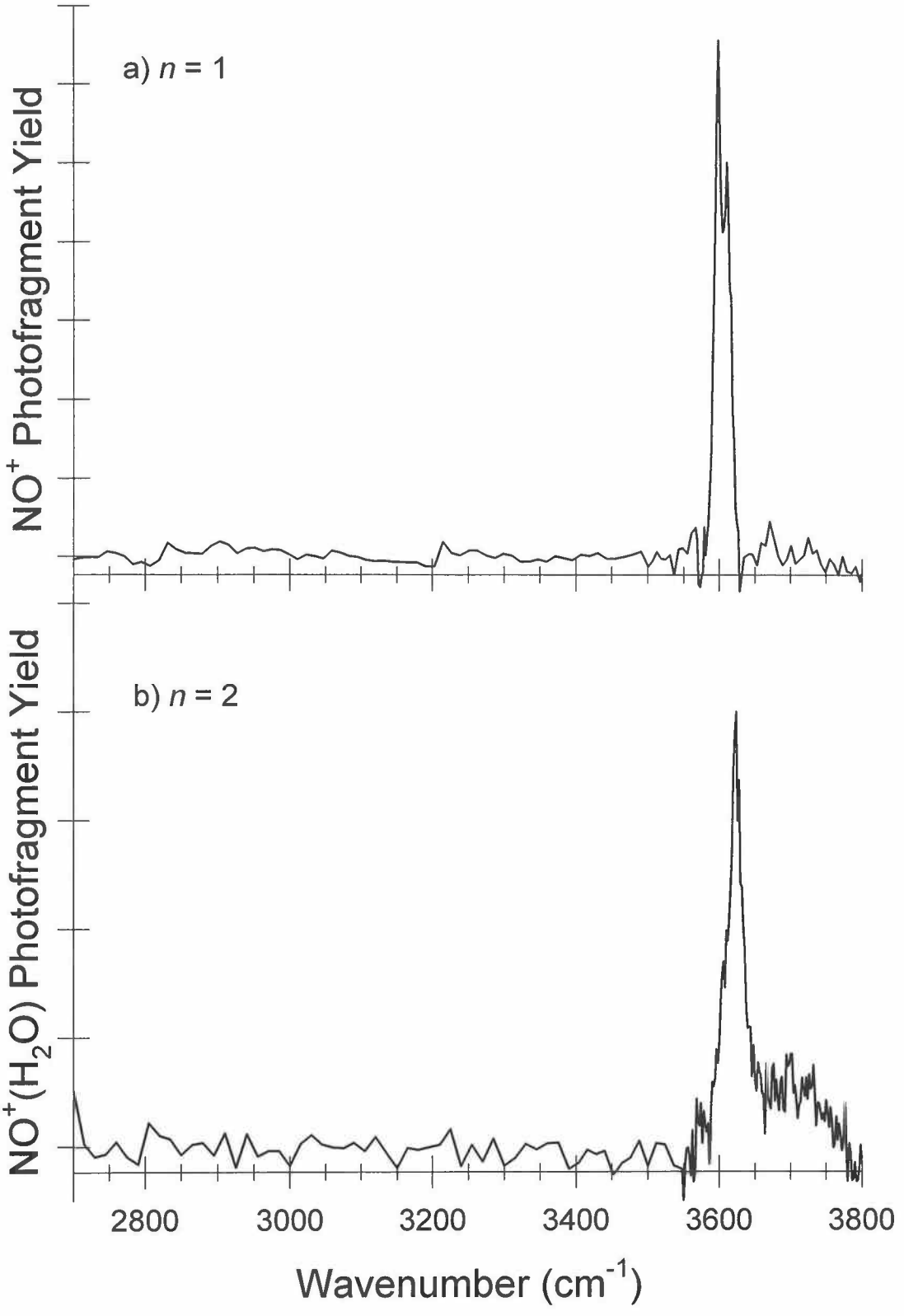

Figures 2a,2b

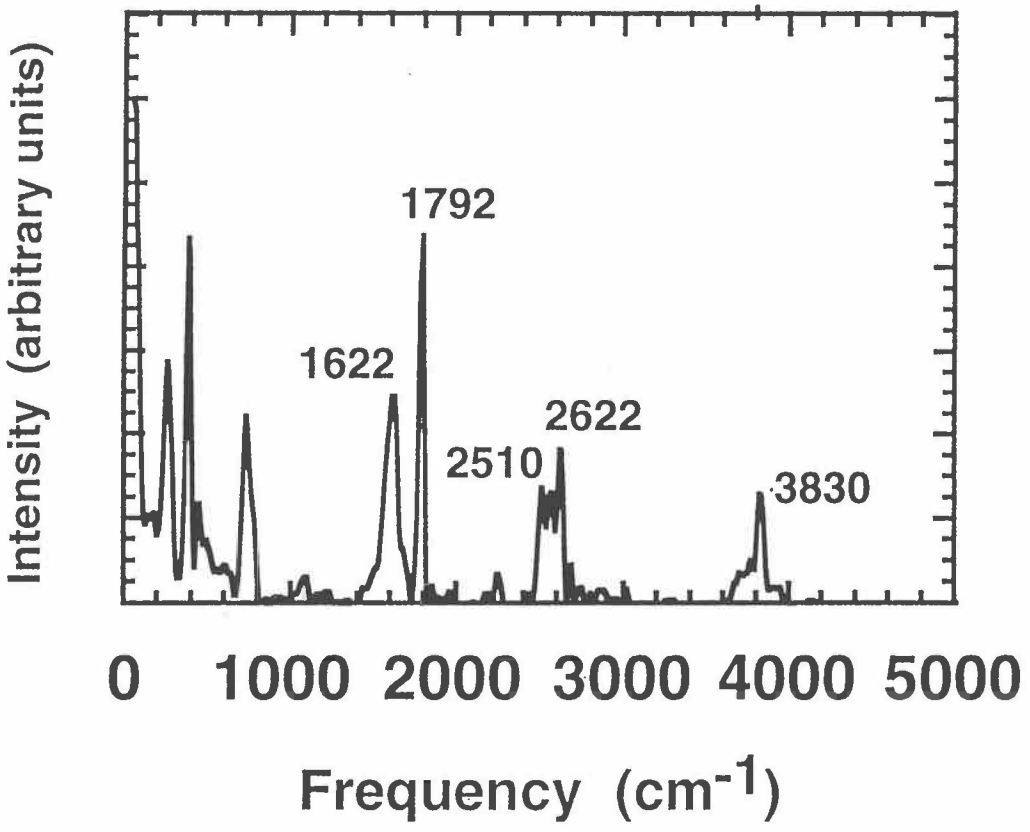
Intensity (arbitrary units)
1792
1622
2622
2510
3830
0
1000
2000
3000
4000
5000
Frequency (cm-1)

Figure 2c

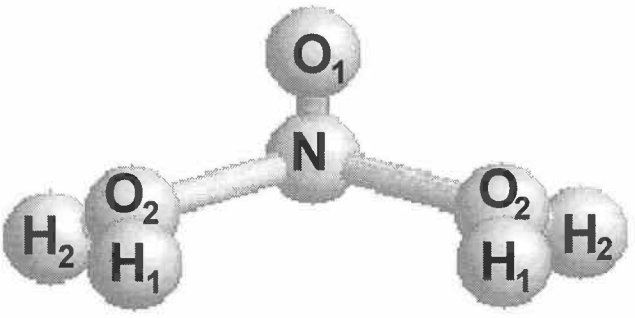

Figure 3a

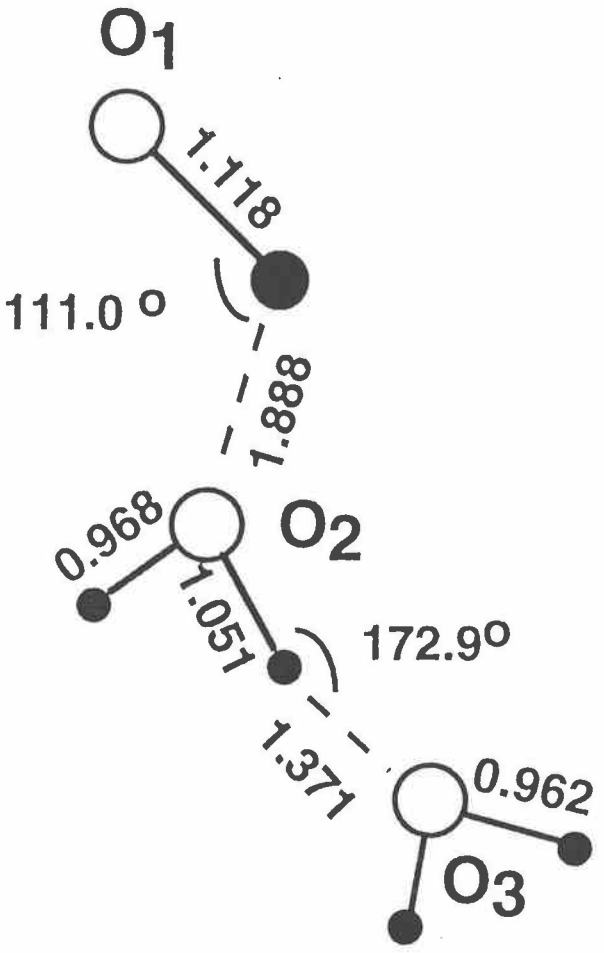

Figure 3b

Figure 4a

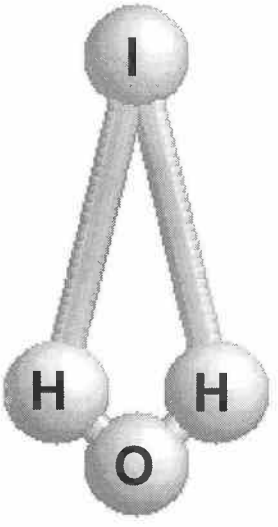

Figure 4b

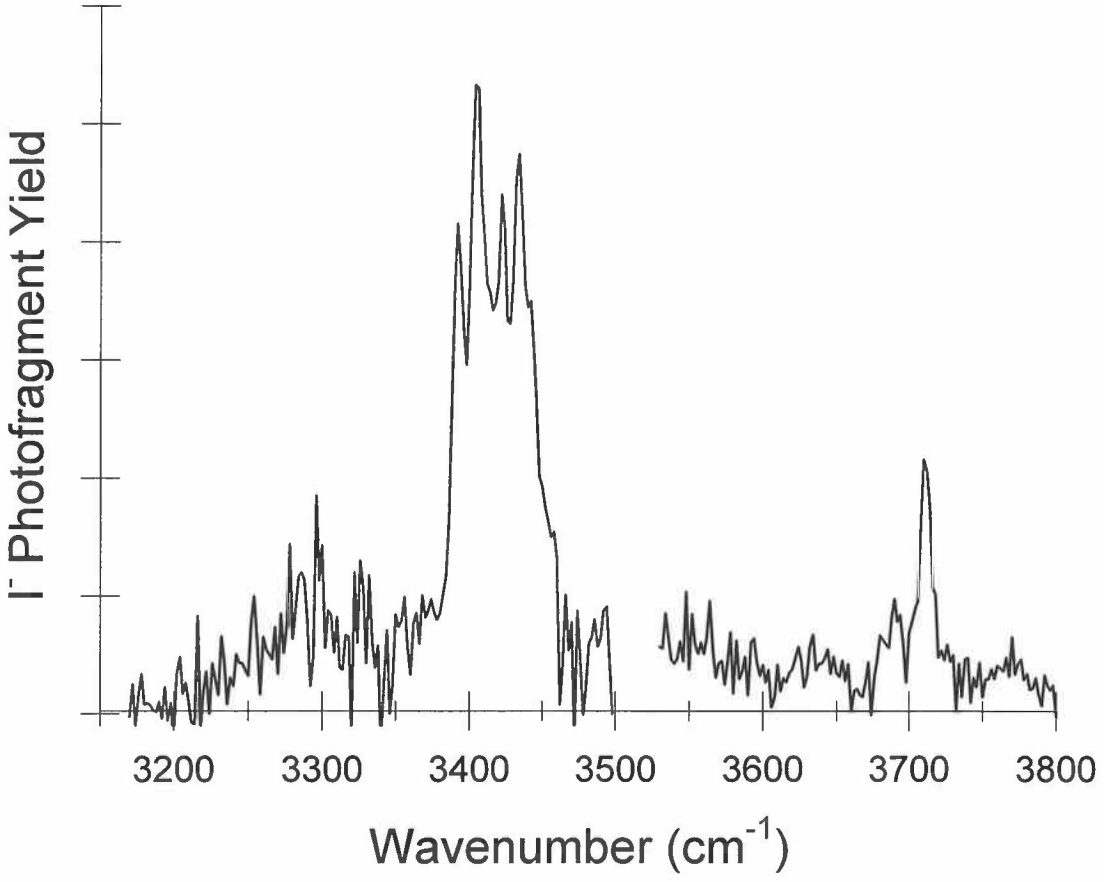
I⁻ Photofragment Yield
3200
3300
3400
3500
3600
3700
3800
Wavenumber (cm-1)

Figure 5

CHAPTER 4

The Gas-Phase Hydration of Chloride Ion: Infrared Spectroscopy and *Ab Initio* Calculations for $Cl^-(H_2O)_n$, n=1-7 and $Cl^-(H_2O)(CCl_4)$

4.1 INTRODUCTION

A. General Considerations. The structures that water molecules form about the chloride ion in the gas phase reflect the competition between solvation of the ion *vs.* hydrogen bonding among the waters. If hydrogen bonding to Cl^- dominates, the ion will move to the interior of a solvation shell. If hydrogen bonding among the waters dominates, Cl^- ion will move to the surface of a neutral water cluster. Computational studies over the past two decades have predicted that surface states dominate in $Cl^-(H_2O)_n$ even at large n, but direct experimental probes of cluster structure have been lacking. In this chapter, we will discuss the application of vibrational predissociation spectroscopy to the gas-phase clusters $Cl^-(H_2O)_n$, n = 1-7 and $Cl^-(H_2O)(CCl_4)$. Infrared spectra of n = 6 and 7 and of $Cl^-(H_2O)(CCl_4)$, are new to this thesis. This chapter also presents *ab initio* calculations of the energetics, optimized geometries, and vibrational frequencies of $Cl^-(H_2O)$, $Cl^-(H_2O)_2$, and $Cl^-(CCl_4)$.

Computational studies of the structure of $Cl^-(H_2O)_n$ were pioneered in the mid 1980's by the molecular mechanics calculations of Lybrand and Kollman.[1] Using many-body potential functions, they found that the waters in the n = 4 system clustered on one side of the Cl^-, hydrogen bonding to each other as well as to the ion. They emphasized the need to account for non-additive effects to obtain good agreement with experimental hydration enthalpies. Subsequent Monte Carlo simulations by Jorgensen and Severance,[2] and molecular dynamics calculations by Jordan and co-workers,[3] Perera and Berkowitz,[4] and Stuart and Berne[5] predicted that Cl^- will be surface solvated with as many as 255 waters, and verified the importance of treating many-body effects explicitly.

However, the role of the polarizability of both Cl^- ion and H_2O in determining cluster structure has been ambiguous. Originally, Perera and Berkowitz[4a] found the polarizability of H_2O to be a critical driving force towards surface solvation. This claim was later disputed by Jorgensen and Severance.[2] More recently, Stuart and Berne[5] supported the original predictions of Perera and Berkowitz, with the proviso that H_2O polarizability becomes essential only for larger ($n > 18$) clusters.

All three groups agreed, however, that Cl^- polarizability was not essential for surface solvation.[6] This conflicted with the original molecular dynamics results of Sung and Jordan,[7] who found that the large chloride ion polarizability (estimated to be 4.1 $Å^3$)[8] was a critical driving force for the asymmetric structure of $Cl^-(H_2O)_3$. The later calculations focused on larger ($n \geq 14$) clusters, and do not exclude the role of Cl^- polarizability for smaller clusters that lack the opportunity for extensive hydrogen bonding among the waters. This possibility is borne out by very recent Monte Carlo simulations by Truong and Stefanovich.[9] Using a hybrid scheme of treating Cl^- with *ab initio* Hartree-Fock (HF) calculations, and the waters with a classical molecular mechanics force field, they find that the Cl^- polarizability plays a significant role in causing surface solvation for $n \leq 7$.

Advances in computer technology have made possible recent systematic *ab initio* studies of $Cl^-(H_2O)_n$ cluster structure. Hartree-Fock calculations by Jortner and co-workers[10] and Okuno,[11] density functional theory (DFT) calculations by Dunbar *et al.*,[12] and second-order Møller-Plesset (MP2) calculations by Caldwell and Kollman[13] and by Xantheas[14] have all predicted that surface isomers of $Cl^-(H_2O)_n$ will dominate.

This straightforward understanding of cluster structure, however, is complicated by consideration of the effects of temperature. In a molecular dynamics study, Berkowitz and co-workers[15] found that the 0 K surface structure of $Cl^-(H_2O)_{11}$ is essentially retained when the system is heated to greater than 200 K. However, Monte Carlo simulations by Asada *et al.*[16] found that $Cl^-(H_2O)_2$ is dominated by interior solvation states at 300 K. The aforementioned *ab initio* calculations of Jortner and co-workers[10] also supported the notion that higher temperatures will favor more interior solvation states for $Cl^-(H_2O)_n$.

The strongly quantum mechanical character of the hydrogen atoms in $Cl^-(H_2O)_n$ could also play a critical role in determining cluster structure. Using path integral Monte Carlo simulations, Dang and co-workers[17] found that the hydrogen atoms in $Cl^-(H_2O)_n$ are highly delocalized for $T \leq 100$ K, weakening the hydrogen bonding between the waters. These large-amplitude zero-point motions, like higher temperature, may favor interior solvation of Cl^- ion within water clusters.

B. Specific $Cl^-(H_2O)_n$ Cluster Structures. To motivate the assignment of cluster structure with our vibrational spectra, we will now discuss the possible structures of different $Cl^-(H_2O)_n$ isomers as predicted by *ab initio* calculations. All previous *ab initio* calculations[18] on $Cl^-(H_2O)$ suggest that Cl^- forms a nearly linear hydrogen bond with H_2O (Figure 1, **Ia**). However, the ion-dipole interaction alone would lead to a bridged structure (Figure 1, **Ib**) in which the Cl^- is equally shared by both H atoms.

When a second water is added, the key issue is its relationship with the first water. HF calculations by Jortner and co-workers[10] indicate that the two waters may bind either

to the same side (Figure 2, **IIa**) or to nearly opposite sides (resembling Figure 2, **IIb**). However, both MP2 and DFT calculations indicate that only **IIa** corresponds to a minimum on the global potential. The minimum is asymmetric, with one H_2O acting as a double hydrogen bond donor, and the other H_2O acting as both a donor and acceptor of hydrogen bonding. However, higher temperatures and the zero-point motion of the hydrogen atoms may greatly weaken the hydrogen bonding interaction between the waters.

Both HF[10,11] and MP2[14] calculations predict that all $n = 3$ isomers are surface structures. The ground state is C_3 pyramidal (Figure 3, **IIIa**) with all waters equivalent. Each H_2O forms one hydrogen bond to Cl^-, and one hydrogen bond to another water. In the ring isomer (Figure 3, **IIIb**), two waters bind to the Cl^- (each has one free OH bond), and the third forms a second solvation shell, binding to the first two waters.

The two $n = 4$ MP2 isomers identified by Xantheas[14] are surface structures. The ground state is C_4 pyramidal (Figure 4, **IVa**) with a structure analogous to the C_3 pyramidal isomer. In the "3+1" isomer, three waters form a pyramid and the fourth H_2O forms a bridge between the base of the pyramid and Cl^- (Figure 4, **IVb**). Jortner and co-workers[10] also find an interior isomer at the HF level with a ring of three waters on one side and an ion-bound H_2O on the other side (Figure 4, **IVc**).

C. Previous Experimental Studies. Experiments have yet to provide detailed cluster structures as a function of n. Mass spectrometry[19,20] reveals no breaks in the stepwise hydration enthalpies of $Cl^-(H_2O)_n$ ($n \leq 6$) that may indicate the closing of solvation shells. The gradual differential change in Cl^- hydration enthalpy led Hiraoka[21]

to suggest that the water ligands in $Cl^-(H_2O)_n$ had almost as much freedom of motion as in neutral water clusters $(H_2O)_n$.

Cheshnovsky and co-workers[22] tried to differentiate surface and interior solvation states of $Cl^-(H_2O)_n$ with photoelectron spectroscopy. The idea was that different cluster structures would have different characteristic ionization potentials (IP), which could be assigned either by *ab initio* calculations or molecular dynamics simulations.[23] The trends revealed by experiment and theory suggest that surface states dominate for $n \leq 6$. However, the differences in the *ab initio* IPs of different isomers (for a given n) were often on the order of the error in the calculation ($\geq$ 2 kcal/mol). (The molecular dynamics simulations did not provide specific structures). This approach, then, did not allow the assignment of specific cluster structures.

Some structural information may be inferred from a kinetics study by Viggiano and co-workers.[24] They used a selected ion flow tube to monitor the reactions of Cl_2 with $Cl^-(D_2O)_n$ ($n \leq 8$) to give the trichloride products $Cl_3^-(D_2O)_{n-1}$ and $Cl_3^-(D_2O)_{n-2}$. The n=6 cluster was found to react two times slower than the n = 5 cluster. Viggiano and co-workers suggested that this reflects a transition to an interior state at n = 6, but this shell closing is not predicted by either simulations or *ab initio* calculations.

In this chapter, we consider the structural information to be had from the vibrational predissociation of chloride-water clusters. Vibrational spectroscopy is a sensitive, size-specific probe of hydrogen bonding in both ionic[25,26,27] and neutral[28] solvated clusters. For example, the predissociation spectrum of $I^-(H_2O)$ has established that the structure contains one strong ionic hydrogen bond. Recent spectroscopy by

Johnson and co-workers[29] have revealed some structural features of the clusters $Br^-(H_2O)_n$ (n = 1-5) and $I^-(H_2O)_n$ (n = 1-6). Here we report the infrared spectra of $Cl^-(H_2O)_n$ (n=1-7) and the adduct $Cl^-(H_2O)(CCl_4)$. We consider cluster structures for n = 1 and 2 with our *ab initio* calculations, and for n = 3 and 4 with the aid of Xantheas'[14] calculations.

4.2 EXPERIMENTAL AND COMPUTATIONAL METHODS

Experimental details have been given elsewhere,[30] and only a brief account is presented here. For the infrared spectra of smaller clusters (n = 1-5) (Figure 9), the ions were generated from a mixture of ~20 Torr H_2O and ~20 Torr CCl_4 vapor seeded in methane at a stagnation pressure of ~1500 Torr. The gas was injected into vacuum (~10^{-4} Torr) by a piezo-driven pulsed valve (width ~200 μs) through a 1 mm nozzle. Clusters of $Cl^-(H_2O)_n$ were formed in the expansion by crossing the jet with a continuous 750 eV electron beam. The plasma was skimmed and entered a time-of-flight mass spectrometer, where the ions were pulse-extracted and mass-analyzed. The typical cluster distribution, shown in Figure 6, was peaked at Cl^-, indicating a hot cluster distribution.

It was possible to enhance clustering of H_2O to Cl^- ion (Figure 7) by increasing the pulse width to ~400 μs and aiming the electron beam closer to the start of the expansion. The cluster distribution, now peaked at n = 5, may have been vibrationally cooler. This enabled us to obtain the infrared spectra of larger clusters (n = 6 and 7), as well as a n = 5 spectrum under these different conditions. The predissociation spectra of ions generated in this distribution are reported in Figure 11.

Attachment of one or more CCl_4 ligands to the $Cl^-(H_2O)_n$ clusters was effected

by increasing the vapor pressure of CCl_4 in the source line to ~300 Torr. The mass spectrum of $Cl^-(H_2O)_n(CCl_4)_m$ is shown in Figure 8. The relative intensities of the $m = 1$ systems (for n = 0-2) agree with the $^{35}Cl/^{37}Cl$ isotopic distribution expected for a five-chlorine system.

A parent ion of a given mass-to-charge ratio was selected by a mass gate and excited by the 0.5 to 5 mJ idler (~3 μm) beam from a Nd:YAG-pumped $LiNbO_3$ optical parametric oscillator (OPO). For the spectra in Figure 11, an absorption by the $LiNbO_3$ crystal due to a water impurity led to negligible idler power from 3460 to 3510 cm^{-1}. Photofragment ions were separated from the parent ions using a reflectron and then detected by a MCP detector. Spectra were obtained by integrating fragment ion signal as a function of the OPO frequency, subtracting the background due to dissociation of metastable parent ions, and normalizing with the laser fluence.

Calculations on $Cl^-(H_2O)$, $Cl^-(H_2O)_2$, $Cl^-(CCl_4)$, and their respective fragments were all performed on a Cray Y-MP using the Gaussian 92 system of programs.[31] For $Cl^-(H_2O)$, geometries and frequencies were calculated at the MP2 and CCSD levels of theory. For $Cl^-(H_2O)_2$, geometries and frequencies were calculated at the MP2 level for all isomers, and at the HF level for the C_1 and C_{2v} isomers. Optimized geometries of $Cl^-(CCl_4)$ and CCl_4 were obtained at the HF and MP2 levels. Limitations in scratch disk space precluded the calculation of MP2 frequencies; the thermochemistry of $Cl^-(CCl_4)$ was therefore estimated based on the (unscaled) HF frequencies. Energetics for $Cl^-(H_2O)$ and $Cl^-(H_2O)_2$ were all based on optimized geometries. One set of CCSD calculations for $Cl^-(CCl_4)$ was based on the MP2 optimized geometries. All MP2 and

CCSD calculations neglected the correlation of core electrons.

For most of the calculations, the standard 6-31+G*, 6-31+G**, 6-311++G**, 6-311+G(2*d*), 6-311+G(2*df*), and 6-311+G(3*d*) basis sets were used, as discussed in Chapter 2. (One asterisk or plus sign designates the presence of polarization or diffuse functions on all atoms except for H; two asterisks or plus signs designates the presence of *p* polarization and *s* diffuse functions on H atom as well.) For $Cl^-(CCl_4)$, MP2 energy calculations with the basis sets containing multiple polarization functions were all based on the MP2/6-31+G* geometry.

Tables 1-7 report the optimized geometries of $Cl^-(H_2O)_n(CCl_4)_m$ stationary points, and Tables 8-15 report their harmonic vibrational frequencies and infrared intensities. Figure 10 shows the *ab initio* vibrational spectra predicted at our highest level of theory for n = 1 and 2, and by Xantheas for n = 3 and 4. The frequencies graphed in Figure 10 have been scaled by 0.9399 for n = 1 and 2, and by 0.9575 for n = 3 and 4. These are the scaling factors required for the level of theory employed to reproduce the average of the experimental OH stretches for H_2O.

4.3 RESULTS AND DISCUSSION

A. General Observations. The only photofragment channel observed upon IR excitation of $Cl^-(H_2O)_n$ (n = 1 to 6) was loss of a single water molecule. For n = 7, a minor photofragment channel with loss of two waters was also observed; the metastable loss of two waters from n = 7 was roughly 50% as probable as the loss of one water. Excitation of $Cl^-(H_2O)(CCl_4)$ gave loss of CCl_4 only.

The clusters $Cl^-(H_2O)_n$ have strong infrared bands in the 3200-3500 cm^{-1} region

(Figures 9 and 11) which dominate the spectra. We assign these bands to OH stretches of ionic hydrogen bonds. A single band in n = 1 splits into an asymmetric doublet in n=2, with the blue band being more intense. The higher frequency band blue shifts 30-40 cm^{-1} with the addition of each water, indicating a weakening of the ionic hydrogen bonds. Adding more waters also makes the blue band progressively more intense than the red band. By n = 4, only one distinct band persists.

The n = 4-7 spectra have an additional band in the 3500-3650 cm^{-1} region which we assign to the OH stretch of water-water hydrogen bonds. This band red-shifts by ~40 cm^{-1} from n = 4 to n = 5. Other bands that appear further to the red are also likely due to cooperative hydrogen bonding among the waters, but we cannot assign them definitively. The spectra of $Cl^-(H_2O)(CCl_4)$ and $Cl^-(H_2O)_n$ (n = 2-7) all possess a weak band appearing at ~3700 cm^{-1}, which we assign to the free OH stretch.

B. $Cl^-(H_2O)$. Our spectrum (Figure 9a) demonstrates that H_2O forms one strong hydrogen bond to Cl^- (Figure 1, **Ia**). This agrees with our *ab initio* predictions of the n = 1 ground state geometry (Table 1) and (scaled) vibrational spectrum (Figure 10a). The only problem with this interpretation is that we do not observe the free OH stretch at ~3700 cm^{-1}. This issue will be addressed in the next section.

The intense band at 3285 cm^{-1} is clear evidence of a strong, nearly linear ionic hydrogen bond. The observed frequency agrees well with the prediction (3266 cm^{-1}) for the ionic OH stretch of **Ia**. The first bending overtone of H_2O at 3156 cm^{-1} is close to the free H_2O monomer frequency[32] of 3151 cm^{-1}. The H_2O bending mode has significant oscillator strength; MP2 theory predicts an absolute intensity of 100-150 km/mol (Table

8). The overtone may gain further intensity through a Fermi resonance interaction with the 3285 cm^{-1} band. We tentatively assign a weak feature at ~3440 cm^{-1} to a combination of the OH bonded stretch and the Cl^---H intermolecular stretch. If our assignment is valid, the frequency of the intermolecular stretch, ~155 cm^{-1}, is somewhat less than the *ab initio* harmonic value of 184 cm^{-1} (Table 8).

All of our *ab initio* calculations predict that the ground state $Cl^-(H_2O)$ structure has C_s symmetry (Table 1). The calculated geometric parameters vary little with basis set or level of theory, except for the length of the hydrogen bond, $r(Cl\text{-}H_1)$. Enlarging the valence basis set at the MP2 level shortens $r(Cl\text{-}H_1)$ by ~0.06 Å; with this larger basis set, CCSD predicts $r(Cl\text{-}H_1)$ is re-lengthened by ~0.04 Å. This lack of consistency is manifested more noticeably in the predicted bonded OH stretch frequencies ω_2 (Table 8). CCSD theory predicts a value more than 100 cm^{-1} than MP2 theory with the same basis set.

The discrepancies in these parameters reflect differing predictions of the strength of the $Cl^-(H_2O)$ hydrogen bond. Table 16 summarizes the theoretical and experimental thermochemistry. We see that the MP2/6-311++G** gives the most accurate prediction of the room temperature bond enthalpy. Since the MP2 formalism neglects destabilizing single excitations out of the zeroth order wave function, it tends to overestimate the strength of intermolecular interactions. On the other hand, the modest 6-311++G** basis set is far from saturated, particularly in the polarization space. A lack of sufficient *d* and *f* basis functions would lead to an underestimate of the strength of intermolecular interactions. The accuracy of the MP2/6-311++G** prediction, then, is likely due to a

cancellation of errors.

We find no spectroscopic evidence for the C_{2v} isomer **Ib** (Figure 1), which is predicted to be a transition state with two highly bent hydrogen bonds (Table 2). The imaginary frequency corresponds to the rocking motion of the H_2O, which connects the two equivalent C_s minima (Table 9). While the barrier to H atom exchange ΔE_o is predicted to be only ~1 kcal/mol, both OH stretches of **Ib** are red-shifted by only 60-90 cm^{-1} (Figure 10a). However, we observe no bands in the 3500-3650 cm^{-1} region.

C. $Cl^-(H_2O)(CCl_4)$. The free OH stretch in $Cl^-(H_2O)$ is predicted to be ~35 times weaker than the bonded OH stretch (Table 8), but the signal-to-noise of our experimental spectrum (Figure 9a) should be sufficient to observe it. This was not the case. We did observe the free OH stretch at 3698 cm^{-1} by loss of CCl_4 from the cluster $Cl^-(H_2O)(CCl_4)$. No loss of H_2O, however, was observed upon infrared excitation of $Cl^-(H_2O)(CCl_4)$.

One would assume that the non-polar CCl_4 only weakly perturbs $Cl^-(H_2O)$. However, the one experimental binding enthalpy for the complex $Cl^-(CCl_4)$, reported by Dougherty *et al.*,[33] is 14.2 kcal/mol, virtually identical to the accepted $Cl^-(H_2O)$ binding enthalpy. There is reason to believe, however, that there was a systematic error in the measurements of Dougherty *et al.* In the same paper, they report that the binding enthalpy in $Cl^-(CHCl_3)$ is 19.1 kcal/mol, which differs greatly from the 15.2 kcal/mol value reported by Yamdagni and Kebarle.[34]

To further verify our assumption that CCl_4 is a messenger ligand which does not strongly perturb $Cl^-(H_2O)$, we undertook a systematic *ab initio* study of the

thermochemistry of $Cl^-(CCl_4)$. Optimized geometries of CCl_4 and $Cl^-(CCl_4)$ are reported in Table 3, and vibrational frequencies are reported in Tables 10 and 11.

As shown in Figure 5, Cl^- forms a stable C_{3v} complex by binding to one of the Cl atoms of CCl_4. Interestingly, the C-Cl bond attacked by the Cl^- ion is predicted (at both the HF and MP2 levels) to be shorter than the free C-Cl bonds and the C-Cl bonds of CCl_4 monomer (Table 3). This is consistent with the blue shift of the bonded C-Cl stretch (928 cm^{-1} in the complex *vs.* 899 cm^{-1} in the monomer) (Tables 10 and 11). Our results are consistent with HF calculations on $Cl^-(CCl_4)$ previously reported by Vetter and Zülicke.[35]

The binding energies of $Cl^-(CCl_4)$ computed with a variety of basis sets and methods are listed in Table 17. The MP2 estimate of ΔH_{298} appears to converge (with increasing number of polarization functions) to ~10 kcal/mol, while the CCSD values may be ~1 kcal/mol smaller. The important point is that at all levels of theory, $Cl^-(CCl_4)$ is predicted to be less strongly bound than $Cl^-(H_2O)$ by 5-6 kcal/mol (see Table 16). This is consistent with Dougherty *et al.*'s[33] 4 kcal/mol overestimate of the $Cl^-(CHCl_3)$ binding enthalpy as compared to the value of Yamdagni and Kebarle.[34] Our computational results, coupled with our observation that H_2O does not predissociate from $Cl^-(H_2O)(CCl_4)$, establishes that CCl_4 forms a significantly weaker bond to Cl^- ion than does H_2O.

Our inability to observe the free OH stretch for $Cl^-(H_2O)$ itself may be due to the predissociation mechanism. Since the complex is bound by ~15 kcal/mol, it dissociates by a stepwise-resonant two-photon process. A large anharmonicity in the free OH stretch

shifts the second step out of resonance by ~200 cm^{-1}, and could greatly reduce the Cl^- photofragment yield. In contrast, one-photon excitation of the broad ionic OH stretch band may couple to a quasi-continuum, allowing for facile dissociation with a second photon. As discussed in Chapter 3, a similar mechanism may account for intensity anomalies in the spectrum of $NO^+(H_2O)$. Support for this mechanism also comes from the fact that the free OH stretch is observed directly[25a,26a] for $I^-(H_2O)$, which is the weakest bound halide monohydrate, but not for $Br^-(H_2O)$.[29]

D. $Cl^-(H_2O)_2$. The spectrum (Figure 9b) demonstrates that Cl^- ion is solvated by two nearly equivalent and independent waters. The dominant doublet with maxima at 3245 cm^{-1} and 3317 cm^{-1} provides clear evidence of two strong ionic hydrogen bonds.[36] The absence of peaks from 3500 to 3650 cm^{-1} indicates that the waters do not hydrogen bond to each other.

In addition to our calculations for the n = 2 minimum (Table 4), we identified three n = 2 isomers (shown in Figure 2) not previously reported in the literature. The relative stabilities presented here were calculated at the MP2/6-311++G** level. Isomer **IIb** (Table 5) is a non-planar C_s transition state for the exchange of the two waters of **IIa**, with a barrier height ΔE_o of ~0.6 kcal/mol. In the absence of hydrogen bonding between the waters, the electrostatic repulsion between the H_2O dipoles causes the H-Cl-H angle to open from 66° to 125°. Rotation of the waters into the H-Cl-H plane gives rise to a W-shaped C_{2v} second-order transition state **IIc** (Table 6) with ΔE_o slightly more than ~0.6 kcal/mol above the C_1 minimum. At this stationary point, the H-Cl-H is opened slightly more, to 130°. Finally, a strictly linear C_{2h} structure **IId** (Table 7) was found to be a

third-order transition state with $\Delta E_o \sim 0.9$ kcal/mol above **IIa**. The MP2 potential energy surface is clearly quite flat, with a barrier against breaking the water-water hydrogen bond of less than 1 kcal/mol. Computationally, the very flat potential made it necessary that the gradients of all $n = 2$ structures be minimized to $\leq 1 \times 10^{-8}$ hartrees/bohr.

Our experimental spectrum is not consistent with the predictions for **IIa**. The spectrum of the *ab initio* minimum (Figure 10b) contains four distinct bands whose intensities decrease monotonically with increasing frequency. The two ion-bound OH stretches are chemically distinct and split by more than 300 cm^{-1} (Table 12). Our experimental spectrum, however, contains only three bands. The two red-shifted bands are of comparable intensity, and are split by only 70 cm^{-1}. The structure probed by our experiment cannot be the asymmetric isomer **IIa** (Figure 2).

The apparent absence of hydrogen bonding between the waters in $Cl^-(H_2O)_2$ suggests that one of the other *ab initio* structures may have been probed by our experiment. The harmonic splittings of 20-30 cm^{-1} predicted for the Cl^--bound OH stretches (Tables 13-15) are also more consistent with the experimental data. Our *ab initio* results demonstrate how the relative intensities of the two bonded OH stretches track the angle between the ionic hydrogen bonds. For **IIb**, which has a H--Cl--H angle of 125°, the more red-shifted antisymmetric stretch band (at 3547 cm^{-1}, unscaled) is predicted to be almost four times more intense than the symmetric stretch band at 3572 cm^{-1}. By the time the angle opens up to 180°, the symmetric band is forbidden by symmetry to have any infrared oscillator strength. However, in the experimental structure, the less red-shifted OH stretch is the more intense band. Therefore, the

structure probed by our experiment is considerably more bent than any of the other three $n = 2$ isomers we identified. Although we did not find an *ab initio* minimum lacking water-water hydrogen bonding, our spectrum is consistent with a very bent structure with two nearly equivalent ionic hydrogen bonds and no water-water hydrogen bonds.

The discrepancy between experiment and theory may be due to large amplitude motions. As noted above, the small differences in the energies of the *ab initio* stationary points reveal a very flat potential. Either zero-point motion or high cluster temperature could make the complex less rigid. The classical Monte Carlo simulations of Asada *et al.*[16] and the quantum molecular dynamics simulations of Dang and co-workers[17] both indicate that the interactions between the waters of $Cl^-(H_2O)_2$ are very dynamic in nature. Quantum chemical methods which can locate only stationary points of the potential are likely inadequate for interpreting experimental probes of cluster structure.

Our results suggest that $Cl^-(H_2O)_2$ is asymmetrically solvated in the absence of water-water hydrogen bonds. This has also been observed for $I^-(CH_3CN)_2$ by Johnson and co-workers.[26b] The stability of this bent geometry may be due not only to residual water-water interactions, but also to a cooperative effect in which the binding of one water to the polarizable Cl^- ion induces a dipole which favors and is enhanced by the binding of a second water to the same side of the ion. As discussed above, the role of ion polarizability in asymmetric solvation has been predicted by the molecular dynamics calculations of Sung and Jordan.[7] This effect is not limited to anions. HF calculations by Bauschlicher *et al.*[37] indicate that any ion with a large enough polarizability will be asymmetrically solvated. They predicted that $Ca^{2+}(H_2O)_2$ is bent by 126°, and that

$Sr^{2+}(H_2O)_2$ is bent by 116°. In their electronic structure calculations, Bauschlicher *et al.* estimate that the polarization of the core 4*s* and 4*p* orbitals in Sr^{2+} stabilizes the bent $Sr^{2+}(H_2O)_2$ geometry by 2.2 kcal/mol.

In spite of the enhancement effect, the removal of one water from $Cl^-(H_2O)_2$ requires less energy than does the removal of one water from $Cl^-(H_2O)$. As seen in Tables 16 and 18, the second H_2O is bound by 1.5-2 kcal/mol less. Interesting, the MP2 calculations miss this trend.

E. $Cl^-(H_2O)_3$ and $Cl^-(H_2O)_4$. Adding a third and fourth water increases the intensity of the water-bound OH stretch. The $n = 3$ spectrum may contain peaks at ~3530 and ~3630 cm^{-1} barely discernible above the background. For $n = 4$, we observe a peak at 3590 cm^{-1} with an intensity ~20% of that of the ion-bound OH stretch. This trend is consistent with the vibrational spectra predicted by Xantheas for the ground state isomers (Figures 10c, 10d). However, no $n = 3$ or $n = 4$ *ab initio* isomer by itself fully accounts for the spectra we observe. As a result, we cannot assign explicit structures for the $n = 3$ and $n = 4$ clusters.

For $n = 3$, a mixture of the pyramidal (**IIIa**) and ring (**IIIb**) isomers (Figure 3) may account for the strong ion-bound OH stretches at 3257 cm^{-1} and 3357 cm^{-1} (Figure 9c). However, any water-bound OH stretches are weak at best, while Xantheas[14] predicts that for either isomer this band has an intensity ≥ 40% of that of the ion-bound OH stretch. It is possible that in $Cl^-(H_2O)_3$ three equivalent waters form hydrogen bonds to Cl^- but not to each other. The splitting of the ionic OH stretches would then be due to modes of A_1 and E symmetry of a C_{3v} complex. Observation of the totally symmetric

stretching mode means that $Cl^-(H_2O)_3$ is not internally solvated in a planar complex. Our spectrum is consistent with a pyramidal-like structure as predicted by *ab initio* theory but without water-water hydrogen bonding. Johnson and co-workers[29] also fail to see water-bound OH stretches in the spectra of $Br^-(H_2O)_3$ and $I^-(H_2O)_3$. Quantum or temperature effects in $n = 3$ may account for the same discrepancy between theory and experiment seen for $n = 2$.

Similarly, theory seems to overestimate the extent of water-water association for $n = 4$ (Figure 10d). The pyramidal isomer **IVa**, with its ring of four waters, has a water-bound OH stretch predicted by Xantheas[14] to be at ~3540 cm^{-1} which is more intense than the ion-bound OH stretch. However, the water-bound OH stretch we see (3590 cm^{-1}) is much weaker than the ionic OH stretch (3408 cm^{-1}) (Figure 9d). The smaller red shift seen for the water-bound OH stretch may be due to a smaller ring of waters, as in the 3+1 isomer **IVb**. This isomer has a series of peaks from 3375 cm^{-1} to 3650 cm^{-1} which is consistent with the broad absorption underlying our spectrum. However, the 3+1 isomer cannot account for the free OH stretch at 3694 cm^{-1}. Our spectrum suggests a more open structure with at least one free OH bond, as in the HF isomer **IVc** identified by Jortner and co-workers.[10] Although MP2 theory indicates that the fourth H_2O is attracted to the remaining waters, this interaction could again be attenuated by quantum or temperature effects. The appearance of several weak peaks may indicate the presence of more than one isomer.

F. $Cl^-(H_2O)_n$, n = 5-7. The spectra of larger $Cl^-(H_2O)_n$ clusters (Figures 9e and 11) differ considerably from the spectra of n = 1-4. They dominated by broad absorptions

from 3100 to 3750 cm^{-1} and resemble the infrared spectra of large neutral water clusters.[38,39] The free OH stretch is clearly present at ~3700 cm^{-1} for all four spectra and implies that not all OH bonds participate in hydrogen bonding.

Although we have no *ab initio* calculations for these larger systems, the trends seen for smaller clusters allow us to assign the distinct features for the $n = 5$ spectrum in Figure 9. We assign the peak at 3441 cm^{-1} to the ion bound OH stretch, based on the blue shift of this band with increasing n. We assign the peak at 3548 cm^{-1} to the water-bound OH stretch, assuming the red shift of this band with increasing n.

Of the remaining bands, the peak at 3233 cm^{-1} is most notable. Although the most red-shifted band of ionic cluster spectra is typically an ion-bound OH stretch, the 3233 cm^{-1} band does not follow the trend we see for smaller clusters. It is even more red-shifted than the ion-bound OH stretch in $n = 1$. Such a large red shift could be caused by cooperative hydrogen bonding in cyclic $(H_2O)_n$ structures. Vernon *et al.*[38] and Huisken[39] have observed a similar band in the spectra of large neutral water clusters. Xantheas and Dunning[40] have predicted that the water-bound OH stretch can red-shift by as much as ~500 cm^{-1} in $(H_2O)_4$. The peak at 3233 cm^{-1} could thus be due to the ring OH stretch of cyclic water structures within the cluster. From the red shift we infer that the n=5 cluster contains rings of at least four waters.

Alternatively, the large red shift could be due to the Cl^--bound OH stretch of waters that are both hydrogen bond donors and acceptors. Our calculations for the $n = 2$ C_1 minimum (Figure 10b) predict that the ion-bound OH stretch of the donor/acceptor is red-shifted to 3204 cm^{-1} (scaled). This band position is also to the red of what is

observed and predicted for the $n = 1$ bonded OH stretch. The 3233 cm^{-1} band, then, could be evidence for the formation of a second solvation shell; one or more H_2Os in the first shell donate an H atom to Cl^- ion, and accept an H atom from an H_2O in the second shell. This picture is reminiscent of that proposed by Viggiano and co-workers,[24] although the transition happens at a different value of n.

Since the spectra reported in Figure 9 were likely taken at high cluster temperatures (*cf.* Figure 6), it is possible that the $n = 5$ parent ion packet contained a mixture of low-lying isomers. This would broaden the spectrum as observed. To test this idea, the vibrational spectrum of $Cl^-(H_2O)_5$ was remeasured with the cluster ion distribution shown in Figure 7. The preliminary results (Figure 11a) substantially resemble the earlier spectrum. While the signal-to-noise in the 3200 cm^{-1} region is not sufficient to tell if the very red-shifted feature is still present, the overall breadth of the spectrum is the same. It is possible that the broad absorption is not due to high temperature. Alternatively, the clusters may still be hot, shifted distribution notwithstanding.

The preliminary spectrum of $n = 6$ (Figure 11b) resembles the spectrum of $I^-(H_2O)_6$ obtained by Johnson and co-workers.[29] There appears to be a prominent red-shifted feature centered at 3296 cm^{-1}. Again, the location of the band does not follow the trend for the ion-bound OH stretches seen for smaller clusters. It may be a signature either of cooperative hydrogen bonding among rings of waters, or of hydrogen bonding between solvation shells.

The preliminary $n = 7$ spectrum (Figure 11c) is broad, again resembling the

spectra of neutral water clusters. It also has a very distinct free OH stretch band centered at 3698 cm^{-1}, indicating that the cluster does not form completely closed structures. An action spectrum (not shown) in the 3500-3750 cm^{-1} was also obtained for the loss of two waters from the $n = 7$ parent. It had the same appearance as the spectrum due to loss of one water. This suggests the importance of statistical dissociation for these larger systems.

4.4 CONCLUSION

The structures we infer from our spectra have less hydrogen bonding than predicted by theory. These discrepancies are most likely due either to zero-point effects or high cluster temperature, which would favor large amplitude motions and lead to the breaking of water-water hydrogen bonds. As a result, we would not observe the *ab initio* ground state isomers, but rather a mixture of low-lying isomers, particularly for $n \geq 5$. Because the clusters are hot, we cannot tell if zero-point motion alone would cause the breaking of hydrogen bonds among the waters.

Despite the ambiguity from high temperature and multiple isomers, the current data provide strong evidence that Cl^- is surface solvated for larger clusters. The $n = 4$-7 spectra reveal water-water hydrogen bonding networks, and the $n = 5$-7 spectrum themselves resemble those of large neutral water clusters. It is noteworthy that we observe surface solvation even at high temperature, which is predicted to favor interior solvation states. For $n = 2$ and 3 we observe that Cl^- ion is asymmetrically solvated without hydrogen bonding between the waters. This disagreement with the ground state *ab initio* structures may be due to temperature or zero-point energy effects which lead to

breaking of the water-water hydrogen bonds.

For further work, it would be worthwhile to study the infrared spectra of larger ($n \geq 5$) clusters more thoroughly, both experimentally and computationally. Features to the red of ~3400 cm^{-1} could reveal more definitive evidence of cooperative hydrogen bonding within rings of water molecules. Very recent work by Wang *et al.*[41] indicates that careful scanning of the free OH region (~3700 cm^{-1}) can also reveal critical details of the coordination numbers of H_2Os within large clusters.

4.5 REFERENCES AND NOTES

(1) Lybrand, T. P.; Kollman, P. A. *J. Chem. Phys.* **1985**, *83*, 2923.

(2) Jorgensen, W. L.; Severance, D. L. *J. Chem. Phys.* **1993**, *99*, 4233.

(3) Lin, S.; Jordan, P. C. *J. Chem. Phys.* **1988**, *89*, 7492.

(4) (a) Perera, L.; Berkowitz, M. L. *J. Chem. Phys.* **1991**, *95*, 1954. (b) Perera, L.; Berkowitz, M. L. *J. Chem. Phys.* **1993**, *99*, 4236.

(5) Stuart, S. J.; Berne, B. J. *J. Phys. Chem.* **1996**, *100*, 11934.

(6) Perera, L.; Berkowitz, M. L. *J. Chem. Phys.* **1992**, *96*, 8288.

(7) Sung, S.-S.; Jordan, P. C. *J. Chem. Phys.* **1986**, *85*, 4045.

(8) Coker, H. *J. Phys. Chem.* **1976**, *80*, 2084.

(9) Truong, T. N.; Stefanovich, E. V. *Chem. Phys.* **1997**, *218*, 31.

(10) (a) Combariza, J. E.; Kestner, N. R.; Jortner, J. *Chem. Phys. Lett.* **1993**, *203*, 423.

(b) Combariza, J. E.; Kestner, N. R.; Jortner, J. *J. Chem. Phys.* **1994**, *100*, 2851.

(11) Okuno, Y. *J. Chem. Phys.* **1996**, *105*, 5817.

(12) Dunbar, R. C.; McMahon, T. B.; Thölmann, D.; Tonner, D. S.; Salahub, D. R.; Wei, D. *J. Am. Chem. Soc.* **1995**, *117*, 12819.

(13) Caldwell, J. W.; Kollman, P. A. *J. Phys. Chem.* **1992**, *96*, 8249.

(14) Xantheas, S. S. *J. Phys. Chem.* **1996**, *100*, 9703.

(15) Sremaniak, L. S.; Perera, L.; Berkowitz, M. L. *J. Phys. Chem.* **1996**, *100*, 1350.

(16) (a) Asada, T.; Nishimoto, K.; Kitaura, K. *J. Phys. Chem.* **1993**, *97*, 7724. (b) Asada, T.; Nishimoto, K.; Kitaura, K. *J. Molec. Struct. (Theochem)* **1994**, *310*, 149.

(17) Gai, H.; Dang, L. X.; Schenter, G. K.; Garrett, B. C. *J. Phys. Chem.* **1995**, *99*, 13303.

(18) (a) Zhao, X. G.; Gonzalez-Lafont, A.; Truhlar, D. G.; Steckler, R. *J. Chem. Phys.* **1991**, *94*, 5544. (b) Zhan, C.-G.; Iwata, S. *Chem. Phys. Lett.* **1995**, *232*, 72.

(19) Keesee, R. G.; Castleman, A. W., Jr. *J. Phys. Chem. Ref. Data* **1986**, *15*, 1011, and references therein.

(20) Hiraoka, K.; Mizuse, S.; Yamabe, S. *J. Phys. Chem.* **1988**, *92*, 3943.

(21) Hiraoka, K. *Bull. Chem. Soc. Jpn.* **1987**, *60*, 2555.

(22) Markovich, G.; Pollack, S.; Giniger, R.; Cheshnovsky, O. *J. Chem. Phys.* **1994**, *101*, 9344.

(23) (a) Perera, L.; Berkowitz, M. L. *Z. Phys. D* **1993**, *26*, 166. (b) Perera, L.; Berkowitz, M. L. *J. Chem. Phys.* **1993**, *99*, 4222. (c) Yeh, I.-C.; Perera, L.; Berkowitz, M. L. *Chem. Phys. Lett.* **1997**, *264*, 31.

(24) Seeley, J. V.; Morris, R. A.; Viggiano, A. A. *J. Phys. Chem.* **1996**, *100*, 15821.

(25) (a) Johnson, M. S.; Kuwata, K. T.; Wong, C.-K.; Okumura, M. *Chem. Phys. Lett.* **1996**, *260*, 551. (b) Cao, Y.; Choi, J.-H.; Haas, B.-M.; Johnson, M. S.; Okumura, M. *J. Chem. Phys.* **1993**, *99*, 9307. (c) Choi, J.-H.; Kuwata, K. T.; Haas, B.-M.; Cao, Y.; Johnson, M. S.; Okumura, M. *J. Chem. Phys.* **1994**, *100*, 7153. (d) Cao, Y.; Choi, J.-H.; Haas, B.-M.; Okumura, M. *J. Phys. Chem.* **1994**, *98*, 12176.

(26) (a) Bailey, C. G.; Kim, J.; Dessent, C. E. H.; Johnson, M. A. *Chem. Phys. Lett.* **1997**, *269*, 122. (b) Dessent, C. E. H.; Bailey, C. G.; Johnson, M. A. *J. Chem. Phys.* **1995**, *103*, 2006.

(27) (a) Weinheimer, C. J.; Lisy, J. M. *Int. J. Mass Spect. Ion Process.* **1996**, *159*, 197. (b) Weinheimer, C. J.; Lisy, J. M. *J. Phys. Chem.* **1996**, *100*, 15305. (c) Weinheimer, C. J.; Lisy, J. M. *J. Chem. Phys.* **1996**, *105*, 2938.

(28) (a) Gruenloh, C. J.; Carney, J. R.; Arrington, C. A.; Zwier, T. S.; Fredericks, S. Y.; Jordan, K. D. *Science* **1997**, *276*, 1678. (b) Pribble, R. N.; Hagemeister, F. C.; Zwier, T. S. *J. Chem. Phys.* **1997**, *106*, 2145. (c) Zwier, T. S. *Ann. Rev. Phys. Chem.* **1996**, *47*, 205, and references therein.

(29) Ayotte, P.; Bailey, C. G.; Johnson, M. A. *J. Phys. Chem.*, submitted.

(30) Choi, J.-H. Ph.D. Thesis, California Institute of Technology, 1995.

(31) Frisch, M. J.; Trucks, G. W.; Head-Gordon, M.; Gill, P. M. W.; Wong, M. W.; Foresman, J. B.; Johnson, B. G.; Schlegel, H. B.; Robb, M. A.; Replogle, E. S.; Gomperts, R.; Andres, J. L.; Raghavachari, K.; Binkley, J. S.; Gonzalez, C.; Martin, R. L.; Fox, D. J.; Defrees, D. J.; Baker, J.; Stewart, J. J. P.; Pople, J. A. *Gaussian 92, Revision D.2.*, Gaussian, Inc., Pittsburgh, PA, 1992.

(32) Herzberg, G. *Molecular Spectra and Molecular Structure. II. Infrared and Raman Spectra of Polyatomic Molecules*; van Nostrand Reinhold: New York, 1945; Chapter 3.

(33) Dougherty, R. C.; Dalton, J.; Roberts, J. D. *Org. Mass Spect.* **1974**, *8*, 77.

(34) Yamdagni, R.; Kebarle, P. *J. Am. Chem. Soc.* **1971**, *93*, 7139.

(35) Vetter, R.; Zülicke, L. *Chem. Phys.* **1986**, *101*, 201.

(36) Both harmonic and anharmonic terms should split the infrared bands of the ionic hydrogen bonds. Alternatively, one of the red-shifted bands may correspond to the bending overtone of one of the H_2O's. However, since the n=1 bending overtone is only ~10% of the intensity of the n=1 bonded OH stretch fundamental, it is unlikely that the n=2 bending overtone could be of comparable intensity to the bonded OH stretch. Also, since the H_2O bending fundamental is predicted to blue shift only ~20 cm^{-1} in going from n=1 to n=2, it is unlikely that the bending overtone will shift from 3156 cm^{-1} to 3245 cm^{-1}.

(37) Bauschlicher, C. W., Jr.; Sodupe, M.; Partridge, H. *J. Chem. Phys.* **1992**, *96*, 4453.

(38) Vernon, M. F.; Krajnovich, D. J.; Kwok, H. S.; Lisy, J. M.; Shen, Y. R.; Lee, Y. T. *J. Chem. Phys.* **1982**, *77*, 47.

(39) Huisken, F. Private communication.

(40) Xantheas, S. S.; Dunning, T. H., Jr. *J. Chem. Phys.* **1993**, *99*, 8774.

(41) Wang, Y.-S.; Jiang, J. C.; Cheng, C.-L.; Lin, S. H.; Lee, Y. T.; Chang, H.-C. *J. Chem. Phys.* **1997**, *107*, 9695.

TABLE 1: Optimized Geometries of the $Cl^-(H_2O)$ C_s Linear Isomer at Various Levels of Theory[a,b]

	MP2/ 6-31+G**	MP2/ 6-311++G**	CCSD/ 6-311++G**
$r(Cl\text{-}H_1)$	2.215	2.151	2.189
$r(H_1\text{-}O)$	0.993	0.984	0.978
$r(O\text{-}H_2)$	0.970	0.959	0.958
$\theta(Cl\text{-}H_1\text{-}O)$	163.9	165.4	164.7
$\theta(H_1\text{-}O\text{-}H_2)$	101.6	100.0	100.4
$\tau(Cl\text{-}H_1\text{-}O\text{-}H_2)$	0.0	0.0	0.0

[a] Bond lengths in Å; bond angles in deg.

[b] Atoms are labeled as in Figure 1a.

TABLE 2: Optimized Geometries of the $Cl^-(H_2O)$ C_{2v} Bridged Isomer at Various Levels of Theory[a]

	MP2/ 6-311++G**	CCSD/ 6-311++G**
r(Cl-H)	2.649	2.675
r(H-O)	0.966	0.963
θ(H-O-H)	96.0	96.6
τ(Cl-H-O-H)	0.0	0.0

[a] Bond lengths in Å; bond angles in deg.

TABLE 3: Optimized Geometries of CCl_4 and $Cl^-(CCl_4)$ at Various Levels of Theory[a,b]

	HF/ 6-31+G*	MP2/ 6-31+G*
CCl_4		
r(C-Cl)	1.767	1.771
$Cl^-(CCl_4)$		
$r(Cl_1\text{--}Cl_2)$	3.234	2.971
$r(C\text{-}Cl_2)$	1.745	1.754
$r(C\text{-}Cl_3)$	1.779	1.788
$\theta(Cl_1\text{-}Cl_2\text{-}C)$	180.0	180.0
$\theta(Cl_2\text{-}C\text{-}Cl_3)$	110.6	110.9
$\theta(Cl_3\text{-}C\text{-}Cl_3)$	108.3	108.0
$\tau(Cl_1\text{-}Cl_2\text{-}C\text{-}Cl_3)$	0, ±120	0, ±120

[a] Bond lengths in Å; bond angles in deg.

[b] Atoms are labeled as in Figure 5.

TABLE 4: Optimized Geometries of the $Cl^-(H_2O)_2$ C_1 Isomer at Various Levels of Theory[a,b]

	HF/ 6-31+G*	MP2/ 6-31+G*	MP2/ 6-311++G**
$r(Cl\text{--}H_1)$	2.336	2.157	2.096
$r(O_1\text{-}H_1)$	0.962	0.995	0.987
$r(O_1\text{-}H_2)$	0.948	0.971	0.959
$r(O_1\text{--}H_3)$	2.228	2.122	2.190
$r(O_2\text{-}H_3)$	0.951	0.977	0.964
$r(O_2\text{-}H_4)$	0.955	0.982	0.972
$r(Cl\text{--}H_4)$	2.644	2.451	2.381
$\theta(H_1\text{-}Cl\text{-}H_4)$	66.2	66.3	66.0
$\theta(Cl\text{-}H_1\text{-}O_1)$	157.8	164.2	167.1
$\theta(H_1\text{-}O_1\text{-}H_2)$	103.2	102.7	101.2
$\theta(H_3\text{-}O_1\text{-}H_1)$	83.4	83.2	80.9
$\theta(O_2\text{-}H_3\text{-}O_1)$	149.6	147.6	144.6
$\theta(H_3\text{-}O_2\text{-}H_4)$	102.8	100.9	99.5
$\theta(Cl\text{-}H_4\text{-}O_2)$	148.2	151.8	156.1
$\tau(Cl\text{-}H_1\text{-}O_1\text{-}H_2)$	39.4	55.0	56.1
$\tau(Cl\text{-}H_1\text{-}O_1\text{-}H_3)$	-58.6	-48.8	-54.7
$\tau(H_1\text{-}O_1\text{-}H_3\text{-}O_2)$	30.9	20.0	14.6
$\tau(O_1\text{-}H_3\text{-}O_2\text{-}H_4)$	-16.6	-11.3	-6.8

[a] Bond lengths in Å; bond angles in deg.

[b] Atoms are labeled as in Figure 2a.

TABLE 5: MP2 Optimized Geometries of the $Cl^-(H_2O)_2$ C_s Isomer with Various Basis Sets[a,b]

	6-31+G*	6-311++G**
r(Cl--H_1)	2.224	2.186
r(O-H_1)	0.982	0.980
r(O-H_2)	0.963	0.959
θ(H_1-Cl-H_1)	125.7	124.8
θ(Cl-H_1-O)	178.6	178.1
θ(H_1-O-H_2)	101.8	100.4
τ(H_1-Cl-H_1-O)	±196.1	±194.6
τ(Cl-H -O-H_2)	±1.9	±2.4

[a] Bond lengths in Å; bond angles in deg.

[b] Atoms are labeled as in Figure 2b.

TABLE 6: Optimized Geometries of the $Cl^-(H_2O)_2$ C_{2v} Isomer at Various Levels of Theory[a,b]

	HF/ 6-31+G*	MP2/ 6-311++G**
$r(Cl\text{--}H_1)$	2.444	2.189
$r(O\text{-}H_1)$	0.958	0.980
$r(O\text{-}H_2)$	0.947	0.959
$\theta(H_1\text{-}Cl\text{-}H_1)$	162.7	129.7
$\theta(Cl\text{-}H_1\text{-}O)$	153.3	165.5
$\theta(H_1\text{-}O\text{-}H_2)$	102.5	100.3
$\tau(O\text{-}H_1\text{-}H_1\text{-}O)$	0.0	0.0

[a] Bond lengths in Å; bond angles in deg.

[b] Atoms are labeled as in Figure 2c.

TABLE 7: Optimized Geometry of the $Cl^-(H_2O)_2$ C_{2h} Linear Isomer[a,b]

	MP2/ 6-311++G**
r(Cl--H_1)	2.223
r(O-H_1)	0.978
r(O-H_2)	0.959
θ(H_1-Cl-H_1)	180.0
θ(Cl-H_1-O)	162.4
θ(H_1-O-H_2)	100.0
τ(O-H_1-H_1-O)	180.0

[a] Bond lengths in Å; bond angles in deg.

[b] Atoms are labeled as in Figure 2d.

TABLE 8: Harmonic Vibrational Frequencies and Infrared Intensities of the $Cl^-(H_2O)$ C_s Linear Isomer at Various Levels of Theory[a,b]

	Approx Description	MP2/ 6-31+G**	MP2/ 6-311++G**	CCSD/ 6-311++G**
$\omega_1(A')$	Free OH stretch	3829(50)	3952(30)	3952
$\omega_2(A')$	Bonded OH stretch	3435(851)	3475(1026)	3577
$\omega_3(A')$	H_2O bend	1747(152)	1708(102)	1734
$\omega_4(A')$	H_2O rock	344(84)	361(73)	348
$\omega_5(A')$	Cl--H intermol stretch	188(20)	184(24)	177
$\omega_6(A'')$	H_2O wag	754(162)	754(120)	739

[a] Frequencies in cm^{-1}; infrared intensities in km/mol.

[b] Infrared intensities not calculated at the CCSD level of theory.

TABLE 9: Harmonic Vibrational Frequencies and Infrared Intensities of the $Cl^-(H_2O)$ C_{2v} Bridged Isomer[a]

	Approx Description	MP2/ 6-311++G**
$\omega_1(A_1)$	OH sym stretch	3844(111)
$\omega_2(A_1)$	H_2O bend	1698(246)
$\omega_3(A_1)$	Cl--H intermol stretch	156(14)
$\omega_4(B_1)$	H_2O wag	643(198)
$\omega_5(B_2)$	OH antisym stretch	3877(59)
$\omega_6(B_2)$	H_2O rock	290*i*(120)

[a] Frequencies in cm^{-1}; infrared intensities in km/mol.

TABLE 10: Harmonic Vibrational Frequencies and Infrared Intensities of $Cl^-(CCl_4)$[a]

	Approx Description	HF/ 6-31+G*
$\omega_1(A_1)$	Bonded C-Cl stretch	928(93)
$\omega_2(A_1)$	Free C-Cl stretch	492(9)
$\omega_3(A_1)$	CCl_3 scissor	344(7)
$\omega_4(A_1)$	Cl--Cl intermol stretch	76(42)
$\omega_5(E)$	Free C-Cl stretch	865(184)
$\omega_6(E)$	CCl_2 wag	349(0)
$\omega_7(E)$	CCl_2 twist	245(0)
$\omega_8(E)$	Cl--Cl-C bend	49(6)

[a] Frequencies in cm^{-1}; infrared intensities in km/mol.

TABLE 11: Harmonic Vibrational Frequencies and Infrared Intensities of CCl_4[a]

	Approx Description	HF/ 6-31+G**	Exp[b]
$\omega_1(A_1)$	C-Cl stretch	502(0)	458
$\omega_2(E)$	Cl-C-Cl bend	242(0)	218
$\omega_3(T_2)$	C-Cl stretch	899(156)	776
$\omega_4(T_2)$	Cl-C-Cl bend	347(0)	314

[a] Frequencies in cm^{-1}; infrared intensities in km/mol.

[b] Taken from ref. 32.

TABLE 12: MP2 Harmonic Vibrational Frequencies and Infrared Intensities of the $Cl^-(H_2O)_2$ C_1 Isomer at Various Levels of Theory[a,b]

	Approx Description	HF/ 6-31+G*	MP2/ 6-31+G*	MP2/ 6-311++G**
ω_1	Free OH stretch	4138(70)	3826(56)	3949(36)
ω_2	H_2O bound OH stretch	4096(201)	3739(218)	3868(146)
ω_3	Cl^- bound OH stretch	3995(196)	3621(294)	3719(401)
ω_4	Cl^- bound OH stretch	3867(480)	3376(846)	3408(1008)
ω_5	DD H_2O bend	1875(223)	1776(194)	1730(125)
ω_6	DD H_2O bend	1860(135)	1751(126)	1704(80)
ω_7	DA H_2O wag	788(292)	832(228)	813(172)
ω_8	DD H_2O wag	679(291)	709(241)	669(192)
ω_9	DD H_2O rock	461(22)	503(18)	474(39)
ω_{10}	DA H_2O rock	374(77)	416(73)	416(61)
ω_{11}	IP H_2O twist	277(46)	353(30)	364(18)
ω_{12}	OOP H_2O twist	208(108)	219(92)	207(32)
ω_{13}	Antisym Cl--H stretch	174(23)	210(48)	180(88)
ω_{14}	Sym Cl--H stretch	141(5)	172(5)	157(2)
ω_{15}	H--Cl--H bend	81(1)	102(1)	88(0)

[a] Frequencies in cm^{-1}; infrared intensities in km/mol.

[b] DA=donor/acceptor; DD=double donor; IP=in phase; OOP=out of phase.

TABLE 13: MP2 Harmonic Vibrational Frequencies and Infrared Intensities of the $Cl^-(H_2O)_2$ C_s Isomer with Various Basis Sets[a,b]

	Approx Description	6-31+G*	6-311++G**
$\omega_1(A')$	IP free OH stretch	3952(55)	3955(55)
$\omega_2(A')$	Sym bonded OH stretch	3595(286)	3572(370)
$\omega_3(A')$	IP H_2O bend	1684(73)	1706(41)
$\omega_4(A')$	IP H_2O wag	742(224)	771(183)
$\omega_5(A')$	OOP H_2O rock	332(127)	342(131)
$\omega_6(A')$	Sym Cl--H stretch	162(4)	160(4)
$\omega_7(A')$	OOP H_2O twist	53(124)	62(124)
$\omega_8(A')$	H--Cl--H bend	20(14)	21(9)
$\omega_9(A'')$	OOP free OH stretch	3950(45)	3954(18)
$\omega_{10}(A'')$	Antisym bonded OH stretch	3574(1190)	3547(1337)
$\omega_{11}(A'')$	OOP H_2O bend	1679(190)	1702(152)
$\omega_{12}(A'')$	OOP H_2O wag	713(54)	732(42)
$\omega_{13}(A'')$	IP H_2O rock	329(40)	342(26)
$\omega_{14}(A'')$	Antisym Cl--H stretch	195(28)	189(33)
$\omega_{15}(A'')$	IP H_2O twist	58*i*(35)	64*i*(33)

[a] Frequencies in cm^{-1}; infrared intensities in km/mol.

[b] IP=in phase; OOP=out of phase.

TABLE 14: Harmonic Vibrational Frequencies and Infrared Intensities of the $Cl^-(H_2O)_2$ C_{2v} Isomer at Various Levels of Theory[a,b]

	Approx Description	HF/ 6-31+G*	MP2/ 6-311++G**
$\omega_1(A_1)$	IP free OH stretch	4142(90)	3954(14)
$\omega_2(A_1)$	IP bonded OH stretch	3946(13)	3574(111)
$\omega_3(A_1)$	IP H_2O bend	1857(59)	1713(70)
$\omega_4(A_1)$	OOP H_2O rock	244(163)	372(43)
$\omega_5(A_1)$	Sym Cl--H stretch	120(0)	152(3)
$\omega_6(A_1)$	H--Cl--H bend	9(2)	24(1)
$\omega_7(A_2)$	OOP H_2O wag	665(0)	712(0)
$\omega_8(A_2)$	IP H_2O twist	40*i*(0)	55*i*(0)
$\omega_9(B_1)$	IP H_2O wag	670(493)	720(263)
$\omega_{10}(B_1)$	OOP H_2O twist	7(5)	36*i*(161)
$\omega_{11}(B_2)$	OOP free OH stretch	4141(49)	3953(57)
$\omega_{12}(B_2)$	OOP bonded OH stretch	3939(745)	3554(1621)
$\omega_{13}(B_2)$	OOP H_2O bend	1847(344)	1703(119)
$\omega_{14}(B_2)$	IP H_2O rock	234(34)	347(114)
$\omega_{15}(B_2)$	Antisym Cl--H stretch	170(30)	194(32)

[a] Frequencies in cm^{-1}; infrared intensities in km/mol.

[b] IP=in phase; OOP=out of phase.

TABLE 15: Harmonic Vibrational Frequencies and Infrared Intensities of the $Cl^-(H_2O)_2$ C_{2h} Linear Isomer[a]

	Approx Description	MP2/ 6-311++G**
$\omega_1(A_g)$	IP free OH stretch	3953(0)
$\omega_2(A_g)$	IP bonded OH stretch	3612(0)
$\omega_3(A_g)$	IP H_2O bend	1711(0)
$\omega_4(A_g)$	IP H_2O rock	314(0)
$\omega_5(A_g)$	Sym Cl--H stretch	137(0)
$\omega_6(A_u)$	IP H_2O wag	561(347)
$\omega_7(A_u)$	IP H_2O twist	25i(40)
$\omega_8(A_u)$	OOP H_2O twist	133i(63)
$\omega_9(B_g)$	OOP H_2O wag	684(0)
$\omega_{10}(B_u)$	OOP free OH stretch	3953(75)
$\omega_{11}(B_u)$	OOP bonded OH stretch	3584(1577)
$\omega_{12}(B_u)$	OOP H_2O bend	1684(228)
$\omega_{13}(B_u)$	OOP H_2O rock	216(167)
$\omega_{14}(B_u)$	Antisym Cl--H stretch	184(29)
$\omega_{15}(B_u)$	H--Cl--H bend	60i(8)

[a] Frequencies in cm^{-1}; infrared intensities in km/mol.

[b] IP=in phase; OOP=out of phase.

TABLE 16: Energetics[a] of the Reaction $Cl^-(H_2O) \rightarrow Cl^- + H_2O$ [b]

Source of Data	ΔE_e	ΔE_0	ΔH_{298}
MP2/6-31+G*	15.4	14.0	14.0
MP2/6-311++G**	15.5	14.2	14.2
CCSD/6-311++G**	15.0	13.6	13.5
Experiment (Ref. 19)			14.7

[a] Energies in kcal/mol.

[b] With reference to the more stable $Cl^-(H_2O)$ linear isomer.

TABLE 17: Energetics[a] of the Reaction $Cl^-(CCl_4) \rightarrow Cl^- + CCl_4$

Source of Data	ΔE_e	ΔE_0[b]	ΔH_{298}[b]
HF/6-31+G*	5.4	5.2	4.2
MP2/6-31+G*	9.2	9.0	8.1
MP2/6-311+G*[c]	9.5	9.3	8.4
MP2/6-311+G(2d)[c]	10.8	10.6	9.7
MP2/6-311+G(2df)[c]	10.9	10.7	9.7
MP2/6-311+G(3d)[c]	11.3	11.1	10.1
CCSD/6-31+G*[c]	8.5	8.3	7.3
Experiment (Ref. 19)			14.7

[a] Energies in kcal/mol.

[b] HF/6-31+G* vibrational frequencies used.

[c] At the MP2/6-31+G* optimized geometry.

TABLE 18: Energetics[a] of the Reaction $Cl^-(H_2O)_2 \rightarrow Cl^-(H_2O) + H_2O$ [b]

Source of Data	ΔE_e	ΔE_0	ΔH_{298}
MP2/6-31+G*	16.2	13.4	14.2
MP2/6-311++G**	15.7	13.1	13.9
Experiment			12.6, 13.0

[a] Energies in kcal/mol.

[b] With reference to the most stable C_1 $Cl^-(H_2O)_2$ isomer and the linear $Cl^-(H_2O)$ isomer.

4.6 FIGURE CAPTIONS

Figure 1. *Ab initio* stationary points predicted at the MP2/6-311++G** level for $Cl^-(H_2O)$. **Ia** is the C_s minimum. **Ib** is the C_{2v} transition state with ΔE_o~1.2 kcal/mol.

Figure 2. *Ab initio* stationary points predicted at the MP2/6-311++G** level for $Cl^-(H_2O)_2$. **IIa** is the C_1 minimum with three hydrogen bonds. **IIb** is a C_s stationary point similar to the interior state predicted by Jortner and co-workers (ref. 10). It is a transition state with ΔE_o ~0.6 kcal/mol. The H atoms not shown for **IIb** are pointing into the plane of the page. **IIc** is the C_{2v} second-order transition state with ΔE_o ~0.6 kcal/mol. **IId** is the C_{2h} third-order transition state with ΔE_o ~0.9 kcal/mol.

Figure 3. *Ab initio* minima of $Cl^-(H_2O)_3$ located by Xantheas (ref. 14) with MP2 theory. **IIIa** is the C_3 pyramidal global minimum. **IIIb** is the C_s ring minimum with ΔE_e=2.6 kcal/mol. Figures taken from ref. 14.

Figure 4. The top two structures are *ab initio* minima of $Cl^-(H_2O)_4$ located by Xantheas (ref. 14) with MP2 theory. **IVa** is the C_4 pyramidal global minimum. **IVb** is the C_1 "3+1" minimum with ΔE_e=2.1 kcal/mol. **IVc** is a minimum with less water-water hydrogen bonding predicted by Jortner and co-workers (ref. 10) with HF theory. Figures taken from refs. 10 and 14.

Figure 5. The weakly bound complex $Cl^-(CCl_4)$ and its fragmentation to CCl_4 and Cl^-. Structures determined at the MP2 level of theory.

Figure 6. The time-of-flight mass spectrum of $Cl^-(H_2O)_n$ typical of the spectra reported in the thesis of J.-H. Choi.

Figure 7. The time-of-flight mass spectrum of $Cl^-(H_2O)_n$ typical of the new $Cl^-(H_2O)_n$

infrared spectra reported for the first time in this thesis.

Figure 8. The time-of-flight mass spectrum of $Cl^-(H_2O)_n(CCl_4)_m$.

Figure 9. Infrared spectra of $Cl^-(H_2O)_n$ recorded by loss of H_2O. The n=1 inset shows loss of CCl_4 from $Cl^-(H_2O)(CCl_4)$ parent. The intensity of the inset peak is arbitrary.

Figure 10. *Ab initio* vibrational stick spectra of $Cl^-(H_2O)_n$ stationary points. Results for n=1 and n=2 are from this work; results for n=3 and n=4 are adapted from the work of Xantheas (ref. 14). The frequencies are scaled by the average of the experimental stretches of H_2O, and all infrared intensities are on the same scale for a given cluster size. In each spectrum, the solid lines correspond to the global minimum; the dotted lines, to the less stable minimum or transition state. (a) C_s minimum and C_{2v} transition state. (b) C_1 minimum and C_s transition state. (c) C_3 pyramidal global minimum and C_s ring minimum with ΔE_e=2.6 kcal/mol. (d) C_4 pyramidal global minimum and C_1 "3+1" minimum with ΔE_e=2.1 kcal/mol.

Figure 11. The vibrational predissociation spectra of larger $Cl^-(H_2O)_n$ clusters. (a) n = 5. (b) n = 6. (c) n = 7.

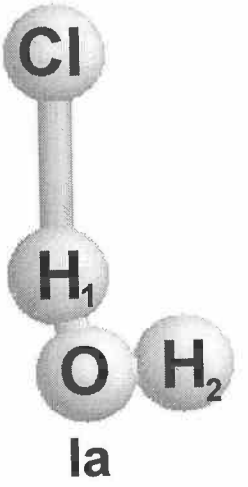

Ia

Figure 1a

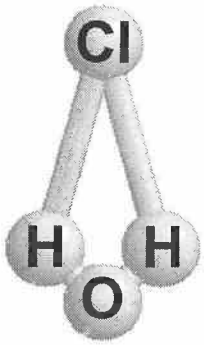

Ib

Figure 1b

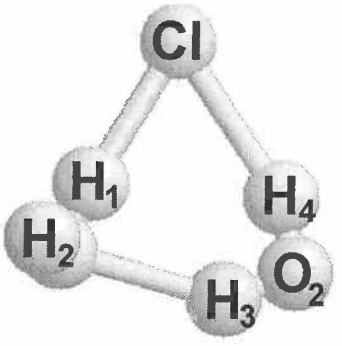

IIa

Figure 2a

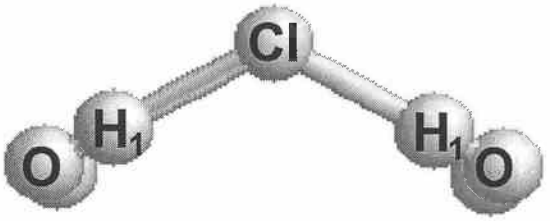

IIb

Figure 2b

IIc

Figure 2c

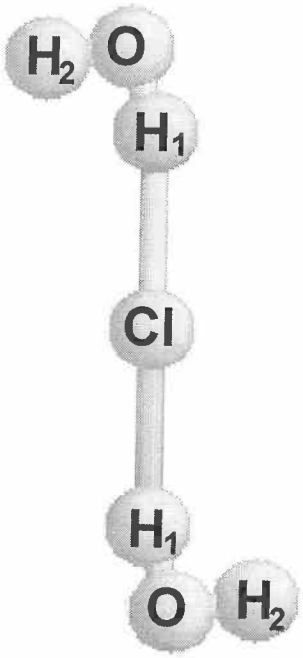

IId

Figure 2d

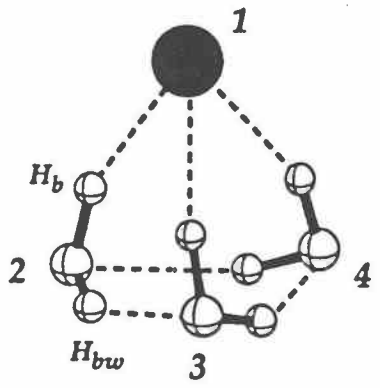

IIIa

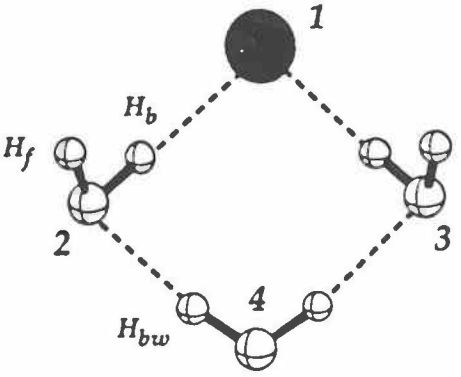

IIIb

Figure 3

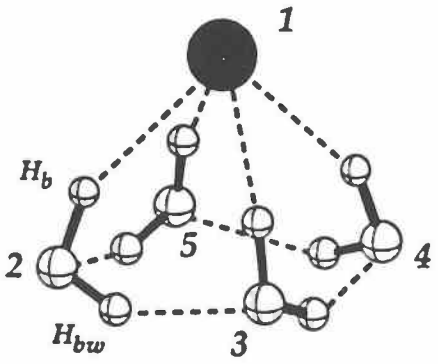

IVa

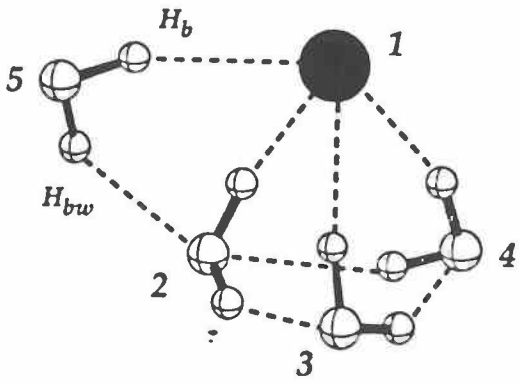

IVb

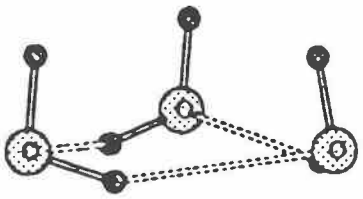

IVc

Figure 4

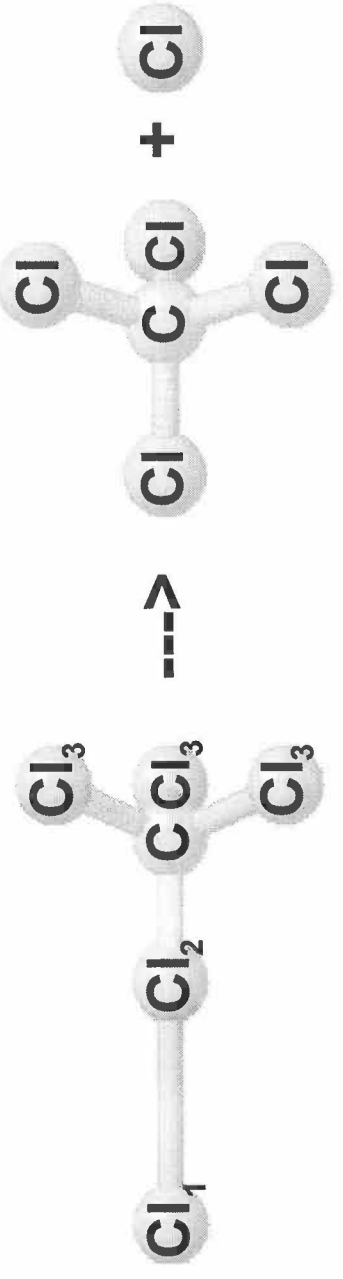

Figure 5

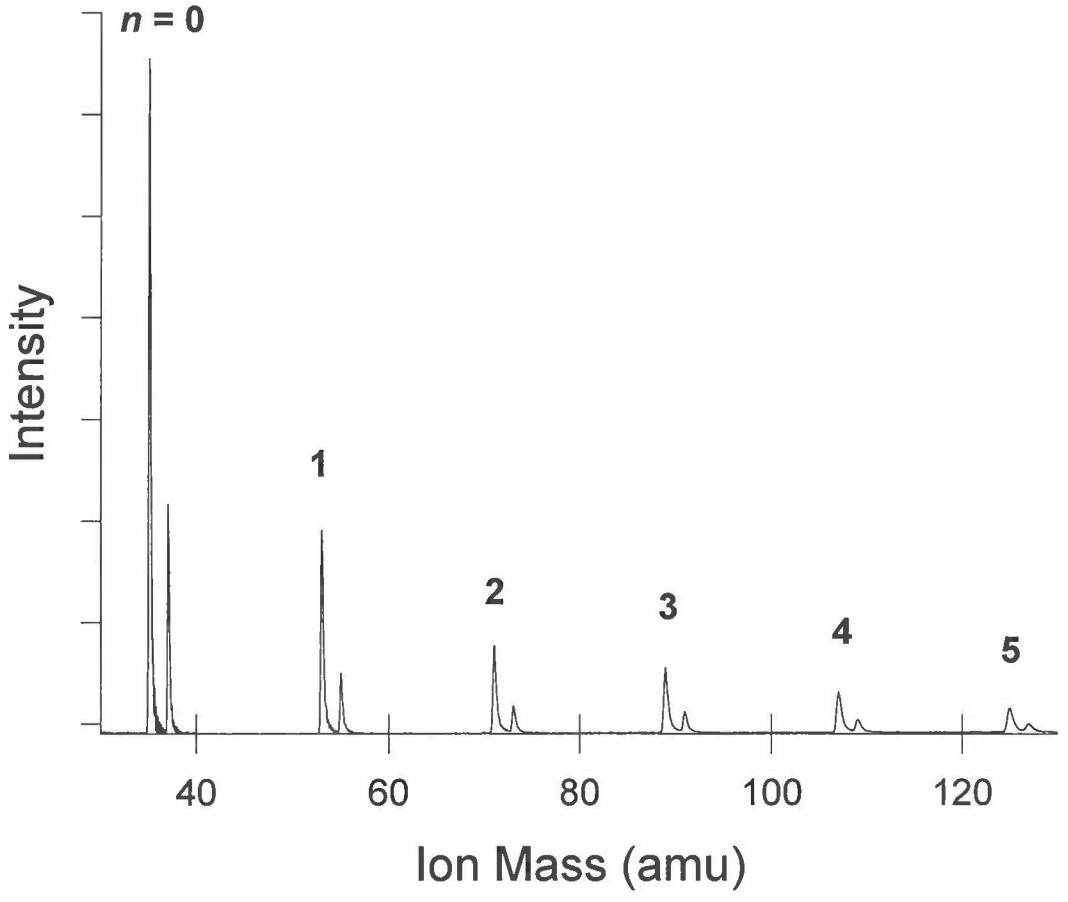

Figure 6

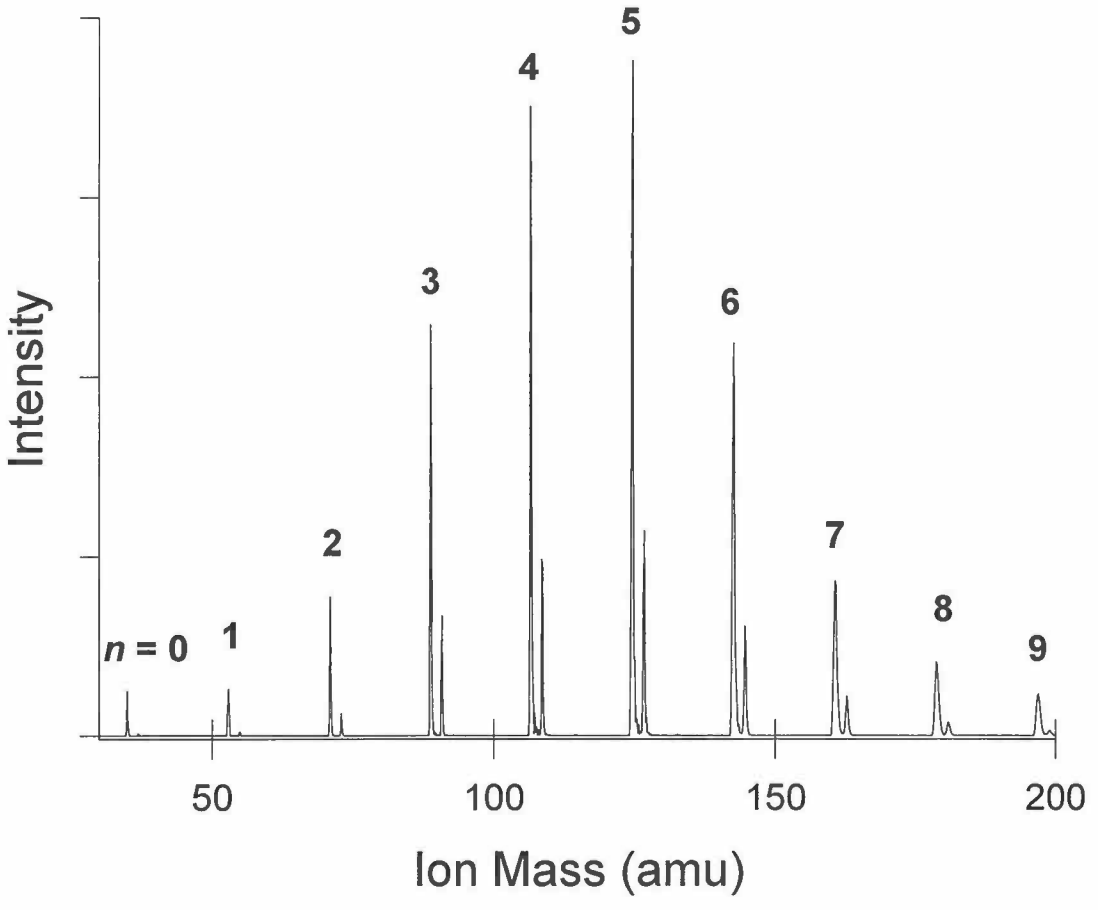

Figure 7

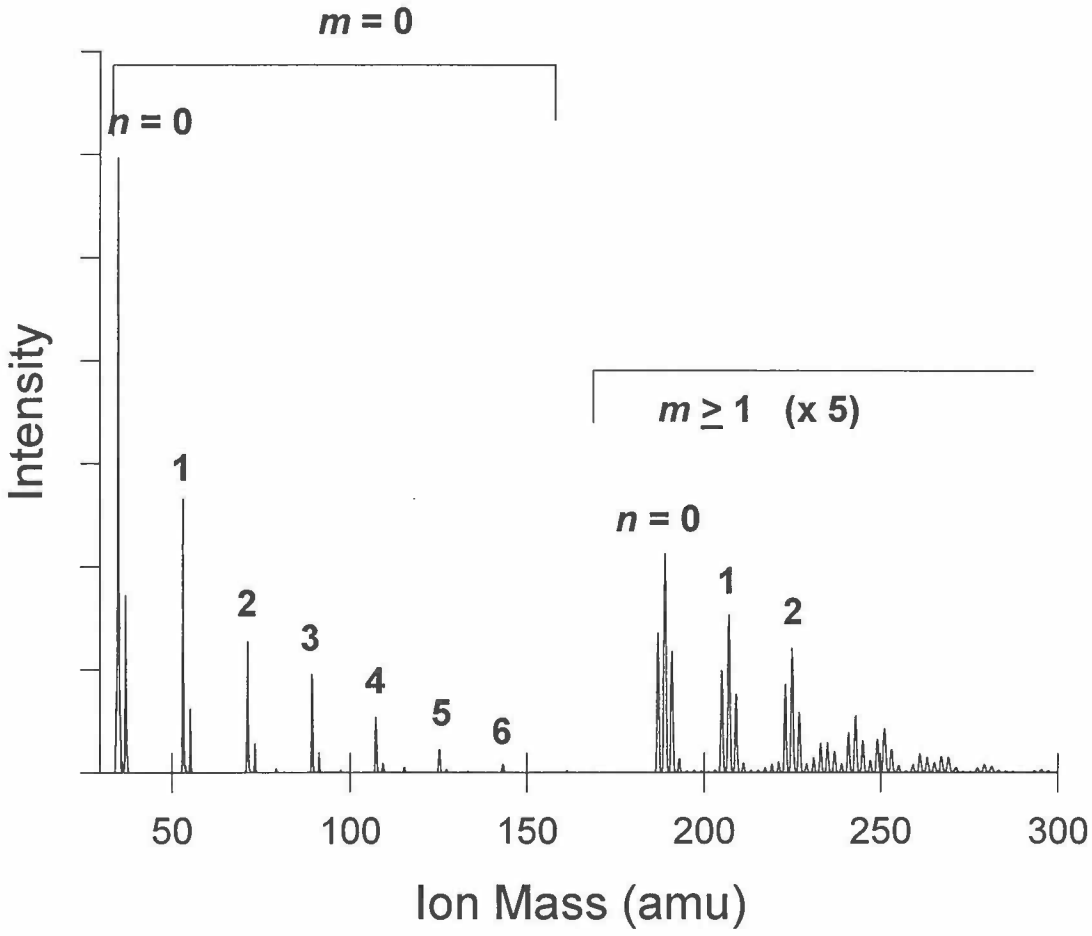
m = 0
n = 0
m ≥ 1 (x 5)
n = 0
1
2
3
4
5
6
1
2
Intensity
50
100
150
200
250
300
Ion Mass (amu)

Figure 8

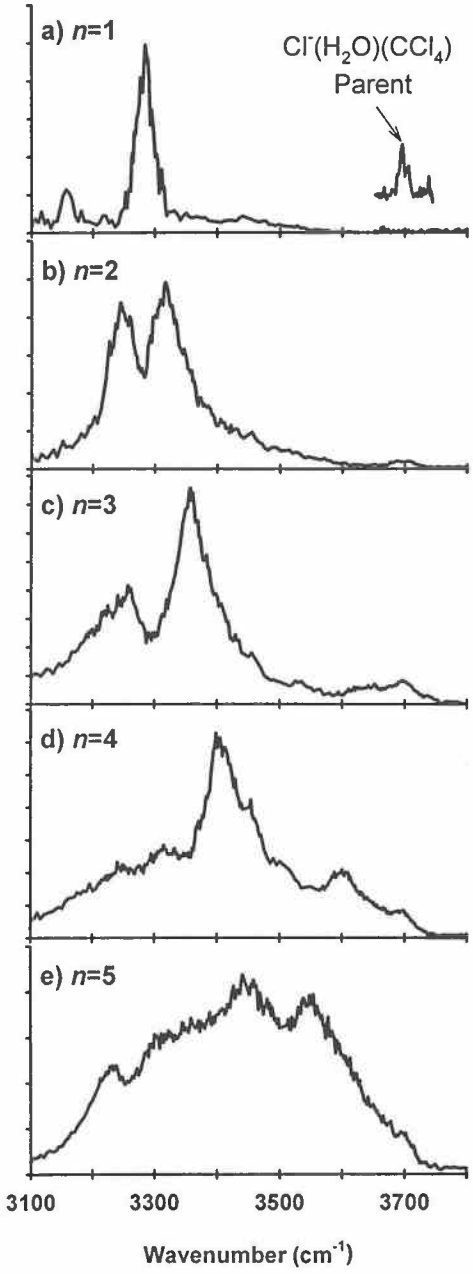
a) n=1
Cl⁻(H2O)(CCl4)
Parent
b) n=2
c) n=3
d) n=4
e) n=5
3100
3300
3500
3700
Wavenumber (cm-1)

Figure 9

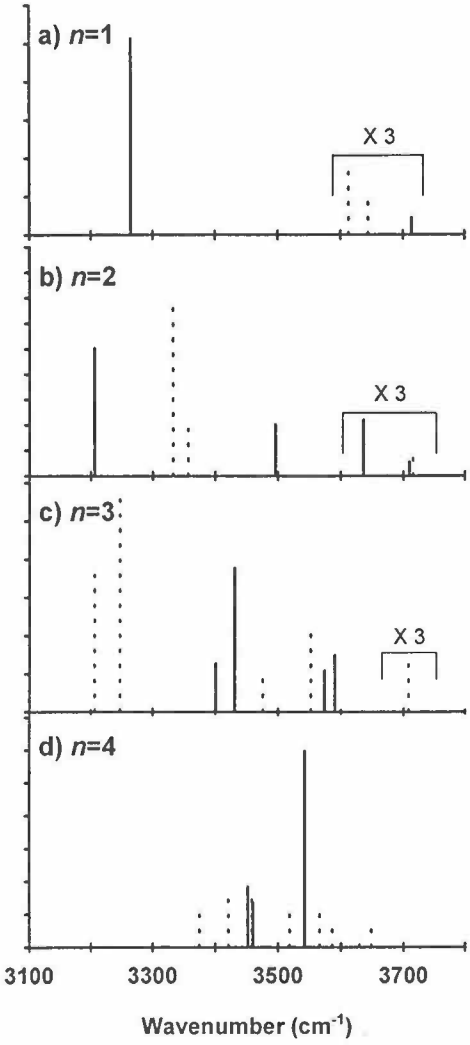

Figure 10

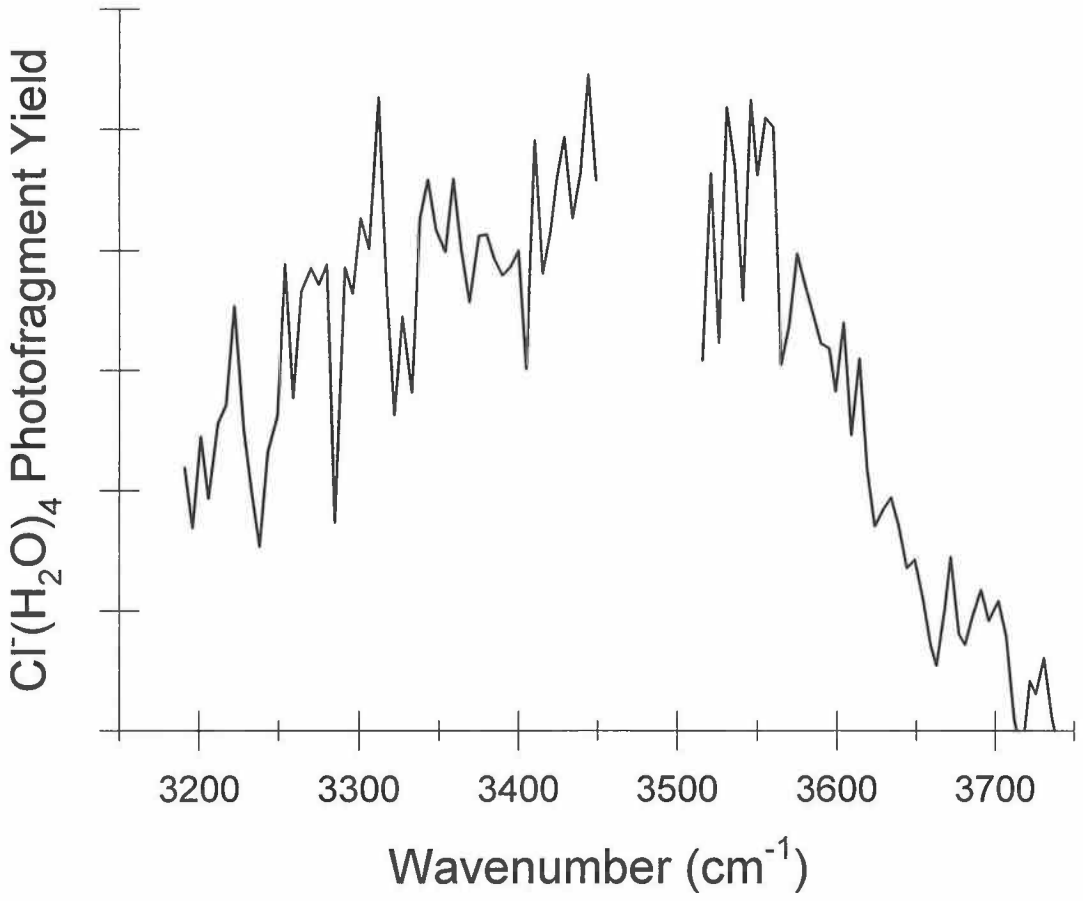
$Cl^-(H_2O)_4$ Photofragment Yield
3200
3300
3400
3500
3600
3700
Wavenumber (cm^{-1})

Figure 11a

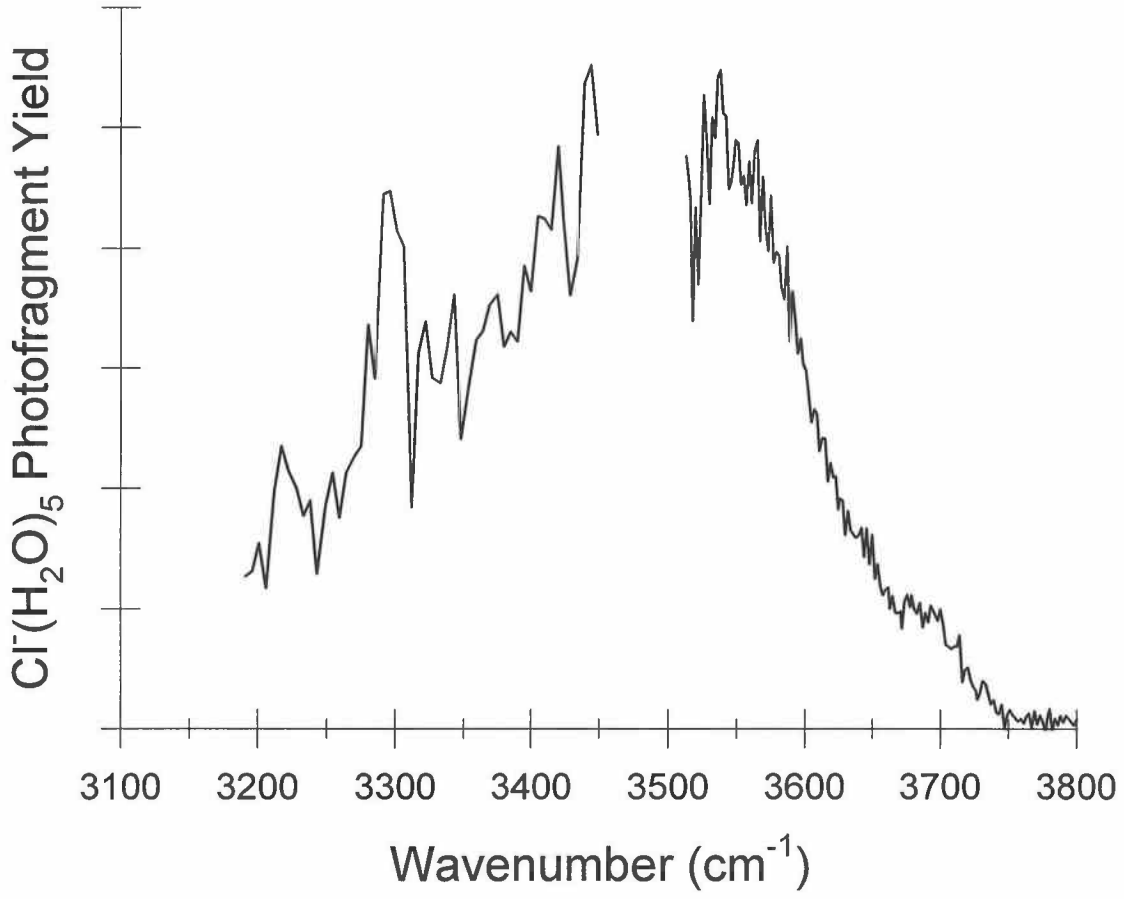
$Cl^-(H_2O)_5$ Photofragment Yield
3100
3200
3300
3400
3500
3600
3700
3800
Wavenumber (cm^{-1})

Figure 11b

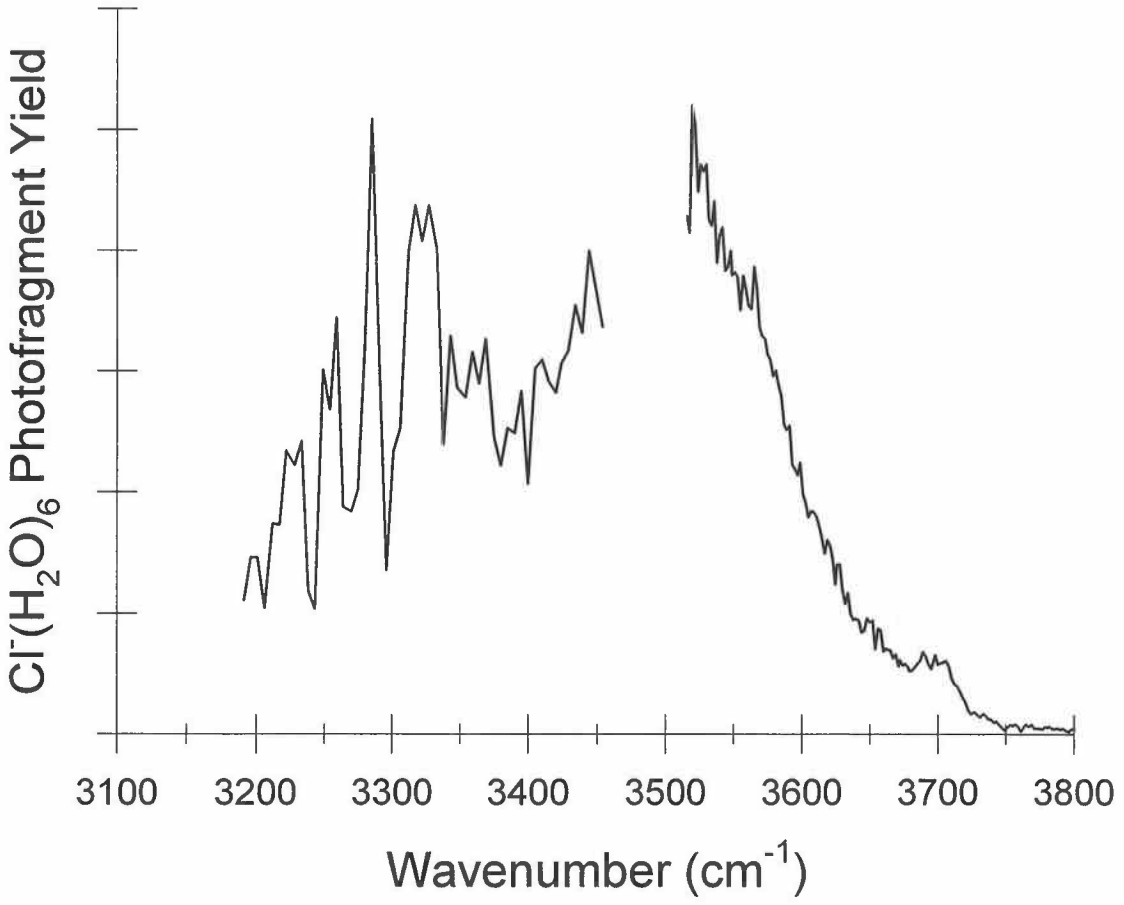
$Cl^-(H_2O)_6$ Photofragment Yield
3100
3200
3300
3400
3500
3600
3700
3800
Wavenumber (cm^{-1})

Figure 11c

CHAPTER 5

The Vibrational Predissociation Spectroscopy of

$Cl^-(NH_3)_n$, n = 1-5

5.1 INTRODUCTION

Unlike the significant amount of experimental and theoretical work done on chloride-water clusters $Cl^-(H_2O)_n$, as discussed in Chapter 4, there is little previous work to guide our discussion of gas-phase chloride-ammonia clusters, $Cl^-(NH_3)_n$. There are only a few experimental and computational studies of $Cl^-(NH_3)$ in the literature, and no study of larger ammonia clusters. In this chapter, we will present the vibrational predissociation spectra of $Cl^-(NH_3)_n$, n = 1-5, and *ab initio* calculations for some of the isomers for n = 1-3. At several points, we will draw comparisons with the $Cl^-(H_2O)_n$ results presented in Chapter 4. Our pioneering spectroscopic and computational work should provide a good foundation for further study.

Mass spectrometry has been used to measure the binding enthalpy of Cl^- to one NH_3 ligand. Using ion cyclotron resonance (ICR), Larson and McMahon[1] reported a ΔH_{298} = 10.5 ± 0.2 kcal/mol. The chloride affinity of NH_3 was measured relative to that of CH_3F, which in turn was referenced to the Cl^- affinity of t-C_4H_9OH; only the last enthalpy had been measured directly at the time of their 1984 study. More recently, Castleman and co-workers,[2] using high-pressure mass spectrometry (HPMS), reported a somewhat lower binding enthalpy of ΔH_{298} = 8.2 ± 0.1 kcal/mol. No values have been reported for any larger chloride-ammonia clusters. Mass spectrometry by itself, then, gives little insight into the solvation structure of these clusters.

Castleman and co-workers[2] also reported calculations on possible structures of the $Cl^-(NH_3)$ cluster. Using Hartree-Fock theory with a small 4-31G basis set, they predicted that the n = 1 minimum is a C_s structure containing one nearly linear hydrogen

bond (**Ia**, Figure 1), with an angle $\theta(\text{Cl-H}_1\text{-N}) = 172°$. Other geometries were considered using electrostatic calculations, with an estimate of the repulsive potential based on He-NH_3 scattering data. Consideration of the ion-dipole term alone would lead to a C_{3v} dipole aligned structure (**Ic**, Figure 3) in which the Cl^- ion is equally shared by all three hydrogens. However, the repulsive charge-quadrupole interaction in **Ic** nearly offsets the attractive ion-dipole interaction. The electrostatic model predicted that the most stable geometry is a C_s bridged structure (**Ib**, Figure 2) in which the Cl^- ion is equally shared by two of the hydrogens of NH_3.

The Hartree-Fock linear minimum was re-examined at a much higher level of theory by Kaldor.[3] The singles-and-doubles coupled cluster (CCSD) calculations gave the same qualitative description of the $Cl^-(NH_3)$ geometry as did the earlier work of Castleman and co-workers.[2] The CCSD binding energy (ΔE_e) of 8.3 kcal/mol was in excellent agreement with the HPMS value. However, no computational studies have been performed on larger clusters (Figures 4-8).

Some experimental confirmation for the linear geometry of $Cl^-(NH_3)$ comes from the photoelectron spectroscopy (PES) of Cheshnovsky and co-workers.[4] They observed vertical ionization potentials (IP) of 4.0 eV, which was assigned to ionization of Cl^- ion, and 6.45 ± 0.15 eV, which was assigned to the formation of a $Cl^-NH_3^+$ charge transfer state. The vertical IP's were reasonably well reproduced by CCSD predictions for the linear isomer **Ia** (3.88 eV and 6.36 eV). However, since ionization potentials were not calculated for other possible isomers, such as **Ib** and **Ic**, we cannot use the combination of PES data and theory to assign the $n = 1$ cluster structure definitively.

In this chapter, we apply the technique of vibrational predissociation spectroscopy to the systems $Cl^-(NH_3)_n$, n = 1-5. As discussed in Chapter 4, the ~3 μm spectra of these clusters should reveal much about hydrogen bonding to the ion and among the solvent molecules as a function of cluster size. We again consider cluster structures with the aid of *ab initio* predictions of vibrational frequencies. Computational results for n = 1-3 have all been obtained in this laboratory.

5.2 EXPERIMENTAL AND COMPUTATIONAL METHODS

The experimental procedure is largely similar to that presented in Chapter 4, and only those details unique to the ammonia experiment are presented here. The ions were generated from a mixture of ~20 Torr CCl_4 vapor seeded into a mixture of ammonia and methane at a stagnation pressure of ~1500 Torr. The gases were mixed during the course of the experiment, with the NH_3 being introduced through a MKS 100 sccm flow meter, and the CH_4 being introduced through a MKS 20 sccm flow meter. Both meters were run at full scale (5 V).

Use of ammonia required special attention to the materials used in the source line. Typically, the heat-tolerant but relatively inexpensive Viton o-rings are used for the static and dynamics seals within the pulsed valve. However, since the Viton material swells when exposed to NH_3, all of the o-rings had to be replaced with Kal-Rez o-rings. In the same vein, halocarbon grease had been used in the $Cl^-(H_2O)_n$ and $I^-(H_2O)$ experiments to protect the piezoelectric ceramic of the pulsed valve from reaction with halogens. The material, however, is a strong Lewis acid which reacts vigorously with NH_3. It was replaced with Krytox grease.

To obtain sufficient ammonia parent ion intensity, the source line had to be kept quite dry. Because H_2O binds almost twice as strongly to chloride ion as does NH_3 (~15 kcal/mol *vs.* ~8 kcal/mol), even a trace of water would largely suppress the production of $Cl^-(NH_3)_n$ clusters. Figure 9 shows the four isotopomers resulting from the solvation of $^{35}Cl^-$ and $^{37}Cl^-$ by a single NH_3 (m/z = 52 and 54) and by a single H_2O (m/z = 53 and 55). Whenever the experiment was not running, the source line was baked out with heating tape and pumped on by a diffusion pump down to a typical pressure of 3×10^{-5} Torr. Figure 10, which was typical of the mass spectra used to obtain infrared spectra, shows this procedure was sufficient to produce only ammonia clusters.

Typically, the piezo-driven pulsed valve was operated at a width of ~200 μs, with a resulting source chamber pressure of $\sim 10^{-4}$ Torr. However, one of the $Cl^-(NH_3)$ infrared spectra (Figure 12, bottom) and the $Cl^-(NH_3)_2$ infrared spectrum (Figure 13) were taken with the pulsed valve not completely opening (width ~30 μs). The source chamber pressure for these spectra was $\sim 1 \times 10^{-5}$ Torr. The two distinct pulsed valve settings nevertheless resulted in the same $Cl^-(NH_3)_n$ cluster distribution that is shown in Figure 10. Also, it was possible to shift the distribution to larger clusters by opening the pulsed valve more (to ~400 μs) and increasing the time delay (by ~50 μs) between triggering of the pulsed valve and triggering of the pulsed repeller. However, the overall ion intensity was decreased, and the mass resolution was severely degraded (Figure 11).

Calculations on NH_3, $Cl^-(NH_3)$, $Cl^-(NH_3)_2$, and $Cl^-(NH_3)_3$ were all performed on a Cray Y-MP using the Gaussian 92 system of programs.[5] All calculations reported in this chapter were performed at the second-order Møller-Plesset (MP2) level of theory,

and neglected the correlation of core electrons. Optimized geometries and harmonic vibrational frequencies of n = 1 stationary points were determined with both the 6-31+G** and 6-311++G** basis sets. With one exception, the n = 2 and 3 stationary points were treated with only the 6-31+G** basis set.

5.3 RESULTS AND DISCUSSION

A. General Experimental Observations. The only photofragment channel observed upon infrared excitation of $Cl^-(NH_3)_n$ (n = 1 to 5) was loss of a single ammonia molecule. The action spectra obtained for these clusters are shown in Figure 12-16, and band centers are summarized in Table 1.

Each of the clusters $Cl^-(NH_3)_n$ studied here has a strong infrared band in the 3100-3200 cm^{-1} region which dominates its spectrum. We assign this band to the stretches of NH groups forming hydrogen bonds to chloride ion. This feature shifts to the blue with each additional NH_3, indicating a weakening of the ionic hydrogen bonds. However, the magnitude of the shift decreases monotonically, from +36 cm^{-1} in going from n = 1 to n = 2, down to +10 cm^{-1} in going from n = 4 to n = 5.

The n = 2-5 spectra have three distinct additional bands in the 3200-3400 cm^{-1} region. The intensity of all three bands increases with cluster size relative to the ion-bound NH stretch. The ~3200 cm^{-1} blue shifts very slightly (by +5 cm^{-1}), but regularly, with additional NH_3 ligands. We assign it to the second bending overtone ($2\nu_4$) of NH_3 ligands within the complex. The other two features always appear at ~3300 and ~3350 cm^{-1} respectively. The highest frequency band at ~3350 cm^{-1} can be assigned to the free NH stretch. The assignment of the ~3300 cm^{-1} cannot be made as definitively, and will

be discussed below.

We also note that the spectra of larger $Cl^-(NH_3)_n$ clusters (n = 4 and 5) are not nearly as broad as the corresponding $Cl^-(H_2O)_n$ spectra discussed in Chapter 4, but rather closely resemble the spectra of n = 2 and 3. This suggests that for as many as five NH_3's, the $Cl^-(NH_3)_n$ cluster has not converged to a liquid-like state, which would be dominated by hydrogen bonding among the ammonias.

B. General Comments on the *Ab Initio* Results. The *ab initio* optimized geometries of $Cl^-(NH_3)_n$ (n = 1-3) are depicted in Figures 1-8 and detailed in Tables 2-9. The predicted harmonic vibrational frequencies are reported in Tables 10-17, and the predicted energetics are reported in Tables 18-21. Increasing the basis set from 6-31+G** to 6-311++G** had a modest effect on the predicted geometries (Tables 2-5). With the larger basis set, the hydrogen bond lengths were almost always predicted to be somewhat shorter (by 0.03-0.06 Å).

The choice of basis set had a much more dramatic effect on the predicted harmonic vibrational frequencies (Tables 10-13). The 6-311++G** basis set always led to significantly lower values for the intramolecular stretching and bending modes, by as much as ~60 cm^{-1}. The relative quality of these two basis sets can be assessed by comparing their results for ammonia monomer. Table 10 compares our NH_3 MP2 predictions with the experimental fundamental[6,7] and harmonic[8,9] frequencies. The larger 6-311++G** basis set provides predictions of the NH harmonic stretch frequencies (ω_1 and ω_3) closer to the recent measurements of Coy and Lehmann,[8] which themselves have uncertainties of > 10 cm^{-1}. Still, there are significant discrepancies. Quantitative

descriptions of the ammonia force field to date remains a challenge for both theory and experiment. Martin *et al.*[10] were able to generate predictions of the harmonic frequencies within the error bars of Coy and Lehmann's values only with the very high CCSD(T) level of theory and a large polarized quadruple-zeta basis set.

What is more, even given accurate harmonic values, accurate predictions of the fundamentals for NH_3 and $Cl^-(NH_3)_n$ are difficult to make. Typically, to predict shifts in monomer frequencies upon complex formation that can be compared to experiment, all *ab initio* harmonic frequencies (within a subset, *e.g.*, the stretching vibrations) are scaled by a single factor to match best the experimental frequencies, thus accounting for the anharmonicities in these modes. For this procedure to be valid, either the anharmonic corrections to the harmonic values must be roughly the same for a given subset of the normal modes, or that the red or blue shifts in the complex must be much larger than the variation in the anharmonic corrections to the monomer values.

Neither situation obtains for the $Cl^-(NH_3)_n$ system. Although there is significant variation among the experimental estimates of x_{11} and x_{33}, Coy and Lehmann's most recent values[8] of x_{11} = -26 cm^{-1} and x_{33} = -44 cm^{-1} differ by nearly a factor of 2. In contrast, the anharmonicity constants for the stretches of H_2O monomer[11] are x_{11} = -43 cm^{-1} and x_{33} = -46 cm^{-1}. Moreover, in $Cl^-(NH_3)$, the most red-shifted feature at 3107 cm^{-1} (Table 1) is red-shifted only -220 cm^{-1} from the symmetric (A_1) NH stretch in free NH_3. These factors conspire to make a direct comparison of *ab initio* and experimental vibrational frequencies difficult. Nevertheless, the trends in the *ab initio* predictions for n = 1 through n = 3 should prove to be informative.

C. $Cl^-(NH_3)$. Our experimental spectra (Figure 12) demonstrate that NH_3 forms one strong hydrogen bond to Cl^-. The structure of the n = 1 cluster is thus well represented by Figure 1, confirming the *ab initio* predictions that **Ia** is the ground state isomer. However, the details of both the experimental and computational data are difficult to explain.

Both spectra in Figure 12 are dominated by an intense band with maximum intensity at 3107 cm^{-1} (Table 1), which is clear evidence of a strong, nearly linear ionic hydrogen bond. In both spectra, the dominant feature rises sharply on the red side (the low frequency half-maximum point is ~3104 cm^{-1}), but falls away more gradually on the blue side. The top spectrum, however, has a much broader feature, and possibly contains a shoulder starting at ~3150 cm^{-1}. Overall, the major absorption in the top spectrum is three times wider than in the bottom spectrum. Both spectra also contain weak, broad absorptions from ~3180 to ~3370 cm^{-1}, with the top spectrum having a more distinct absorption centered at ~3340 cm^{-1}.

As discussed above, the top spectrum was taken with the pulsed valve completely open and with a high source chamber pressure. The resulting expansion should have led to greater vibrational cooling. The ability to observe a (more) distinct free NH stretch band at ~3340 cm^{-1}, which is not discernible in the bottom spectrum, is consistent with this understanding of source conditions. However, the great breadth of the ionic NH stretch suggests the population of excited vibrational states, or of multiple isomers. This effect should be worse for the bottom spectrum, recorded with ions generated by choking the source gas flow. However, the ionic NH stretch band is rather narrow and sharp (full

width at half maximum (FWHM) of ~20 cm^{-1}), suggesting a simple resonant one-photon excitation of the bonded NH stretch, leading to predissociation.

Differences notwithstanding, both experimental spectra (Figure 12) agree best with the spectrum predicted for the C_s linear isomer (Figure 1, Table 10). Structure **Ia** possesses one ion-bound NH stretch band ~7 times more intense than the symmetric free NH stretch, and red-shifted from this band by ~185 cm^{-1}. This reflects the presence of one nearly linear (167°) hydrogen bond (Table 2). Theory also predicts that the antisymmetric free NH stretch will have virtually no oscillator strength.

The discrepancies among the two spectra, and the detailed discrepancies between each spectrum and theory, may be accounted for in part by the presence of other isomers. As summarized in Table 18, isomers **Ib** and **Ic** are both only ~1 kcal/mol less stable than the ground-state minimum **Ia**, when zero-point effects are accounted for. The global potential for $Cl^-(NH_3)$ is quite flat and it is possible that the $Cl^-(NH_3)$ generated in the experiment sampled regions of the potential represented by Figures 2 and 3.

The bridged structure **Ib** (Figure 2), which is predicted to be a transition state, has two highly bent (114°) hydrogen bonds (Table 3). The symmetric and antisymmetric linear combinations of the bonded NH stretches should be split by ~100 cm^{-1}, and comparable in intensity with each other and with the free NH stretch (Table 11). The two weak hydrogen bonds red shift the bonded NH stretches by only ~30 cm^{-1} and ~130 cm^{-1} from the free NH stretch. The dipole-aligned isomer **Ic** (Figure 3), in which all three hydrogen atoms bond (weakly) to Cl^-, is a second-order transition state. Its A_1 and E NH stretch bands are predicted to have frequencies ~15 cm^{-1} to the blue of the bonded NH

stretch bands of **Ib**.

The absolute intensities of all the NH stretch modes in **Ib** and **Ic** are less than 10% of that predicted for the bonded NH stretch of **Ia** (Table 10), and may be expected to contribute weakly to the experimental $n = 1$ spectrum. Nevertheless, it is possible that these structures contribute to the absorption seen from ~3180 cm^{-1} to ~3370 cm^{-1}, particularly for the top spectrum (Figure 12).

It is also possible that excitation of other vibrational modes of the ground state $Cl^-(NH_3)$ isomer results in the observed predissociation. The second bending overtone ($2\nu_4$), observed for NH_3 monomer[11] at 3219 cm^{-1}, has significant oscillator strength, and may gain further intensity through a Fermi resonance interaction with the 3107 cm^{-1} band of the cluster. This feature may be present in both experimental spectra in the vicinity of the monomer value. In addition, the Cl^---H intermolecular stretch, which is predicted to have a frequency of 140 cm^{-1} (Table 10), could be observed in a combination mode with the NH bonded stretch. Such a mode was possibly observed in the $Cl^-(H_2O)$ spectrum. The combination band would occur at ~3250 cm^{-1}, which is a weak feature of the top experimental spectrum.

Use of the $Cl^-(NH_3)$ *ab initio* spectrum to understand the experimental results is complicated if we attempt to use the NH_3 *ab initio* spectrum (Table 10) to calibrate our complex predictions. With the larger basis set, the *E* stretch in NH_3 is predicted to red shift by 38 cm^{-1} in forming the $Cl^-(NH_3)$ complex (correlating with the *A"* stretch). However, the A_1 stretch in NH_3 is predicted to *blue* shift by 43 cm^{-1} (correlating with the *A'* stretch of the complex). If these shifts were taken as quantitative predictions of the

perturbation in NH_3 effected by the binding of Cl^- ion, the two NH stretch bands would be shifted to within ~25 cm^{-1} of each other in the complex. As it is, since the harmonic splitting between the NH_3 A_1 and E stretching modes is predicted to be ~150 cm^{-1} (*vs.* the splitting between the experimental fundamentals of 107 cm^{-1}), the *A'* and *A"* stretching modes in $Cl^-(NH_3)$ are predicted to remain apart by ~70 cm^{-1}.

While the *A"* free NH stretch has no IR oscillator strength, the *A'* free NH stretch should be observable (with an absolute intensity of ~50 km/mol), and we do indeed see a broad feature in the top $n = 1$ spectrum at ~3340 cm^{-1}. This is precisely the location of the A_1 stretch in NH_3 monomer; the MP2 prediction of a +43 cm^{-1} shift for this mode appears to be inaccurate.

In the calculation, the blue shift in the A_1/A' free NH stretching mode reflects a strong degree of coupling with the *A'* bonded NH stretch. The normal mode vectors reveal a significant amount of bonded NH stretch character in the "free" NH stretch mode, and vice versa. Moreover, this only reflects the harmonic coupling between the two totally symmetric modes. The significant mixing and diverging of these two modes could account for the very large red shift in the observed ionic NH stretch. This band, peaked at 3107 cm^{-1}, is 230 cm^{-1} to the red of the experimental A_1 stretch of NH_3 monomer. In contrast, the bonded NH stretch is predicted to be only ~140 cm^{-1} to the red of the predicted A_1 stretch of free NH_3. The MP2 underestimate of the size of the red shift could also reflect an underestimate of the strength of the $Cl^-(NH_3)$ bond. The MP2/6-311++G** level of theory predicts a bond enthalpy of ΔH_{298} = 7.7 kcal/mol, lower than either of the experimental measurements (Table 19).

D. $Cl^-(NH_3)_2$. Our $n = 2$ experimental spectrum (Figure 13) differs significantly from both $n = 1$ spectra (Figure 12). Besides the main Cl^--bound NH stretch band at 3143 cm^{-1}, there is a very distinct band at 3347 cm^{-1} attributable to a free NH stretch. The assignment of the other two distinct bands at 3212 cm^{-1} and 3293 cm^{-1} (Table 1) will be discussed in light of the *ab initio* findings that follow.

Our MP2 calculations revealed two minima on the $n = 2$ potential energy surface, an asymmetric isomer **IIa** with hydrogen bonding between the ammonias (Figure 4), and a C_2 isomer **IIb** in which the ammonias bind to water, but not to each other (Figure 5). Both are true minima; all vibrational frequencies of both isomers are real (Tables 13 and 14). This is in contrast to the MP2 predictions for $Cl^-(H_2O)_2$, as discussed in Chapter 4, which indicated that the only true minimum on the global potential involved hydrogen bonding between the waters. Interestingly, while the larger 6-311++G** basis predicts shorter lengths of all the ionic hydrogen bonds, the hydrogen bond between the NH_3s in **IIa** is predicted to be 0.03 Å longer with the larger basis set. A more thorough study of basis set effects on the predicted geometry of **IIa** could be warranted.

We note that the MP2 calculations predict that Cl^- ion will be asymmetrically solvated by two NH_3's, both in the presence (Figure 4) and absence (Figure 5) of hydrogen bonding between the NH_3's. Nevertheless, the H--Cl--H bending potential in $Cl^-(NH_3)_2$ is very flat, flatter even than the bending potential in $Cl^-(H_2O)_2$. The relative stabilities of $n = 2$ isomers (Table 20) bear this out.

In the global C_1 minimum (Figure 4), the ion-solvent hydrogen bonds are 63° apart (Table 5). (In order to compare the C_1 geometry directly with the other $n = 2$

stationary points, the angle predicted with the smaller 6-31+G** basis set is used.) For the C_2 minimum (Figure 5), in the absence of hydrogen bonding between the waters, the electrostatic repulsion between the NH_3 dipoles causes the H--Cl--H angle to open from 63° to 122°. The net energy cost is only ΔE_o = +0.3 kcal/mol. Rotation of the nitrogen atoms into the H-Cl-H plane gives rise to a C_{2v} transition state **IIc** (Figure 6) with ΔE_o = +0.4 kcal/mol above the C_1 minimum. At this stationary point, the H--Cl--H is opened slightly more, to 123°. Finally, a strictly linear C_{2h} structure **IId** (Figure 7) was found to be a second-order transition state with $\Delta E_o \sim 0.6$ kcal/mol above **IIa**. The MP2 potential energy surface is clearly quite flat, the barrier against breaking the ammonia-ammonia hydrogen bond being only ~0.5 kcal/mol.

Like the $Cl^-(H_2O)_2$ minimum, **IIa** demonstrates the strong enhancement in ion solvation by donor/acceptor ligands. The ammonia ligand $N_1H_1H_3H_4$ (labeling in Figure 4) that serves both as a donor and acceptor in hydrogen bonding has an ionic hydrogen bond length r(Cl--H_1) ~0.06 Å shorter than the hydrogen bond in the $Cl^-(NH_3)$ minimum **Ia** (Tables 2 and 5). On the same note, the ion-bound N_1-H_1 stretch is almost 25 cm^{-1} more red-shifted than the ionic NH stretch of **Ia** (Tables 10 and 13). Moreover, the evaporation of one NH_3 ligand from $Cl^-(NH_3)_2$ is actually predicted to require more energy (~0.4 kcal/mol at 298 K) than evaporation of the NH_3 from $Cl^-(NH_3)$ (Tables 19 and 21). As noted above, no experimental thermochemistry exists to confirm this prediction. Moreover, as discussed in Chapter 4, while the second hydration enthalpy of $Cl^-(H_2O)_n$ is predicted to be only 0.3 kcal/mol smaller, the experimental data predict a drop-off of ~2 kcal/mol. In any case, it is clear that the presence of a second NH_3 ligand

strengthens the interaction of the first NH_3 ligand with Cl^- ion.

In isomer **IIa**, the donor/acceptor (DA) Cl^--bound NH stretch is predicted to be separated from the double-donor (DD) Cl^--bound NH stretch by ~100 cm^{-1}, and is predicted to be 3-4 times more intense. Unlike for the predicted spectrum of the $Cl^-(H_2O)_2$ minimum, in $Cl^-(NH_3)_2$ the three NH stretch modes of the double donor--the Cl^--bound NH stretch, the NH_3-bound NH stretch, and the free NH stretch--all mix significantly with each other. (This is reflected in the approximate descriptions of the normal modes in Table 13.) This results in a qualitative difference between the *ab initio* spectrum of **IIa** and the *ab initio* spectrum of the $Cl^-(H_2O)_2$ minimum. In each spectrum, there are four distinct bands corresponding roughly (in order of increasing frequency) to the DA Cl^--bound stretch, the DD Cl^--bound stretch, the DD solvent-bound stretch, and the free stretch. However, in the $Cl^-(NH_3)_2$ spectrum, the two middle bands are predicted to have roughly the same intensity. In contrast, in the $Cl^-(H_2O)_2$ spectrum, the relative intensities decreased monotonically with increasing frequency.

Our experimental $n = 2$ spectrum also has four distinct bands, and the two most red-shifted bands are split significantly, by ~70 cm^{-1}. One might thus assign the 3143 cm^{-1} band to the DA ionic NH stretch, and the 3212 cm^{-1} band to the DD ionic NH stretch. The feature at 3293 cm^{-1} would reflect hydrogen bonding between the NH_3's. However, it is more likely that the experimental data do not reflect the *ab initio* ground state structure. The dominant feature observed is 36 cm^{-1} to the blue of the $n = 1$ dominant feature, indicating the absence of a donor-acceptor ligand. The features at 3212 cm^{-1} and 3293 cm^{-1} are also far less intense than predicted for isomer **IIa**.

The $Cl^-(NH_3)_2$ structure probed by our experiment likely resembles isomer **IIb** (Figure 5). The symmetric and antisymmetric linear combinations of the ion-bound NH stretches are virtually unsplit (Table 14), and should be observed as one dominant band, which agrees with the experimental data (Figure 13). The bound NH stretches of **IIb** are predicted to blue shift ~70 cm^{-1} relative to the $n = 1$ spectrum (Table 10), indicating that the C_2 isomer lacks cooperativity in solvation. The observed blue shift is only ~35 cm^{-1}, but the experimental trend matches the predicted trend.

While the 3212 cm^{-1} band cannot be assigned to a NH stretch mode of the C_2 isomer, it is quite reasonable to assign it to the NH_3 bending overtone ($2\nu_4$). As discussed before, this mode has moderate intensity in the NH_3 monomer spectrum, and will gain further oscillator strength in a Fermi resonance interaction with the 3143 cm^{-1} band. This band has been observed in the IR spectra of larger ($n \geq 4$) $NH_4^+(NH_3)_n$ clusters by Price *et al.*[12]

By analogy with the $n = 1$ spectrum, the least red-shifted feature at 3347 cm^{-1} is assigned to a free NH stretch. However, assignment of the symmetry of this mode, and the assignment of the 3293 cm^{-1} band, require more careful consideration.

The 3293 cm^{-1} band, like the 3347 cm^{-1} band, could involve the free NH stretch. These two bands would then represent the symmetric and antisymmetric linear combinations within each monomer. (As seen in Table 14, there are *A* and *B* modes of both the symmetric and antisymmetric stretch, due to the in-phase and out-of-phase linear combinations of the monomer stretching modes. The splitting between the *A* and *B* combinations of each monomer mode is negligible.) The symmetric and antisymmetric

free NH stretches for the C_2 minimum are predicted to be split by ~70 cm^{-1}, which agrees well with the ~50 cm^{-1} of the two highest frequency bands in the observed spectrum. Also, the positions of the two distinct bands in the $n = 2$ experimental spectrum correlate well with the broad absorptions in the $n = 1$ experimental spectra.

However, the uncertainties in scaling preclude our using the *ab initio* band positions to assign definitively the 3293 cm^{-1} band as the symmetric mode and the 3347 cm^{-1} band as the antisymmetric mode. Moreover, the higher frequency antisymmetric stretches (both at 3694 cm^{-1}, unscaled) are predicted to have no oscillator strength. In contrast, the experimental data indicates that these two bands are of comparable intensity. As noted in the $n = 1$ discussion, the position of what is undoubtedly a free NH stretch band, 3347 cm^{-1}, agrees well with the position of the *symmetric* NH stretch band of free NH_3, 3337 cm^{-1}.

Nevertheless, other plausible assignments for the 3293 cm^{-1} band are lacking. The antisymmetric intermolecular stretch is predicted to have significant oscillator strength (23 km/mol), and a combination of this mode (at 157 cm^{-1}) with the bonded NH stretch mode (3143 cm^{-1}) would be at the right position to account for the 3293 cm^{-1} band. However, it is doubtful that a combination band could have oscillator strength comparable to the NH stretch fundamental at 3347 cm^{-1}.

Invoking the presence of isomers **IIc** and **IId** in our ion beam does not help us assign this band. Their spectra vary from that of **IIb** only in the relative intensities of the bonded NH stretches (Tables 15 and 16), which, as noted above, are virtually unsplit. **IIc** and **IId** have the same predicted splitting for the free NH stretch modes as **IIb**, and their

antisymmetric NH stretch modes are also predicted to have virtually no intensity.

At this point, then, the most reasonable assignments for the 3293 cm^{-1} and the 3347 cm^{-1} bands are as the symmetric and antisymmetric free NH stretches, respectively. Since the MP2 band positions cannot be reconciled with experiment, it is possible that the MP2 infrared intensities are also suspect. A more exact *ab initio* treatment of the $Cl^-(NH_3)$ and $Cl^-(NH_3)_2$ force field, which includes the anharmonic corrections and even higher order terms, would likely do a better job of accounting for our experimental data.

E. $Cl^-(NH_3)_n$, n = 3-5. Adding additional ammonias decreases the relative intensity of the ion-bound NH stretch mode, and causes this band to shift to the blue. Overall, the main band of the spectrum shifts by more than +80 cm^{-1} from $Cl^-(NH_3)$ to $Cl^-(NH_3)_5$. However, the differential blue shift decreases with increasing n. This indicates that the frequency of the $Cl^-(NH_3)_n$ is slowly approaching some bulk value.

The three additional bands seen in the n = 2 spectrum persist in the spectra of larger clusters. While there is some variation in their location, all three features remain roughly at the same frequencies. We again assign the 3220-3230 cm^{-1} band to the NH_3 bending overtone. The nearly constant position of this feature with increasing solvation is further evidence that this band is not an ion-bound NH stretch of another symmetry. Similarly, the fixed position of the ~3300 cm^{-1} band is evidence that this is not a combination mode of the ion-bound NH stretch and the intermolecular Cl--H stretch. If it were, it should blue shift with the main absorption feature. Instead, we assign the ~3300 cm^{-1} and the 3350-3360 cm^{-1} bands to free NH stretches in the larger clusters.

Our preliminary MP2 calculations have revealed one stationary point of the $n = 3$ surface. Isomer **III** (Figure 8) appears to be of planar D_{3h} symmetry, but is strictly of C_{3v} symmetry; the N atoms are very slightly out of the plane of the Cl^- ion and the three ion-bound H atoms. This structure, which is a true stationary point (maximum Cartesian force is $\sim 3 \times 10^{-9}$ hartree/bohr), is a third order transition state. The imaginary modes break the σ_v planes of symmetry, but maintain the C_3 rotational symmetry. It is likely that at least one of the minima of the $Cl^-(NH_3)_3$ surface is a C_3 pyramidal isomer analogous to the $Cl^-(H_2O)_3$ global minimum, in which each solvent molecule forms one hydrogen bond to the Cl^- ion, and a second hydrogen bond to the neighboring solvent molecule. The absence of any dramatic difference in the $Cl^-(NH_3)_2$ and $Cl^-(NH_3)_3$ spectra is evidence that our experiment did not probe this putative pyramidal structure.

Further *ab initio* calculations are necessary to understand the spectrum predicted for isomer **III**. At the MP2/6-31+G** level of theory, all structures with two free NH bonds per NH_3 (*i.e.*, isomers **Ia**, **IIb**, **IIc**, and **IId**) were predicted to have free NH stretch frequencies of ~3625 cm^{-1} and ~3695 cm^{-1} (Tables 10, 14, 15, and 16). While there was difficulty in scaling these values to predict experimental fundamentals, there was at least a physically reasonable self-consistency: differences in the number of NH_3 ligands and in the angle separating the NH_3 ligands should not affect the free NH stretch frequencies.

However, the free NH stretches for **III** are blue shifted by 120-140 cm^{-1} (Table 17). The bonded NH stretch is likewise blue shifted ~100 cm^{-1} from the $n = 2$ values, far more than the ~20 cm^{-1} blue shift in the experimental data. At the same time, the NH_3 bending modes in isomer **III** are some 70-100 cm^{-1} to the red of the $n = 2$ bending modes.

Moreover, the magnitude of the (imaginary) umbrella modes are a full 300-400 cm^{-1} lower than the $n = 2$ umbrella modes. In the region of the potential about structure **III**, there is apparently a great deal of coupling among the high frequency intramolecular modes. Distortion of the complex by the umbrella motions of the NH_3 would likely reduce this coupling. The fact that the observed free NH stretch modes in the $n = 3$ spectrum are virtually unshifted from the $n = 2$ values suggests that our experiment is not probing such a highly symmetric structure as in Figure 8. Whether we have asymmetric solvation in the absence of hydrogen bonding among the solvent ligands (as was the case for $Cl^-(H_2O)_3$) is a question only more extensive calculations can answer.

The four main features observed in the $Cl^-(NH_3)_2$ spectrum remain distinct and relatively unbroadened even in the $Cl^-(NH_3)_5$ spectrum. This suggests that we have successively built up a first solvation shell about Cl^- ion, and that up to five NH_3 ligands do not interact with each other. If there were significant bonding among the ammonias, we would expect broadening as has been seen for the spectra of liquid ammonia.[13,14] Preliminary scanning of $n = 4$ and $n = 5$ to the red of 3150 cm^{-1} did not indicate very red-shifted ionic NH bands. These features would have been indicative of a DA NH_3 in the first solvation shell. Unlike the discussion above for the $Cl^-(NH_3)_2$ asymmetric minimum (Figure 4), the donor to the DA NH_3 would have been an NH_3 starting a second solvation shell. The fact that the region from 3200-3350 cm^{-1} appears unperturbed for the $n = 4$ and $n = 5$ spectrum is further evidence that these clusters, at least in our experiment, do not contain hydrogen bonds between any NH_3s.

5.4 CONCLUSION

Our experimental spectra indicate that in gas-phase $Cl^-(NH_3)_n$ clusters, the first five NH_3 ligands will each form one strong hydrogen bond to the ion, but will not form hydrogen bonds with each other. While the free NH stretch was difficult to observe for the $n = 1$ cluster (a common theme in these studies), both the symmetric and antisymmetric linear combinations of the free NH stretches are clearly observable for all larger clusters. The $n = 2$-5 spectra also clearly reveal the NH_3 bending overtone, which is comparable in intensity to the free NH stretches. These last three monomer bands grow in intensity relative to the Cl^--bound NH stretch as n increases, suggesting a gradual weakening of the ionic hydrogen bonds.

Difficulties in treating the NH_3 force field accurately at our modest level of theory precludes any straightforward scaling of the MP2 harmonic frequencies to predict experimental fundamental frequencies. Nevertheless, our calculations identified minima consistent with the $n = 1$ and $n = 2$ spectra. This goal was realized only for the $n = 1$ cluster for the $Cl^-(H_2O)_n$ system.

For further work, it would be worthwhile to study the infrared spectra of larger ($n \geq 6$) clusters. We expect that we will see dramatic changes in the spectra indicative of the formation of a second solvation shell. More thorough scanning of the $n = 1$ spectrum could reveal rotational structure or distinct bands characteristic of higher energy isomers. Computationally, a more detailed search for $n = 3$ stationary points, as well as studies of larger clusters, could help determine if the surface solvation predicted for $Cl^-(H_2O)_n$ clusters is also operative for $Cl^-(NH_3)_n$ clusters.

5.5 REFERENCES AND NOTES

(1) Larson, J. W.; McMahon, T. B. *J. Am. Chem. Soc.* **1984**, *106*, 517.

(2) Evans, D. H.; Keesee, R. G.; Castleman, Jr., A. W. *J. Chem. Phys.* **1987**, *86*, 2927.

(3) Kaldor, U. *Z. Phys. D* **1994**, *31*, 279.

(4) Markovich, G.; Cheshnovsky, O.; Kaldor, U. *J. Chem. Phys.* **1993**, *99*, 6201.

(5) Frisch, M. J.; Trucks, G. W.; Head-Gordon, M.; Gill, P. M. W.; Wong, M. W.; Foresman, J. B.; Johnson, B. G.; Schlegel, H. B.; Robb, M. A.; Replogle, E. S.; Gomperts, R.; Andres, J. L.; Raghavachari, K.; Binkley, J. S.; Gonzalez, C.; Martin, R. L.; Fox, D. J.; Defrees, D. J.; Baker, J.; Stewart, J. J. P.; Pople, J. A. *Gaussian 92, Revision D.2.*, Gaussian, Inc., Pittsburgh, PA, 1992.

(6) Koops, T.; Visser, T.; Smit, W. M. A. *J. Mol. Struct.* **1983**, *96*, 203.

(7) Job, V. A.; Patel, N. D.; D'Cunha, R.; Kartha, V. B. *J. Mol. Spectrosc.* **1983**, *101*, 48.

(8) Coy, S. L.; Lehmann, K. K. *Spectrochim. Acta A* **1989**, *45*, 47.

(9) Hoy, A. R.; Mills, I. M.; Strey, G. *Mol. Phys.* **1972**, *24*, 1265.

(10) Martin, J. M. L.; Lee, T. J.; Taylor, P. R. *J. Chem. Phys.* **1992**, *97*, 8361.

(11) Herzberg, G. *Molecular Spectra and Molecular Structure. II. Infrared and Raman Spectra of Polyatomic Molecules*; van Nostrand Reinhold: New York, 1945; Chapter 3.

(12) Price, J. M.; Crofton, M. W.; Lee, Y. T. *J. Phys. Chem.* **1991**, *95*, 2182.

(13) Corset, J.; Lascombe, J. *J. Chim. Phys.* **1967**, *64*, 665.

(14) Bertrán, J. F. *J. Mol. Struct.* **1982**, *95*, 9.

TABLE 1: Experimental Vibrational Frequencies of $Cl^-(NH_3)_n$ Clusters[a]

	Approx Description	Frequencies
$n = 1$	Cl^--bound NH stretch	3107
	Free NH stretch	~3340
$n = 2$	Cl^--bound NH stretch	3143
	NH_3 bending overtone	3212
	Free NH stretch	3293
	Free NH stretch	3347
$n = 3$	Cl^--bound NH stretch	3165
	NH_3 bending overtone	3218
	Free NH stretch	3304
	Free NH stretch	3353
$n = 4$	Cl^--bound NH stretch	3179
	NH_3 bending overtone	3222
	Free NH stretch	3293
	Free NH stretch	3353
$n = 5$	Cl^--bound NH stretch	3189
	NH_3 bending overtone	3228
	Free NH stretch	3299
	Free NH stretch	3361

[a] Frequencies in cm^{-1}.

TABLE 2: MP2 Optimized Geometries of the $Cl^-(NH_3)$ C_s Linear Isomer with Various Basis Sets[a,b]

	6-31+G**	6-311++G**
$Cl^-(NH_3)$		
$r(Cl\text{--}H_1)$	2.426	2.393
$r(H_1\text{-}N)$	1.025	1.028
$r(N\text{-}H_2)$	1.014	1.016
$\theta(Cl\text{-}H_1\text{-}N)$	165.3	166.8
$\theta(H_1\text{-}N\text{-}H_2)$	105.4	104.7
$\theta(H_2\text{-}N\text{-}H_2)$	106.1	105.2
$\tau(Cl\text{-}H_1\text{-}N\text{-}H_2)$	±55.9	±55.2
NH_3		
r(N-H)	1.012	1.013
θ(H-N-H)	110.8	111.6

[a] Bond lengths in Å; bond angles in deg.

[b] Atoms are as labeled in Figure 1.

TABLE 3: MP2 Optimized Geometries of the $Cl^-(NH_3)$ C_s Bridged Isomer with Various Basis Sets[a,b]

	6-31+G**	6-311++G**
$Cl^-(NH_3)$		
$r(Cl\text{--}H_1)$	2.949	2.921
$r(H_1\text{-}N)$	1.016	1.018
$r(N\text{-}H_2)$	1.015	1.016
$\theta(Cl\text{-}H_1\text{-}N)$	113.2	113.5
$\theta(H_1\text{-}N\text{-}H_2)$	105.1	104.5
$\theta(H_2\text{-}N\text{-}H_2)$	100.7	100.3
$\tau(H_1\text{-}Cl\text{-}N\text{-}H_2)$	±99.1	±98.6
NH_3		
r(N-H)	1.012	1.013
θ(H-N-H)	110.8	111.6

[a] Bond lengths in Å; bond angles in deg.

[b] Atoms are as labeled in Figure 2.

TABLE 4: MP2 Optimized Geometries of the $Cl^-(NH_3)$ C_{3v} Dipole-Aligned Isomer with Various Basis Sets[a,b]

	6-31+G**	6-311++G**
$Cl^-(NH_3)$		
r(Cl--H)	3.261	3.209
r(N-H)	1.016	1.018
θ(Cl-H_1-N)	99.4	99.8
θ(H-N-H)	102.6	101.8
τ(Cl-H-N-H)	±120	±120
NH_3		
r(N-H)	1.012	1.013
θ(H-N-H)	110.8	111.6

[a] Bond lengths in Å; bond angles in deg.

[b] Atoms are as labeled in Figure 3.

TABLE 5: MP2 Optimized Geometries of the $Cl^-(NH_3)_2$ C_1 Isomer[a,b]

	6-31+G**	6-311++G**
$r(Cl\text{--}H_1)$	2.364	2.336
$r(Cl\text{--}H_2)$	2.574	2.554
$r(N_1\text{-}H_1)$	1.025	1.028
$r(N_2\text{-}H_2)$	1.020	1.023
$r(N_1\text{-}H_3)$	1.014	1.016
$r(N_1\text{-}H_4)$	1.014	1.016
$r(N_2\text{-}H_5)$	1.016	1.018
$r(N_2\text{-}H_6)$	1.014	1.016
$r(N_1\text{--}H_5)$	2.513	2.542
$\theta(H_1\text{-}Cl\text{-}H_2)$	63.1	63.7
$\theta(Cl\text{-}H_1\text{-}N_1)$	177.1	177.7
$\theta(Cl\text{-}H_2\text{-}N_2)$	156.3	157.3
$\theta(H_1\text{-}N_1\text{-}H_3)$	106.1	105.5
$\theta(H_1\text{-}N_1\text{-}H_4)$	106.2	105.5
$\theta(H_2\text{-}N_2\text{-}H_5)$	104.0	103.5
$\theta(H_2\text{-}N_2\text{-}H_6)$	105.6	105.0
$\tau(N_1\text{-}H_1\text{-}Cl\text{-}H_2)$	240.5	235.9
$\tau(N_2\text{-}H_2\text{-}Cl\text{-}H_1)$	-27.3	-28.2
$\tau(H_3\text{-}N_1\text{-}H_1\text{-}Cl)$	13.5	17.3
$\tau(H_4\text{-}N_1\text{-}H_1\text{-}Cl)$	-99.6	-94.3
$\tau(H_5\text{-}N_2\text{-}H_2\text{-}Cl)$	24.8	25.4
$\tau(H_6\text{-}N_2\text{-}H_2\text{-}Cl)$	-86.9	-85.0

[a] Bond lengths in Å; bond angles in deg. [b] Atoms are as labeled in Figure 4.

TABLE 6: MP2 Optimized Geometry of the $Cl^-(NH_3)_2$ C_2 Isomer[a,b]

	6-31+G**
$Cl^-(NH_3)_2$	
r(Cl--H_1)	2.432
r(N-H_1)	1.024
r(N-H_2)	1.014
r(N-H_3)	1.014
θ(H_1-Cl-H_1)	122.2
θ(Cl-H_1-N)	165.9
θ(H_1-N-H_2)	105.3
θ(H_1-N-H_3)	105.3
τ(N-H_1-Cl-H_1)	93.4
τ(H_2-N-H_1-Cl)	58.1
τ(H_3-N-H_1-Cl)	-53.9
NH_3	
r(N-H)	1.012
θ(H-N-H)	110.8

[a] Bond lengths in Å; bond angles in deg.

[b] Atoms are as labeled in Figure 5.

TABLE 7: MP2 Optimized Geometry of the $Cl^-(NH_3)_2$ C_{2v} Isomer[a,b]

	6-31+G**
$Cl^-(NH_3)_2$	
$r(Cl\text{--}H_1)$	2.433
$r(N\text{-}H_1)$	1.024
$r(N\text{-}H_2)$	1.014
$\theta(H_1\text{-}Cl\text{-}H_1)$	123.2
$\theta(Cl\text{-}H_1\text{-}N)$	166.1
$\theta(H_1\text{-}N\text{-}H_2)$	105.5
$\theta(H_2\text{-}N\text{-}H_2)$	106.3
$\tau(N\text{-}H_1\text{-}Cl\text{-}H_1)$	0.0
$\tau(Cl\text{-}H_1\text{-}N\text{-}H_2)$	±56.1
NH_3	
$r(N\text{-}H)$	1.012
$\theta(H\text{-}N\text{-}H)$	110.8

[a] Bond lengths in Å; bond angles in deg.

[b] Atoms are as labeled in Figure 6.

TABLE 8: MP2 Optimized Geometry of the $Cl^-(NH_3)_2$ C_{2h} Linear Isomer[a,b]

	6-31+G**
$Cl^-(NH_3)_2$	
$r(Cl\text{--}H_1)$	2.458
$r(N\text{-}H_1)$	1.023
$r(N\text{-}H_2)$	1.014
$\theta(H_1\text{-}Cl\text{-}H_1)$	180.0
$\theta(Cl\text{-}H_1\text{-}N)$	165.4
$\theta(H_1\text{-}O\text{-}H_2)$	105.3
$\theta(H_2\text{-}O\text{-}H_2)$	106.2
$\tau(O\text{-}H_1\text{-}H_1\text{-}O)$	180.0
NH_3	
$r(N\text{-}H)$	1.012
$\theta(H\text{-}N\text{-}H)$	110.8

[a] Bond lengths in Å; bond angles in deg.

[b] Atoms are as labeled in Figure 7.

TABLE 9: MP2 Optimized Geometry of the $Cl^-(NH_3)_3$ C_{3v} Isomer[a,b]

	6-31+G**
$Cl^-(NH_3)_3$	
r(Cl--H_1)	2.387
r(N-H_1)	1.013
r(N-H_2)	0.998
θ(H_1-Cl-H_1)	120.0
θ(Cl-H_1-N)	180.0[c]
θ(H_1-N-H_2)	120.3
θ(H_2-N-H_2)	119.3
τ(Cl-H_1-N-H_2)	0, 180
NH_3	
r(N-H)	1.012
θ(H-N-H)	110.8

[a] Bond lengths in Å; bond angles in deg.

[b] Atoms are as labeled in Figure 8.

[c] The N atoms are very slightly out of the H--Cl--H plane.

TABLE 10: MP2 Harmonic Vibrational Frequencies and Infrared Intensities of the $Cl^-(NH_3)$ C_s Linear Minimum, with Comparison to NH_3 Frequencies[a]

	Approx Description	*Ab Initio*		Experimental	
		6-31+G**	6-311++G**	Harmonic[b]	Fundamental[c]
$Cl^-(NH_3)$					
$\omega_1(A')$	Sym free NH stretch	3620(73)	3573(51)		
$\omega_2(A')$	Bonded NH stretch	3445(279)	3388(351)		
$\omega_3(A')$	Sym NH_3 bend	1690(23)	1646(16)		
$\omega_4(A')$	NH_3 umbrella	1235(184)	1233(152)		
$\omega_5(A')$	NH_3 wag	332(76)	336(71)		
$\omega_6(A')$	Cl--H intermol stretch	146(17)	140(17)		
$\omega_7(A'')$	Antisym free NH str	3692(0)	3644(0)		
$\omega_8(A'')$	Antisym NH_3 bend	1746(19)	1709(12)		
$\omega_9(A'')$	NH_3 twist	259(35)	268(30)		
NH_3					
$\omega_1(A_1)$	Sym NH stretch	3564(2)	3530(2)	3485 ± 11	3337
$\omega_2(A_1)$	NH_3 umbrella	1048(245)	1069(207)	1022	932, 968
$\omega_3(E)$	Degen NH stretch	3734(7)	3682(6)	3624 ± 12	3444
$\omega_4(E)$	Degen NH_3 bend	1705(29)	1665(25)	1678 ± 6	1627

[a] Frequencies in cm^{-1}; infrared intensities in km/mol.

[b] From refs. 8 and 9.

[c] From refs. 6 and 7.

TABLE 11: MP2 Harmonic Vibrational Frequencies and Infrared Intensities of the $Cl^-(NH_3)$ C_s Bridged Transition State[a]

	Approx Description	6-31+G**	6-311++G**
$Cl^-(NH_3)$			
$\omega_1(A')$	Free NH stretch	3682(7)	3634(8)
$\omega_2(A')$	Sym bonded NH stretch	3538(9)	3507(12)
$\omega_3(A')$	Sym NH_3 bend	1704(49)	1669(42)
$\omega_4(A')$	NH_3 umbrella	1263(225)	1261(198)
$\omega_5(A')$	NH_3 wag	202(100)	209(88)
$\omega_6(A')$	Cl--H intermol stretch	110(10)	122(11)
$\omega_7(A'')$	Antisym bonded NH stretch	3655(14)	3604(12)
$\omega_8(A'')$	Antisym NH_3 bend	1696(19)	1654(13)
$\omega_9(A'')$	NH_3 twist	248*i*(78)	227*i*(73)

[a] Frequencies in cm^{-1}; infrared intensities in km/mol.

TABLE 12: MP2 Harmonic Vibrational Frequencies and Infrared Intensities of the $Cl^-(NH_3)$ C_{3v} Dipole-Aligned Second-Order Transition State[a]

	Approx Description	6-31+G**	6-311++G**
$Cl^-(NH_3)$			
$\omega_1(A_1)$	Sym bonded NH stretch	3549(0)	3518(0)
$\omega_2(A_1)$	NH_3 umbrella	1274(228)	1259(214)
$\omega_3(A_1)$	Cl--H intermol stretch	95(13)	95(13)
$\omega_4(E)$	Degen bonded NH stretch	3671(7)	3620(6)
$\omega_5(E)$	Degen NH_3 bend	1708(18)	1661(12)
$\omega_6(E)$	Degen NH_3 wag + twist	193*i*(106)	214*i*(100)

[a] Frequencies in cm^{-1}; infrared intensities in km/mol.

TABLE 13: MP2 Harmonic Vibrational Frequencies and Infrared Intensities of the $Cl^-(NH_3)_2$ C_1 Minimum with Various Basis Sets[a,b]

	Approx Description	6-31+G**	6-311++G**
ω_1	DA free NH stretch	3696(0)	3646(0)
ω_2	DD NH_3-bound + free NH stretches	3683(13)	3634(11)
ω_3	DD Cl^- bound + NH_3-bound NH stretches	3627(107)	3577(91)
ω_4	DD free NH stretch	3619(28)	3572(15)
ω_5	DD Cl^- bound NH stretch	3497(95)	3460(117)
ω_6	DA Cl^- bound NH stretch	3421(334)	3364(392)
ω_7	DA + DD NH_3 bend	1753(31)	1711(19)
ω_8	DA + DD NH_3 bend	1737(24)	1697(17)
ω_9	DD NH_3 bend	1704(17)	1659(13)
ω_{10}	DA NH_3 bend	1690(14)	1648(10)
ω_{11}	DD NH_3 umbrella	1248(104)	1242(91)
ω_{12}	DA NH_3 umbrella	1215(246)	1211(190)
ω_{13}	DA NH_3 wag	422(147)	414(120)
ω_{14}	DD NH_3 wag	330(15)	319(18)
ω_{15}	DA NH_3 twist	285(75)	286(49)
ω_{16}	DD NH_3 twist	252(31)	259(40)
ω_{17}	H_1--Cl--H_2 wag	215(24)	198(31)
ω_{18}	Cl--H_1 stretch	162(20)	157(21)
ω_{19}	Cl--H_2 stretch	130(13)	125(11)
ω_{20}	H_1--Cl--H_2 bend	84(8)	80(6)
ω_{21}	H_1--Cl--H_2 twist	73(30)	58(30)

[a] Frequencies in cm^{-1}; infrared intensities in km/mol.

[b] DA=donor/acceptor; DD=double donor.

TABLE 14: MP2 Harmonic Vibrational Frequencies and Infrared Intensities of the $Cl^-(NH_3)_2$ C_2 Minimum[a]

	Approx Description	6-31+G**
$\omega_1(A)$	IP antisym free NH stretch	3694(0)
$\omega_2(A)$	IP sym free NH stretch	3626(35)
$\omega_3(A)$	Sym bonded NH stretch	3463(90)
$\omega_4(A)$	IP antisym NH_3 bend	1749(23)
$\omega_5(A)$	IP sym NH_3 bend	1692(5)
$\omega_6(A)$	IP NH_3 umbrella	1229(56)
$\omega_7(A)$	IP NH_3 wag	329(25)
$\omega_8(A)$	IP NH_3 twist	262(51)
$\omega_9(A)$	Sym Cl--H stretch	131(5)
$\omega_{10}(A)$	H--Cl--H wag	40(79)
$\omega_{11}(A)$	H--Cl--H bend	16(5)
$\omega_{12}(B)$	OOP antisym free NH stretch	3694(0)
$\omega_{13}(B)$	OOP sym free NH stretch	3625(122)
$\omega_{14}(B)$	Antisym bonded NH stretch	3457(407)
$\omega_{15}(B)$	OOP antisym NH_3 bend	1744(9)
$\omega_{16}(B)$	OOP sym NH_3 bend	1691(45)
$\omega_{17}(B)$	OOP NH_3 umbrella	1228(306)
$\omega_{18}(B)$	OOP NH_3 wag	328(130)
$\omega_{19}(B)$	OOP NH_3 twist	255(18)
$\omega_{20}(B)$	Antisym Cl--H stretch	157(23)
$\omega_{21}(B)$	H--Cl--H twist	9(31)

[a] Frequencies in cm^{-1}; infrared intensities in km/mol. [b] IP=in phase; OOP=out of phase.

TABLE 15: MP2 Harmonic Vibrational Frequencies and Infrared Intensities of the $Cl^-(NH_3)_2$ C_{2v} Transition State[a,b]

	Approx Description	6-31+G**
$\omega_1(A_1)$	IP sym free NH stretch	3628(35)
$\omega_2(A_1)$	IP bonded NH stretch	3462(190)
$\omega_3(A_1)$	IP sym NH_3 bend	1692(41)
$\omega_4(A_1)$	IP NH_3 umbrella	1228(28)
$\omega_5(A_1)$	IP NH_3 wag	334(97)
$\omega_6(A_1)$	Sym Cl--H stretch	135(5)
$\omega_7(A_1)$	H--Cl--H bend	16(0)
$\omega_8(A_2)$	IP antisym free NH stretch	3696(0)
$\omega_9(A_2)$	IP antisym NH_3 bend	1745(0)
$\omega_{10}(A_2)$	IP NH_3 twist	253(0)
$\omega_{11}(A_2)$	H--Cl--H twist	23*i*(0)
$\omega_{12}(B_1)$	OOP antisym free NH stretch	3696(0)
$\omega_{13}(B_1)$	OOP antisym NH_3 bend	1746(35)
$\omega_{14}(B_1)$	OOP NH_3 twist	254(67)
$\omega_{15}(B_1)$	H--Cl--H wag	15(96)
$\omega_{16}(B_2)$	OOP sym free NH stretch	3626(121)
$\omega_{17}(B_2)$	OOP bonded NH stretch	3455(297)
$\omega_{18}(B_2)$	OOP sym NH_3 bend	1691(7)
$\omega_{19}(B_2)$	OOP NH_3 umbrella	1216(348)
$\omega_{20}(B_2)$	OOP NH_3 wag	333(57)
$\omega_{21}(B_2)$	Antisym Cl--H stretch	153(25)

[a] Frequencies in cm^{-1}; infrared intensities in km/mol. [b] IP=in phase; OOP=out of phase.

TABLE 16: MP2 Harmonic Vibrational Frequencies and Infrared Intensities of the $Cl^-(NH_3)_2$ C_{2h} Linear Second-Order Transition State[a]

	Approx Description	6-31+G**
$\omega_1(A_g)$	IP sym free NH stretch	3629(0)
$\omega_2(A_g)$	IP bonded NH stretch	3469(0)
$\omega_3(A_g)$	IP sym NH_3 bend	1693(0)
$\omega_4(A_g)$	IP NH_3 umbrella	1227(0)
$\omega_5(A_g)$	IP NH_3 wag	321(0)
$\omega_6(A_g)$	Sym Cl--H stretch	116(0)
$\omega_7(A_u)$	IP antisym free NH stretch	3696(0)
$\omega_8(A_u)$	IP antisym NH_3 bend	1743(40)
$\omega_9(A_u)$	IP NH_3 twist	233(71)
$\omega_{10}(A_u)$	H--Cl--H twist	16(108)
$\omega_{11}(A_u)$	H--Cl--H bend	29*i*(0)
$\omega_{12}(B_g)$	OOP antisym free NH stretch	3696(0)
$\omega_{13}(B_g)$	OOP antisym NH_3 bend	1745(0)
$\omega_{14}(B_g)$	OOP NH_3 twist	239(0)
$\omega_{15}(B_u)$	OOP sym free NH stretch	3627(157)
$\omega_{16}(B_u)$	OOP bonded NH stretch	3463(474)
$\omega_{17}(B_u)$	OOP sym NH_3 bend	1692(49)
$\omega_{18}(B_u)$	OOP NH_3 umbrella	1123(381)
$\omega_{19}(B_u)$	OOP NH_3 wag	312(156)
$\omega_{20}(B_u)$	Antisym Cl--H stretch	154(29)
$\omega_{21}(B_u)$	H--Cl--H bend	26*i*(6)

[a] Frequencies in cm^{-1}; infrared intensities in km/mol. [b] IP=in phase; OOP=out of phase.

TABLE 17: MP2 Harmonic Vibrational Frequencies and Infrared Intensities of the $Cl^-(NH_3)_3$ C_{3v} Third-Order Transition State[a,b]

	Approx Description	6-31+G**
$\omega_1(A_1)$	IP antisym free NH stretch	3933(77)
$\omega_2(A_1)$	IP sym free NH stretch	3844(0)
$\omega_3(A_1)$	Sym bonded NH stretch	3563(0)
$\omega_4(A_1)$	IP antisym NH_3 bend	1671(88)
$\omega_5(A_1)$	IP sym NH_3 bend	1603(0)
$\omega_6(A_1)$	IP NH_3 rock	232(0)
$\omega_7(A_1)$	Sym Cl--H stretch	118(0)
$\omega_8(A_1)$	H--Cl--H bend	19(9)
$\omega_9(A_2)$	IP NH_3 wag	549(0)
$\omega_{10}(A_2)$	Sym NH_3 twist	59*i*(0)
$\omega_{11}(A_2)$	Sym NH_3 umbrella	801*i*(0)
$\omega_{12}(E)$	Degen antisym free NH stretch	3933(0)
$\omega_{13}(E)$	Degen sym free NH stretch	3840(238)
$\omega_{14}(E)$	Degen bonded NH stretch	3549(677)
$\omega_{15}(E)$	Degen antisym NH_3 bend	1669(0)
$\omega_{16}(E)$	Degen sym NH_3 bend	1602(37)
$\omega_{17}(E)$	Degen NH_3 wag	583(13)
$\omega_{18}(E)$	Degen NH_3 rock	230(0)
$\omega_{19}(E)$	Degen Cl--H stretch	156(22)
$\omega_{20}(E)$	Degen H--Cl--H bend	24(2)
$\omega_{21}(E)$	Degen NH_3 twist	18(0)
$\omega_{22}(E)$	Degen NH_3 umbrella	784*i*(618)

[a] Frequencies in cm^{-1}; infrared intensities in km/mol. [b] IP=in phase; OOP=out of phase.

TABLE 18: Stabilities[a] of the C_s Bridged (Ib) and C_{3v} Dipole-Aligned (Ic) Isomers Relative to the Ground State C_s Linear $Cl^-(NH_3)$ Isomer

	Bridged		Dipole-Aligned	
Level of Theory	ΔE_e	ΔE_o	ΔE_e	ΔE_o
MP2/6-31+G**	+1.5	+1.1	+1.9	+1.2
MP2/6-311++G**	+1.4	+1.0	+1.9	+1.2

[a] Energies in kcal/mol.

TABLE 19: Energetics[a] of the Reaction $Cl^-(NH_3) \rightarrow Cl^- + NH_3$[b]

Source of Data	ΔE_e	ΔE_o	ΔH_{298}
MP2/6-31+G**	8.5	7.5	7.2
MP2/6-311++G**	8.9	8.0	7.7
Experiment (Refs. 1, 2)			8.2, 10.5

[a] Energies in kcal/mol.

[b] With reference to the ground state linear $Cl^-(NH_3)$ isomer (**Ia**).

TABLE 20: Stabilities[a] of the C_s (IIb), C_{2v} (IIc) and C_{2h} (IId) Isomers Relative to the Ground State C_1 $Cl^-(NH_3)_2$ Isomer with Three Hydrogen Bonds (IIa)

	C_2 Minimum		C_{2v} Transition State		C_{2h} 2nd Order TS	
Level of Theory	ΔE_e	ΔE_o	ΔE_e	ΔE_o	ΔE_e	ΔE_o
MP2/6-31+G**	+0.9	+0.3	+1.1	+0.4	+1.4	+0.6

[a] Energies in kcal/mol.

TABLE 21: Energetics[a] of the Reaction $Cl^-(NH_3)_2 \rightarrow Cl^-(NH_3) + NH_3$[b]

Source of Data	ΔE_e	ΔE_o	ΔH_{298}
MP2/6-31+G**	9.1	7.4	7.6
MP2/6-311++G**	9.6	8.0	8.1
Experiment			---

[a] Energies in kcal/mol.

[b] With reference to the ground state C_1 $Cl^-(NH_3)_2$ isomer (**IIa**).

5.6 FIGURE CAPTIONS

Figure 1. The ground state $n = 1$ isomer, with one strong hydrogen bond.

Figure 2. The bridged $n = 1$ transition state.

Figure 3. The dipole-aligned $n = 1$ second-order transition state.

Figure 4. The ground state $n = 2$ minimum, with three hydrogen bonds.

Figure 5. The $n = 2$ C_2 minimum, with no hydrogen bonding between the ammonias.

Figure 6. The $n = 2$ C_{2v} transition state.

Figure 7. The $n = 2$ C_{2h} second-order transition state.

Figure 8. A $n = 3$ C_{3v} (nearly D_{3h}) third-order transition state.

Figure 9. A time-of-flight mass spectrum showing the two isotopes of Cl^- ion (at masses 35 and 37), and the complexes of Cl^- with one NH_3 or one H_2O.

Figure 10. A time-of-flight mass spectrum of $Cl^-(NH_3)_n$ typical of the experimental conditions under which the infrared spectra were recorded.

Figure 11. A time-of-flight mass spectrum showing the production of larger $Cl^-(NH_3)_n$ clusters.

Figure 12. The predissociation spectrum of $Cl^-(NH_3)$. The top and bottom spectra reflect different source conditions. See discussion in the text.

Figure 13. The predissociation spectrum of $Cl^-(NH_3)_2$.

Figure 14. The predissociation spectrum of $Cl^-(NH_3)_3$.

Figure 15. The predissociation spectrum of $Cl^-(NH_3)_4$.

Figure 16. The predissociation spectrum of $Cl^-(NH_3)_5$.

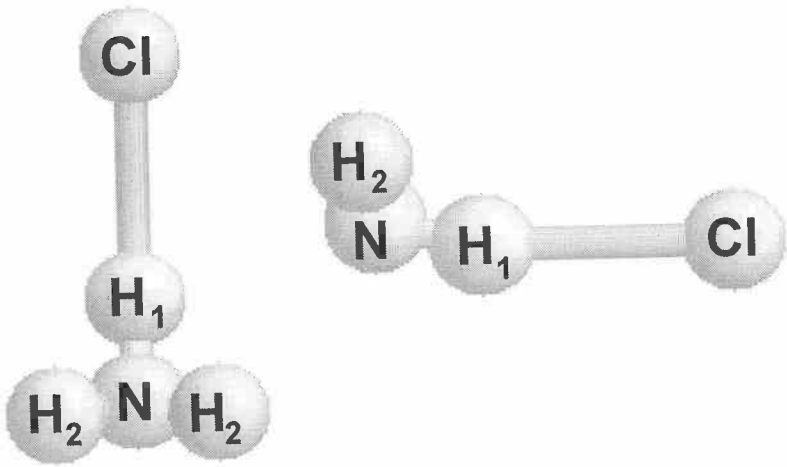

Ia

Figure 1

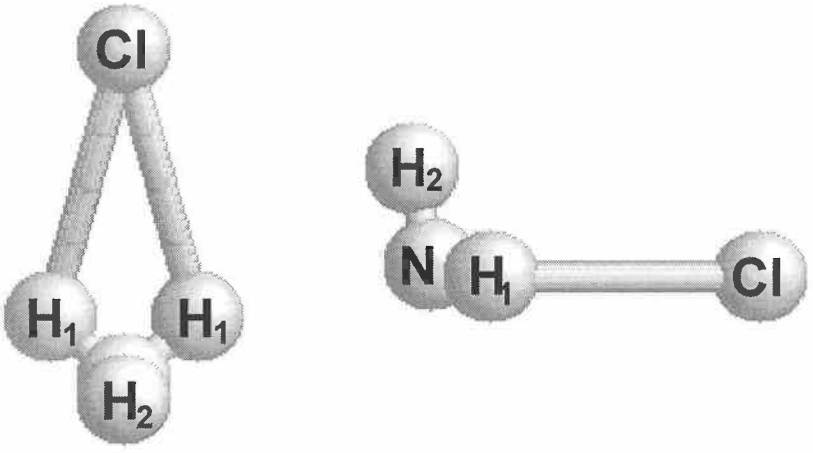

Ib

Figure 2

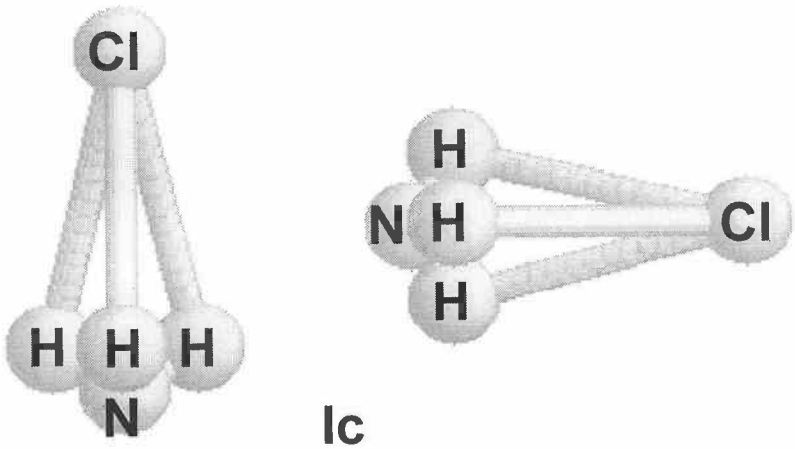

Figure 3

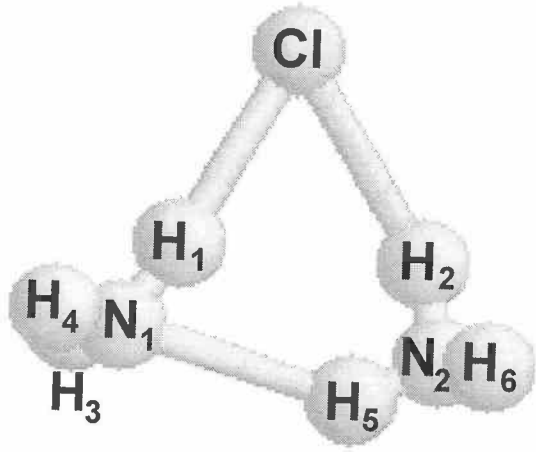

IIa

Figure 4

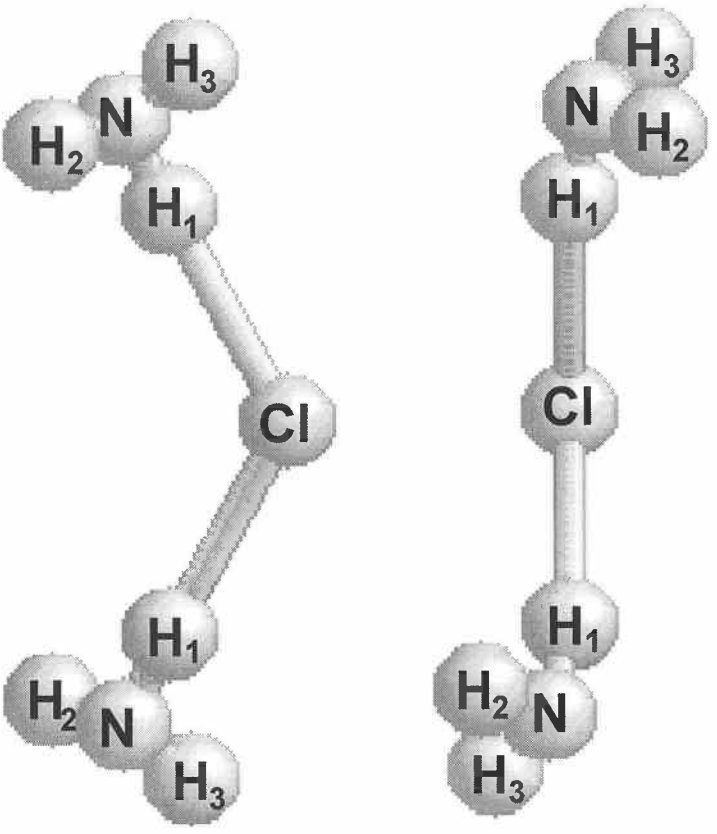

IIb

Figure 5

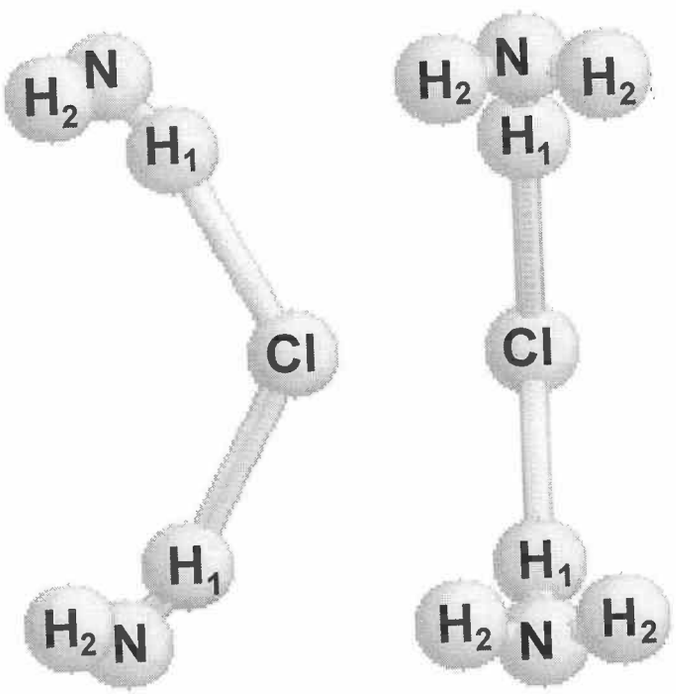

IIc

Figure 6

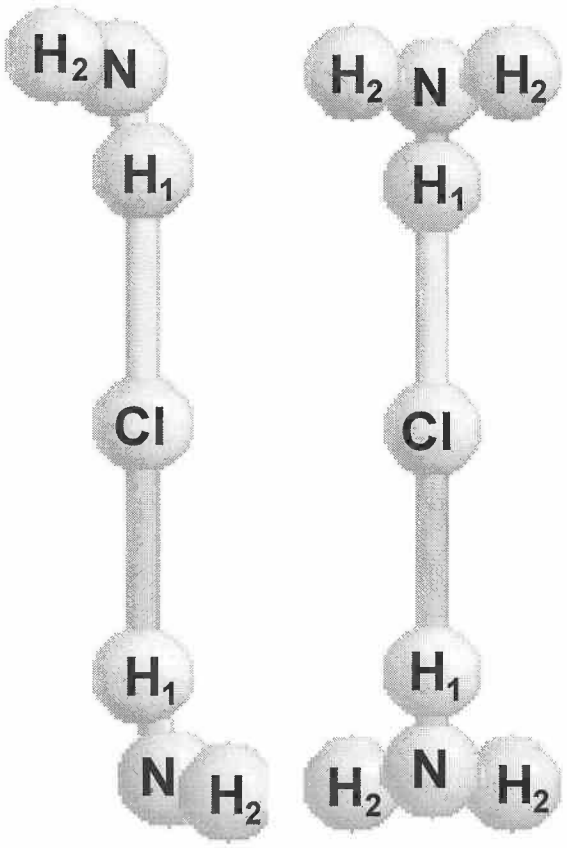

IId

Figure 7

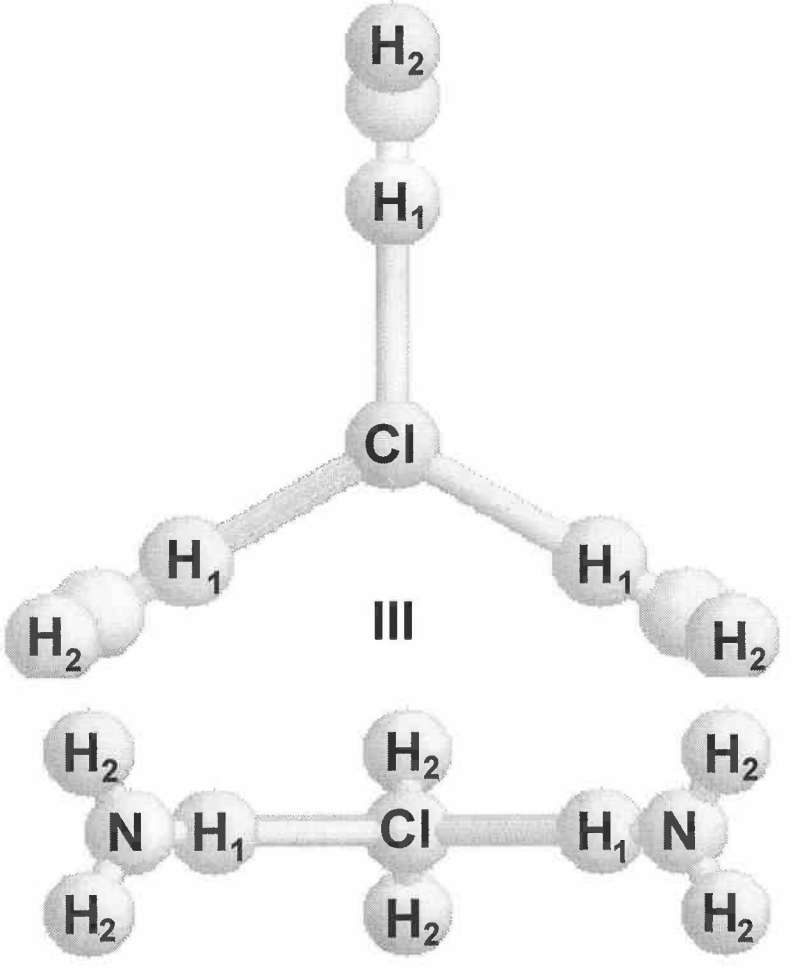

Figure 8

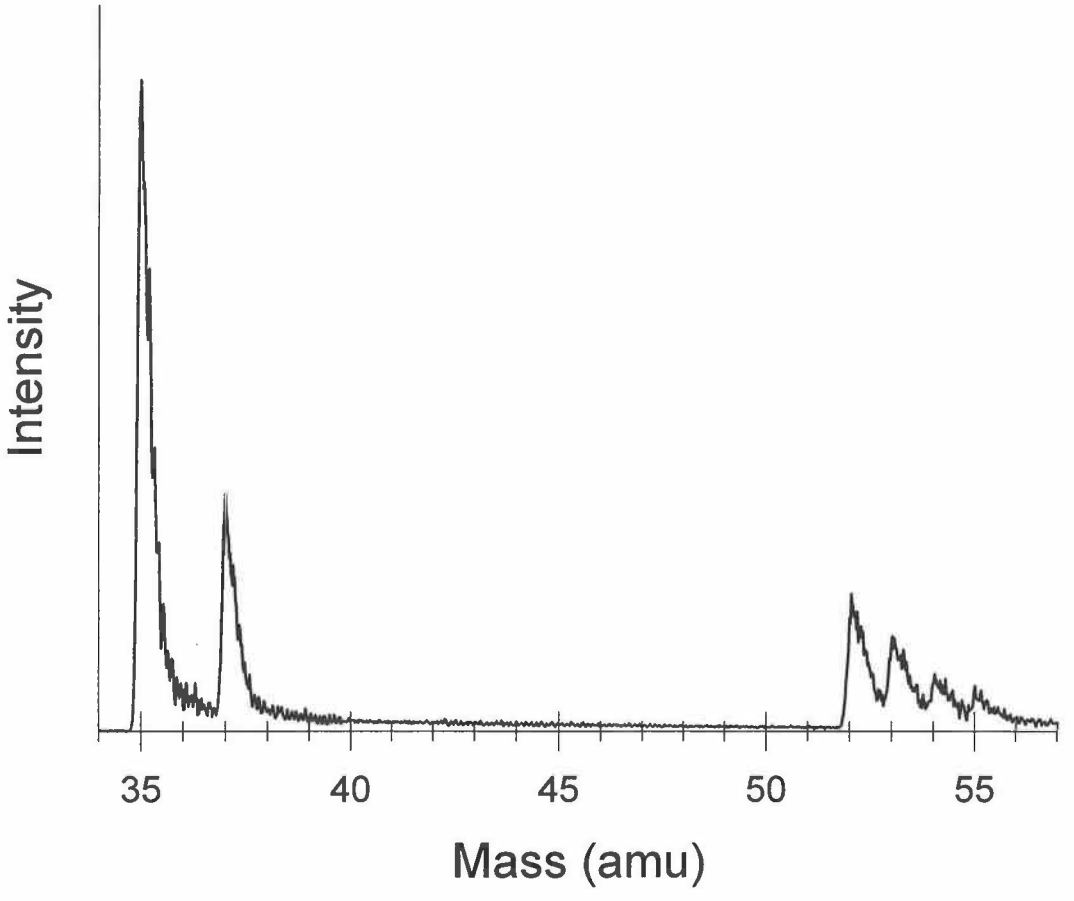

Figure 9

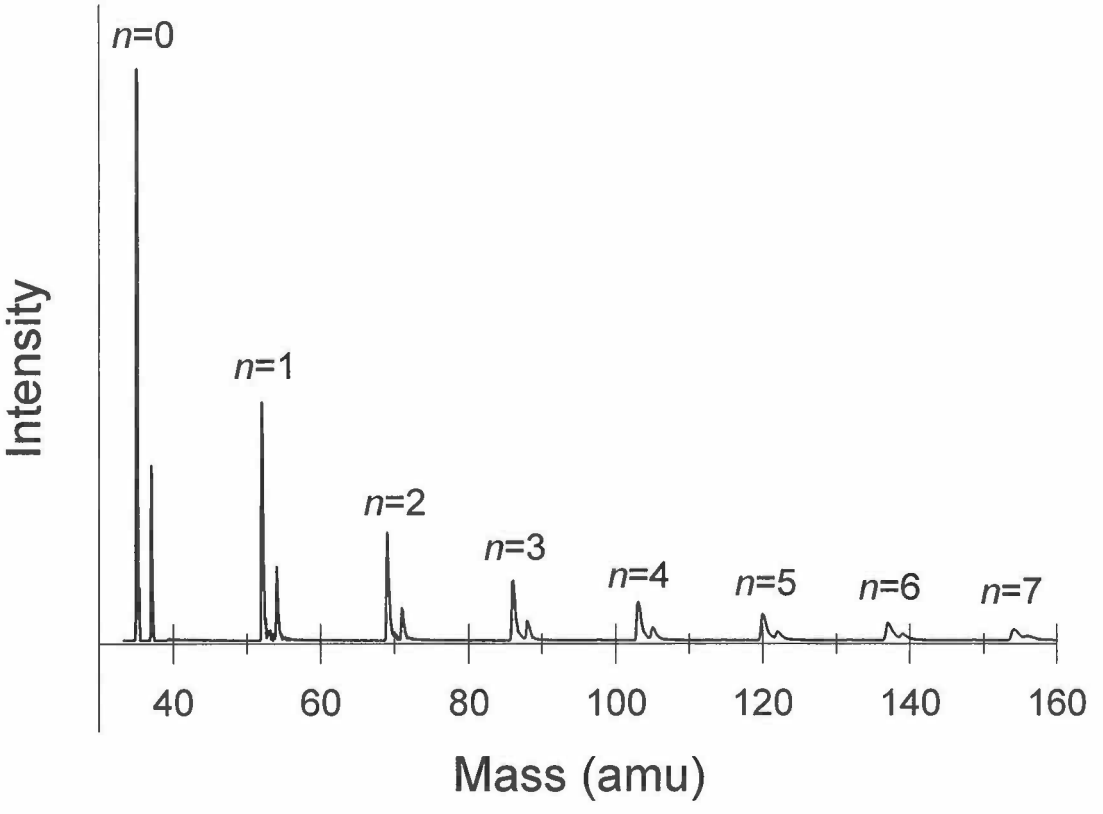
n=0
n=1
n=2
n=3
n=4
n=5
n=6
n=7
Intensity
40
60
80
100
120
140
160
Mass (amu)

Figure 10

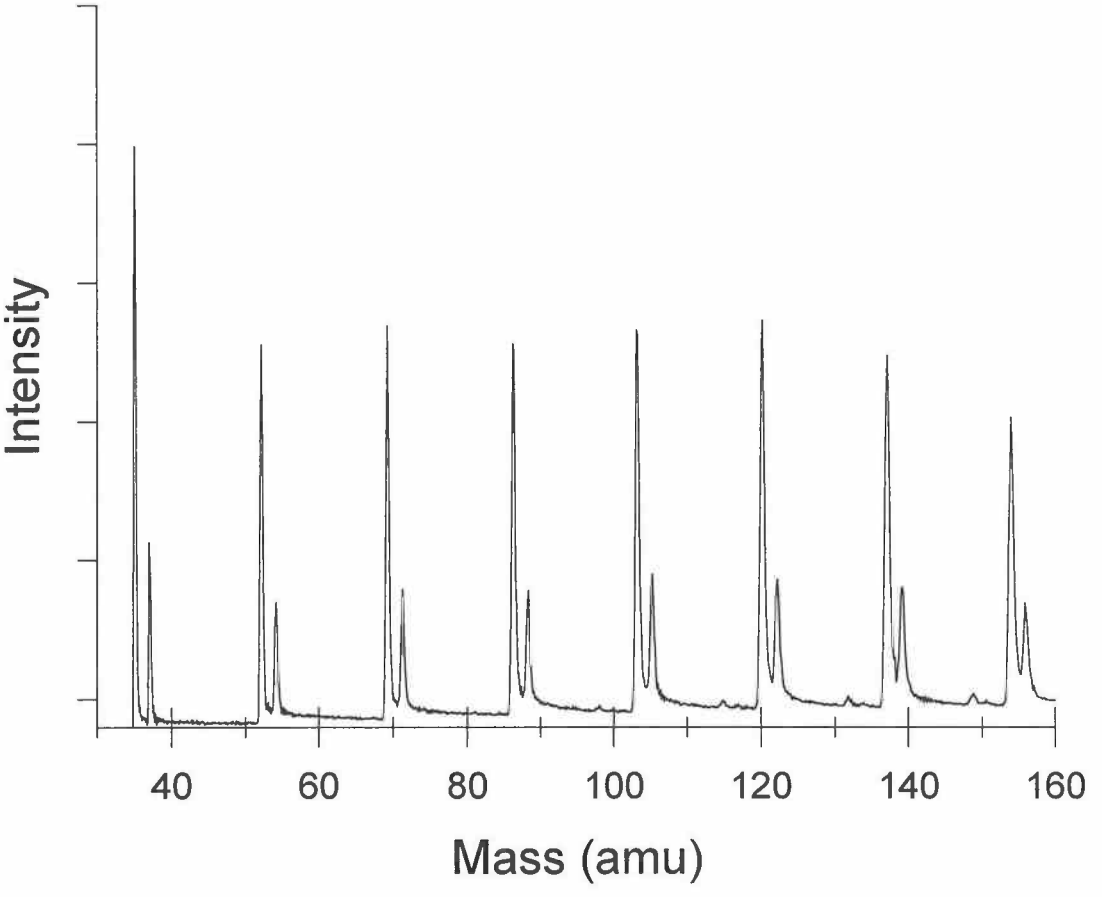

Figure 11

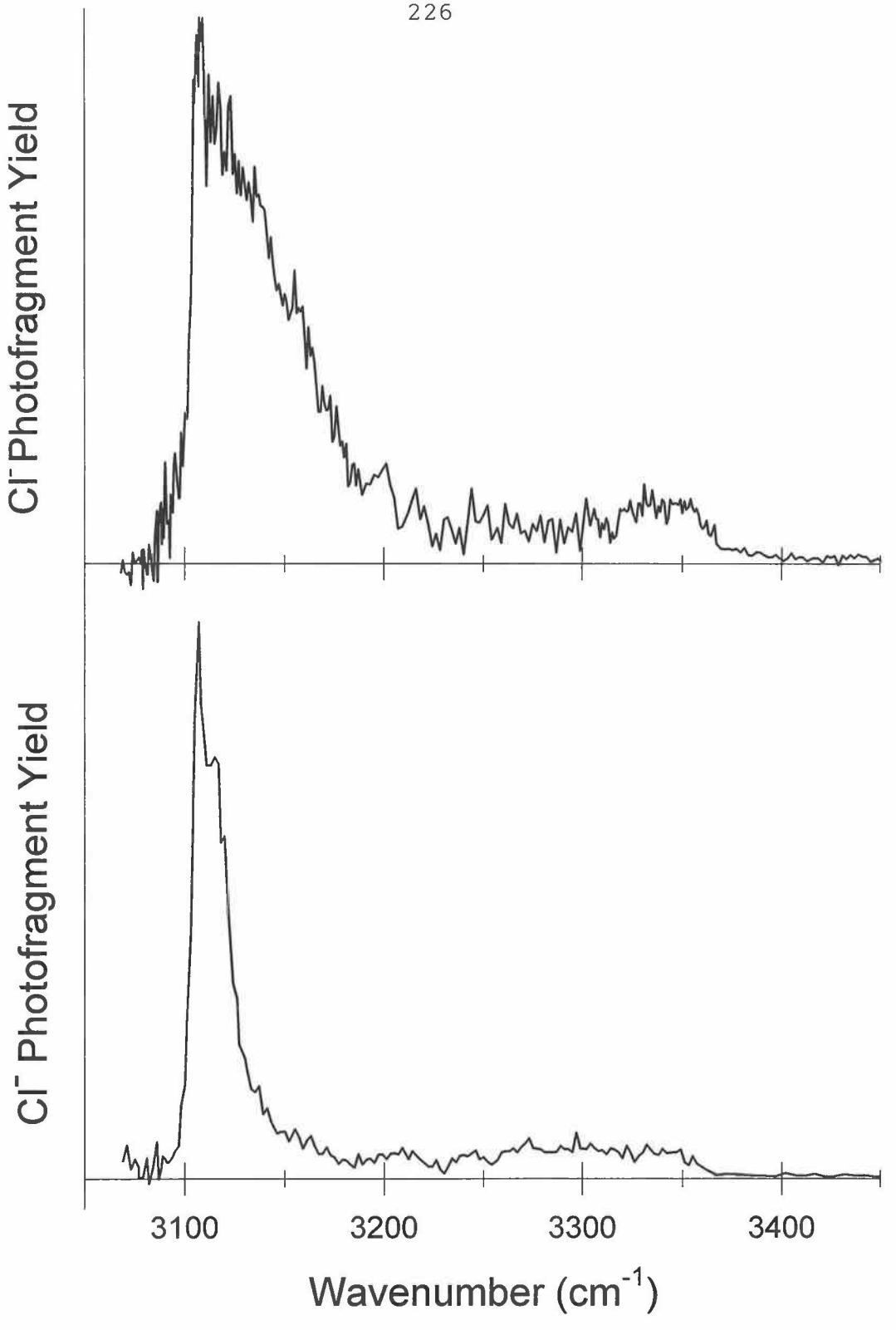
Cl⁻ Photofragment Yield
Cl⁻ Photofragment Yield
3100
3200
3300
3400
Wavenumber (cm⁻¹)

Figure 12

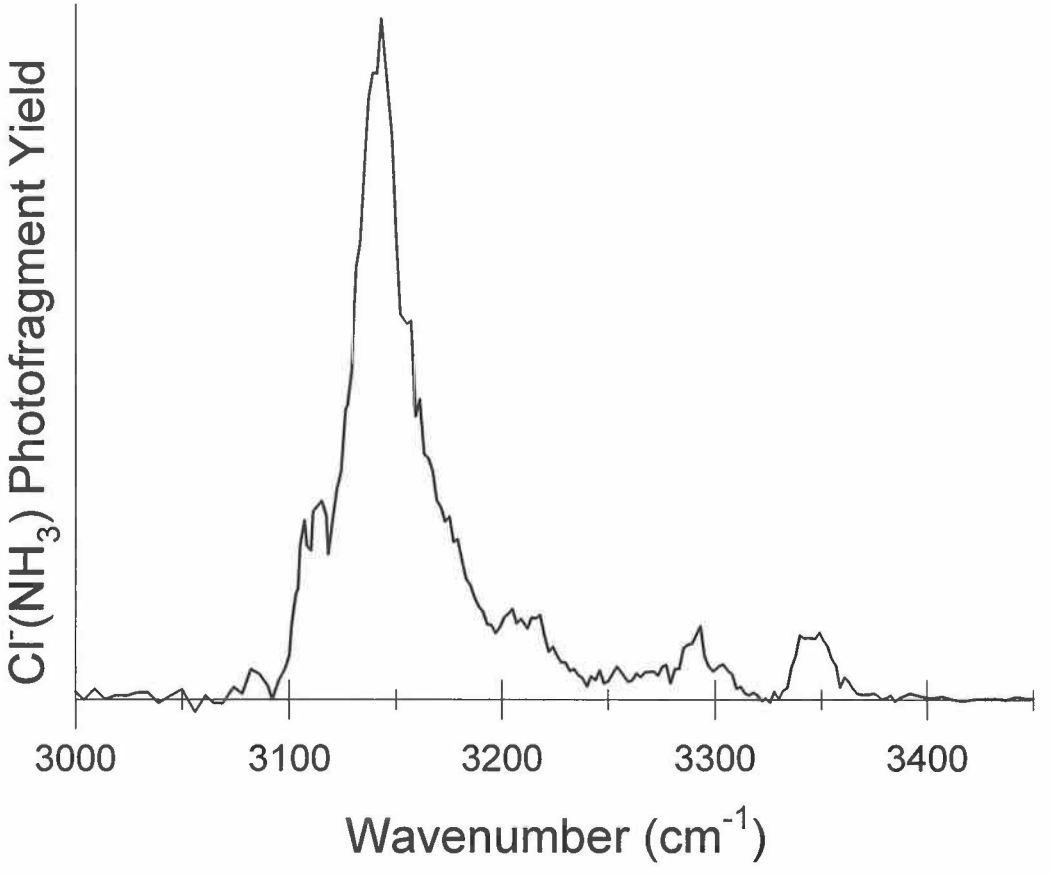
Cl⁻(NH3) Photofragment Yield
3000
3100
3200
3300
3400
Wavenumber (cm-1)

Figure 13

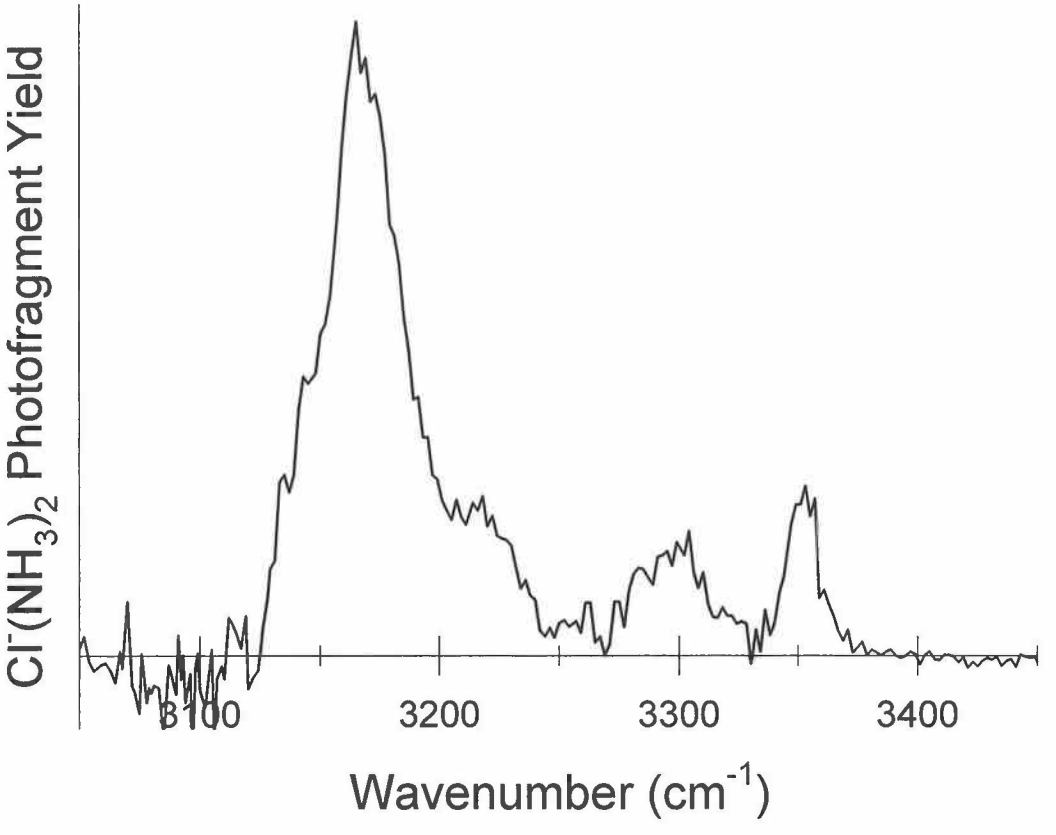
Cl⁻(NH3)2 Photofragment Yield
3100
3200
3300
3400
Wavenumber (cm-1)

Figure 14

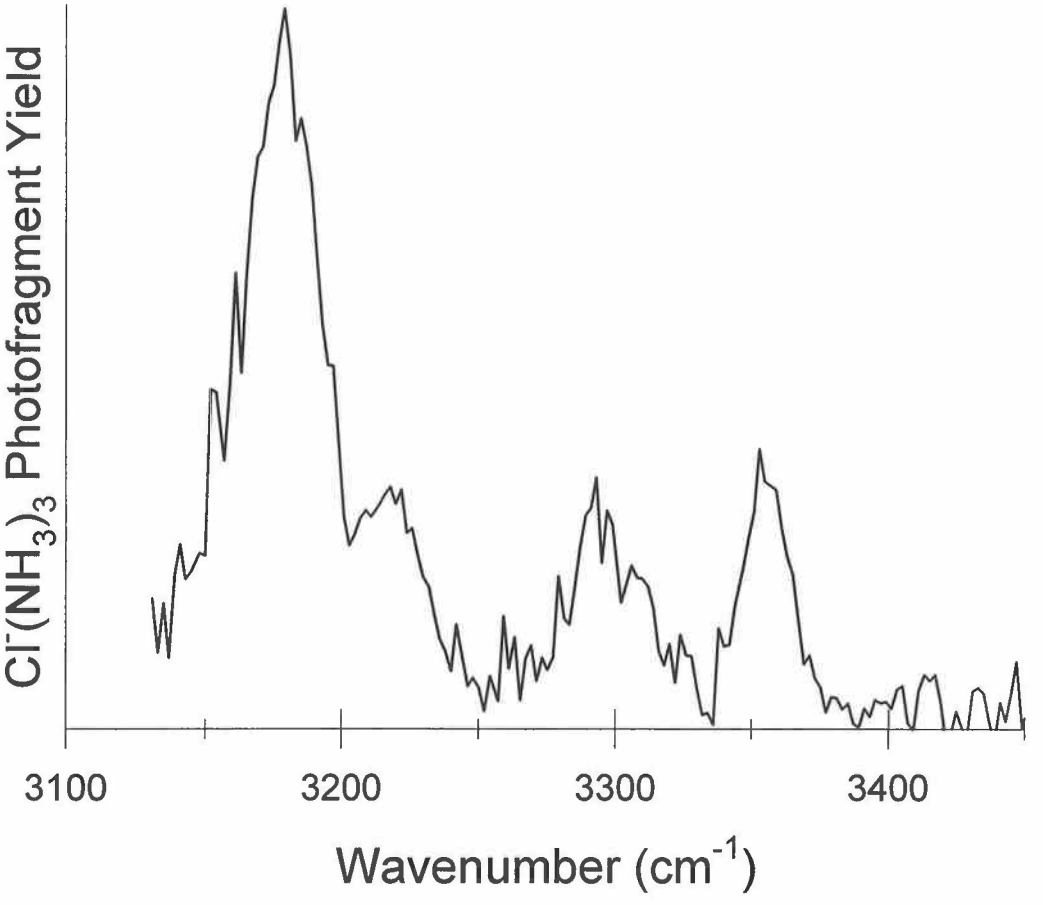
$Cl^-(NH_3)_3$ Photofragment Yield
3100
3200
3300
3400
Wavenumber (cm^{-1})

Figure 15

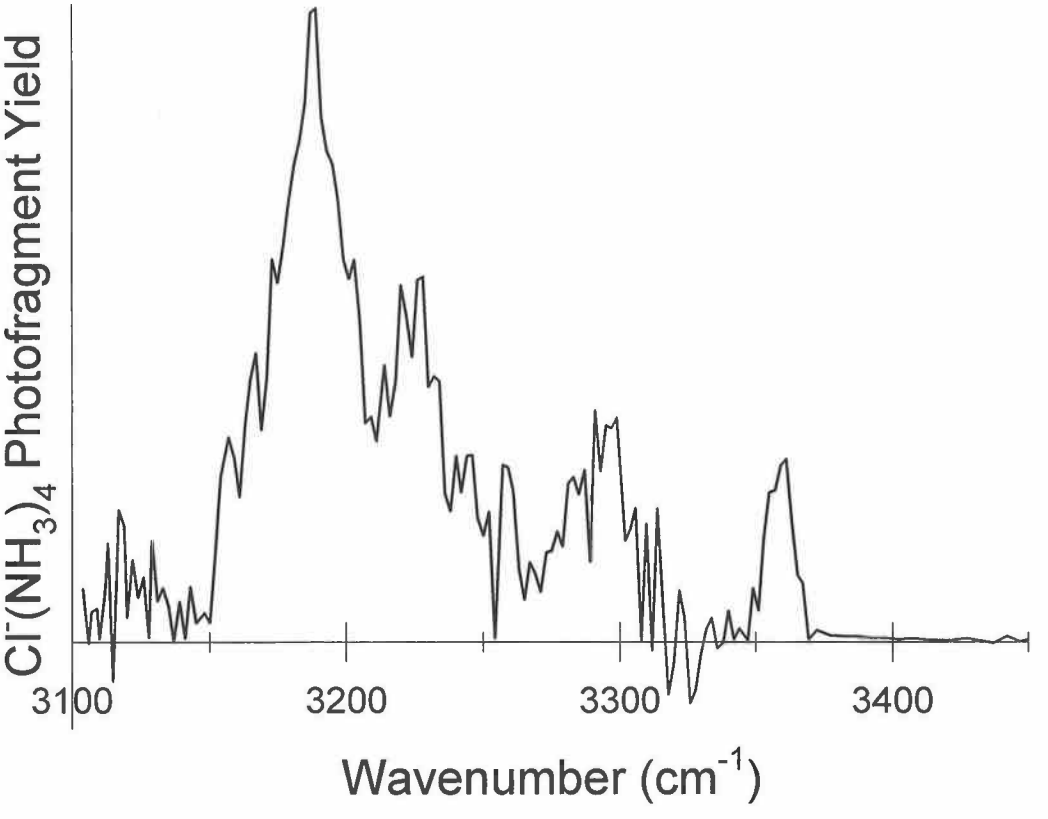
$Cl^-(NH_3)_4$ Photofragment Yield
3100
3200
3300
3400
Wavenumber (cm^{-1})

Figure 16